Impact of human activities on water level and clarity and underwater light climate of *Vallisneria spiralis L.* in Poyang Lake, China

Wu, Guofeng

Promotors:

Prof. Dr. Andrew K. Skidmore
Professor of Vegetation and Agricultural Land Use Survey, International Institute for Geo-Information Science and Earth Observation (ITC), Enschede and Wageningen University, the Netherlands

Prof. Dr. Herbert H. T. Prins
Professor of Resource Ecology, Wageningen University, the Netherlands

Co-promotor:

Dr. Jan De Leeuw
Associate Professor, International Institute for Geo-Information Science and Earth Observation (ITC), Enschede, the Netherlands

Examining Committee:

Prof. Dr. Ir. H. van Keulen
Wageningen University, the Netherlands

Prof. P. Herman
KNAW, Centre for Estuarine and Marine Ecology, Yerseke, the Netherlands

Prof. Dr. Z. Su
University of Twente, Enschede, the Netherlands

Prof. P. Pilesjö
Lund University, Lund, Sweden

This research is carried out within the C. T. de Wit Graduate School for Production Ecology and Resource Conservation (PE&RC) in Wageningen University, the Netherlands

Impact of human activities on water level and clarity and underwater light climate of *Vallisneria spiralis L.* in Poyang Lake, China

Wu, Guofeng

Thesis
To fulfil the requirements for the degree of Doctor
on the authority of the Rector Magnificus of Wageningen University
Prof. Dr. M.J. Kropff
to be publicly defended on Thursday 7 February, 2008 at 15:00 hrs
in the auditorium at ITC, Enschede, the Netherlands

Impact of human activities on water level and clarity and underwater light climate of *Vallisneria spiralis L.* in Poyang Lake, China

Cover photograph: Footsteps in Lake Dahuchi. Photograph taken during emergence of the sediments at low water on 2nd December 2004

ISBN: 978-90-8504-907-4
International Institute for Geo-information Science & Earth Observation, Enschede, the Netherlands (ITC)
ITC Dissertation Number: 151

Dedicated to my wife and parents

CONTENTS

FIGURES

TABLES

SUMMARY

Almost 95% of the world population of Siberian crane (*Grus leucogeranus*) winter in Poyang Lake, China. Here they forage on the tubers of the submerged aquatic macrophyte *Vallisneria spiralis L.* The growth and production of *V. spiralis* are regulated by the local hydrology, which might also be influenced by the changed hydrology of the Yangtze River induced by engineering projects. This thesis investigated the impact of dredging activities in the northern Poyang Lake and the Three Gorges Dam in the Yangtze River on the water turbidity and water level of Poyang Lake, analyzed how these hydrological changes influenced the underwater light climate of *V. spiralis*, and discussed their potential impacts on the growth and productivity of *V. spiralis* and further on the food habitat of Siberian crane in Poyang Lake. The principal results obtained can be summarized as follows:

(1) Moderate resolution imaging spectroradiometer (MODIS) and Landsat thematic mapper (TM) images were compared for mapping the tempo-spatial dynamics of water clarity. Two multiple regression models including the blue and red bands of Landsat TM and MODIS respectively explained 83% and 88% of the variation of the natural logarithm of Secchi disk depth. On the basis of the comparison of water clarity predicted from Landsat TM and MODIS data as well as the advantages and contras of both sensors, it is concluded that MODIS offers the possibility to monitor the dynamics of water clarity more regularly and cheaply in relatively big and frequently cloud covered lakes like Poyang Lake.

(2) The performance of the various Landsat TM bands for detecting dredging ships was explored in the turbid water of the northern Poyang Lake. The result revealed that the TM bands 1 to 4 had limitation especially in turbid water, while bands 5 and 7 better discriminated vessels from surrounding waters. Therefore, it is recommended using the mid-infrared bands of Landsat TM for operational ship monitoring in turbid water.

(3) The possibility to strengthen inference of dredging impact while simultaneously monitoring vessels and water turbidity with remote sensing techniques was investigated in the northern Poyang Lake. Time-series MODIS images revealed a significant increase in water turbidity from 2001 onwards, while Landsat TM image analysis indicated a simultaneous increase in the number of vessels. Regression analysis further showed a highly significant positive relation (R^2 = 0.92) between water turbidity and vessel number. On the basis of discussion of ship-related resuspension, final destinations of vessels and coincidence of vessel clusters with irregular dented patterns and turbid plume development, it is confirmed that dredging caused the increase in water turbidity. Therefore, it is concluded that simultaneously monitoring water turbidity and vessels enhanced the strength of evidence in remotely sensed dredging impact assessments.

(4) Three extrapolation and interpolation methods were compared for predicting daily photosynthetically active radiation reaching the earth surface over the Poyang Lake national nature reserve. The result revealed that the triangulated irregular network (TIN) and inverse distance weighted (IDW)-based interpolation method produced more reliable result than the extrapolation methods.

(5) The photosynthetically active radiation reaching the top of *V. spiralis* (PAR_{tc}) in Lake Dahuchi from 1998 to 2006 was modelled. The results revealed significant between year differences in PAR_{tc}, which were determined primarily by

fluctuation in water level. Six years of Secchi disk depth records revealed seasonal switching of the lake from turbid at low water level in autumn, winter and spring to clear at high water level in summer. The highest PAR_{tc} occurred at intermediate water levels, which were reached when the Yangtze River forces Lake Dahuchi out of its turbid state in spring. The operation of the Three Gorges Dam, which will increase water level of Yangtze River from May to June may force Lake Dahuchi out of its turbid state earlier and increase the light intensity reaching the canopy and the production of *V. spiralis.* It is concluded that the operation of the Three Gorges Dam might at the short term increase the light regime and productivity of *V. spiralis* and possibly affect the food habitat of Siberian crane in Poyang Lake.

(6) A conceptual framework to integrate a simulation model of plant biomass for *V. spiralis* with remote sensing and a geographical information system was introduced. It is expected that the system, once implemented, could contribute to evaluate the impact of possible hydrological changes on the growth and productivity of *V. spiralis*, and assess whether tuber feeding bird populations are constrained by the regional availability of food resources in Lake Poyang.

It is anticipated that these results provide a basis for the future research and necessary information for decision-making that need to be made by the responsible authorities to decide how to rationally manage this unique lake ecosystem.

SAMENVATTING

Bijna 95% van de wereldpopulatie van de Siberische kraanvogel overwintert in het Poyang meer in China, waar ze foerageren op de wortelknolletjes van de ondergedoken waterplant *Vallisneria spiralis L.* De groei en productie van Vallisneria wordt gereguleerd door de locale hydrologie, die beïnvloed zou kunnen worden door verschillende projecten op de hydrologie van de Yangtze. Deze thesis bestudeert de invloed van baggeren in het noorden van Poyang meer en de drie kloven dam in de Yangtze rivier op de troebelheid en het niveau van het water in het meer, analyseert hoe deze hydrologische veranderingen het onderwater licht regime van Vallisneria beïnvloeden en bediscussieert de potentiële invloed hiervan op de groei en productie van Vallisneria en het voedselhabitat van Siberische kraanvogels in Poyang meer. De belangrijkste resultaten kunnen als volgt worden samengevat:

(1) Moderate resolution imaging spectroradiometer (MODIS) en Landsat thematic mapper (TM) beelden werden vergeleken voor het karteren van de temporeel ruimtelijke dynamiek van de helderheid van water. Twee multipele regressie modellen gebaseerd op de rode en blauwe band verklaarden respectievelijk 83% and 88% van de variatie van de natuurlijke logaritme van de Secchi schijf diepte. Op basis van vergelijking van de voorspellingen met Landsat en MODIS en de voordelen van beide sensoren werd geconcludeerd dat MODIS de betere mogelijkheid biedt om de helderheid van water regelmatig en op goedkope wijze te monitoren voor een relatief groot en frequent door wolken bedekt meer zoals het Poyang meer.

(2) De prestatie van Landsat TM banden voor het detecteren van baggerschepen werd bestudeerd in de troebele wateren van noordelijk Poyang meer. De resultaten toonden aan dat TM band 1 tot 4 beperkingen hebben in troebel water, terwijl band 5 en 7 de schepen veel beter wisten te onderscheiden. Aangeraden wordt de middel infrarode banden te gebruiken voor het operationeel monitoren van schepen in troebel water.

(3) In dit hoofdstuk wordt bestudeerd of het simultaan monitoren van schepen en water troebelheid gevolgtrekkingen ten aanzien van bagger impact meer kracht kan bijzetten. Tijdsseries van MODIS beelden toonden een significante toename in water troebelheid vanaf 2001, terwijl Landsat TM een simultane toename van het aantal schepen aantoonde. Regressie analyse toonde een hoogst significante positieve relatie (R^2 = 0.92) tussen water troebelheid en het aantal schepen. De aannemelijkheid dat baggeren de toename in water troebelheid veroorzaakte werd verder versterkt op basis van argumenten gebaseerd op het ontbreken van resuspensie van sediment door schepen, de uiteindelijke bestemming van de schepen en het samenvallen van clusters van baggerschepen met troebelheids pluimen en onregelmatig getande patronen in het sediment. Er werd daarom geconcludeerd dat het simultaan met behulp van aardobservatie monitoren van water troebelheid en schepen de kracht van bewijsvoering verstrekt in bagger impact studies.

(4) Dit hoofdstuk vergelijkt drie extra- en interpolatie methodes voor het voorspellen van de dagelijkse fotosynthetisch actieve straling die het oppervlak van Poyang meer bereikt. De resultaten tonen aan dat een onregelmatig driehoeks netwerk (TIN) en een inverse afstand gewogen (IDW) interpolatie methode betrouwbaarder resultaten leverden dan de extrapolatie methode.

(5) De fotosynthetisch actieve straling die de top van de bladeren van *V. spiralis* bereikt (PAR_{tc}) werd gemodelleerd voor het Dahuchi meer over de periode van 1998 tot 2006. De resultaten toonden significante verschillen in PAR_{tc} tussen jaren, hetgeen vooral werd veroorzaakt door fluctuerende waterhoogte. Zes jaar Secchi schijf metingen toonden een seizoensgebonden omschakeling van het meer aan van troebel tijdens lage waterstanden in de late herfst, winter en het voorjaar naar transparant onder hogere waterstanden in de zomer. De hoogste PAR_{tc} waardes werden waargenomen bij gemiddelde waterstanden, die bereikt werden op het moment dat de stijging van de Yangtze in het voorjaar het Dahuchi meer uit haar troebele staat drukt. Het beheer van de drie kloven dam dat zal leiden tot verhoging van de waterhoogte op de Yangtze in Mei en Juni zou het Dahuchi meer daarom op een vroeger tijdstip uit haar troebele staat kunnen forceren. Het beheer van de driekloven dam zou dus kunnen leiden tot een toename van de lichtintensiteit en de productiviteit van *V. spiralis* en beïnvloed mogelijk daarmee het voedselhabitat van de Siberische kraanvogels in Poyang meer.

(6) Dit hoofdstuk introduceert een conceptueel raamwerk voor het integreren van een biomassa simulatie model voor *V. spiralis* met aardobservatie en een geografisch informatie systeem. Het geïmplementeerde systeem zou het bij kunnen dragen aan het evalueren van de invloed van hydrologische veranderingen op de groei en productie van *V. spiralis*, en het inschatten of populaties van wortelknolletjes etende vogels beperkt worden door het regionale voedselaanbod in het Poyang meer.

De resultaten van deze thesis vormen een basis voor verder onderzoek en levert noodzakelijke informatie voor besluitvorming door verantwoordelijke autoriteiten hoe dit unieke meer ecosysteem op rationele wijze te beheren.

ACKNOWLEDGEMENTS

With starting the acknowledgements, I know my PhD research at ITC (International Institute for Geo-information Science and Earth Observation) really comes to the end. It is difficult to find words to express my appreciations to the organizations and people who have helped me in some ways or the other to complete this work, but I want to take this opportunity to use simple words to describe my deepest gratitude.

First of all I am grateful to the excellent supervising team behind me: Prof. Andrew K. Skidmore of ITC, Prof. Herbert T. Prins of Wageningen University and Dr. Jan de Leeuw of ITC for their innovative ideas, contributions, invaluable guidance and encouragements throughout my research period. Without your supports none of this was possible.

Especial gratitude goes to Prof. Liu Yaolin of Wuhan University for his invaluable suggestion to my research and what he has done during my absence from my position.

I thank WOTRO (the Netherlands Foundation for the Advancement of Tropical Research) and ITC for their financial support, which allowed me to peruse this research in the Netherlands.

I also thank my organization: School of Resource of Environmental Sources of Wuhan University for the supporting during my absence and fieldworks. Thanks also go to the Bureau of Jiangxi Poyang Lake National Nature Reserve (PLNNR), China and the International Crane Foundation (ICF) for their helps in data sharing and fieldwork.

During this period, I also had discussions with many faculty members of ITC, and they gave me lots of invaluable suggestion and helps. Prof. Zongbo Su, Prof. Alfred Stein, Dr. Chris Mannaerts, Dr. Tom Rientjes, Dr. Zoltan Vekerdy, Dr. Henk Kloosterman, Dr. Patrick van Laake, Dr. Martin Schlerf, M.Sc. Valentijn Venus, Dr. David Rossiter and others, thank all of you.

I thank Prof. Martin Hale and Ms. Loes Colenbrander, who ensured that I had excellent research administration. I also express my gratitude to the education affairs department, financial department, library, information technology department and international hotel of ITC for their dynamic support. I also owe a great deal to Esther Hondebrink for her supports.

I express my gratitude to Jeb Barzen, James Burnham of ICF and Ji Weitao, Zeng Nanjing, Zhou Feilong and Yi Wusheng of PLNNR, who have been engaged on the research of Poyang Lake for long time, for sharing their rich knowledge on Poyang Lake. Also I thank Dr. Elly P. H. Best for her suggestion and helps.

My sincerest thanks go to my generation of PhD candidates, especially to Dr. Jella Ferwerda, Dr. Peter Minang, Dr. Moses Cho, Dr. Chudamani Joshi, Dr. Ulanbek Turdukulov, Dr. Peter Beck, Nicky Knox, Jane Bemigisha, Roshanak Darvishzadeh, Mhosisi Masocha, Filiz Bektas, Tyas Mutiara Basuki and Ajay Bhakta Mathema etc.

Big Chinese group at ITC, I got so much happiness and encourages from you. Thank all of you, especially to Tiejun, Pu Shi, Ningrui, Yanqiu, Zhenshan, Langyue, Zhigao, Li Xia, Wenjing Wenbo, Zeng Yu, Huang Fang, Yijian, Zhong Lei, Yali, Bian Meng, Fei Teng, Ouyang Wei, Guangyi, Qiuju, Yixiang, Tian Xin, Longhui, Changbo, Tangtang, Liu Gang, Zongbin, Shen Xin, Weihua, Ruoxiao, Xiankun, Zhengquan and Ai Ping. I also thank my Chinese friends in the Netherlands, Mr. Zheng Ding, Ms. Wang Lichun, Ms. Sun Yuxian

and Mr. Sun Zhongwei for their helps.

Many thanks go to my Chinese colleagues and friends for their suggestion and helps in various ways: Song Aihong, Liu Yanfang, Du Qingyun, Liu Xiao, Li Lin, Guo Qingsheng, Cai Zhongliang, Wang Mingjun, Weng Min, Jiang Wenping, Yang Yuli, Hong Jiewen, Zhan Qingming, Xiao Yinghui, Huang Zhengdong, Chen Jianquan, Tang Xinmin, Chen Xiaoling, Liao Mingsheng, Song Yanling, Cui Lijuan, Zhang Huaiqing, Bao Shuming, Ji Wei, Fan Zhewen, Fang Yu, Liu Xuehua, Jia Haifeng, Wang Xuelei, Li Wei, Chang Zheng, Wang Wei, Liu Ying and Lai Geying.

I thank my family as they always kept sending me good wishes and encouragement. The last but not the least my deepest gratitude goes to my wife, Ms. Gao Wenxiu, for her support and love.

Wu, Guofeng

at ITC, the Netherlands

January 2008

CHAPTER 1

INTRODUCTION

1.1 Problem statement

Lakes are important for human development and preservation of ecosystems and biodiversity (ILEC 2005), for they provide multiple goods and services in commerce, aesthetics, tourism, recreation and biodiversity conservation (Jorgensen et al. 2005, O'Sullivan and Reynolds 2005). Currently, however, many lakes are facing a number of problems such as eutrophication, water-level change, increased erosion and sediment, loss of biodiversity and habitat, human health risks, accumulation of litter and garbage, and invasive species (ILEC&UNEP 2003). These problems may hamper the sustainable developments of multiple lake functions.

Poyang Lake is the largest freshwater lake in China, and now it is suffering from a series of problems, e.g., water and soil erosion, land desertification, land degradation and environmental pollution (Huang 2006), which could influence the hydrological conditions of Poyang Lake. Especially, recent reports (e.g. Zhong and Chen 2005, Fok and Pang 2006) suggest that the sand dredging in the northern Poyang Lake, which started around 2001 for construction purpose, reduces the water clarity and has a negative impact on this ecosystem.

The hydrological conditions in Poyang Lake are not only influenced by the local factors. They also could be modified by the changed hydrology of the Yangtze River induced by ongoing and proposed engineering projects. For example, the Three Gorges Dam in the Yangtze River, which is scheduled for completion by 2009 (Wang 2002), will change the discharge and water level of the Yangtze River (Liu and Xu 1994, Jiang and Huang 1997, Kanai et al. 2002). Similarly, the South-to-North Water Transfer Project will reduce the water level of the middle and lower Yangtze (Cai et al. 2002). All these changes in water level in the Yangtze River will influence the water level of Poyang Lake.

Poyang Lake is one of the biggest bird conservation areas in the world (Wu and Ji 2002). The lake is particularly important for the conservation of the endangered Siberian crane (Li et al. 2005), as more than 95% of its world population winter here (Wu and Ji 2002). During the wintering period, together with swans and the endangered swan goose, Siberian crane forage on the tubers of *Vallisneria spiralis L.* (Meine and Archibald 1996).

V. spiralis is a submerged aquatic macrophyte species widely distributed in Poyang Lake (Wu and Ji 2002). It sprouts in April, flowers in June, reaches its maximum aboveground biomass in mid-September and fills its tubers from mid-July until shoots senesce in late October (Wu and Ji 2002). The production and biomass of the *V. spiralis* mostly depend on the local hydrological conditions such as light intensity, water level, water clarity, chemical properties and water temperature (Wu and Ji 2002). Among these, light availability is likely of primary importance due to the highly fluctuating water depth and turbidity in Poyang Lake.

The changes of hydrological conditions induced by human activities in Poyang Lake or the Yangtze River thus could influence the light intensity reaching the vegetation canopy, and thus have impact on the growth and production of *V. spiralis* and further on the food habitats of tuber-feeding bird species, including Siberian crane. The relevant research was, however, rarely carried out. It thus remains interesting to explore the potential impact of these human activities on the hydrological conditions, the growth and productivity of *V. spiralis* and the Siberian crane in Poyang Lake.

1.2 Study objective and questions

This study aimed to explore how the dredging activities and the Three Gorges Dam change the water turbidity and water level, to analyze how these hydrological changes influence the underwater light climate, and to discuss its potential impacts on the growth and productivity of *V. spiralis* and further on the Siberian crane in Poyang Lake. The study questions are as follows:

(1) To compare moderate resolution imaging spectroradiometer (MODIS) and Landsat thematic mapper (TM) images for mapping tempo-spatial dynamics of water clarity;

(2) To analyze the performance of Landsat TM bands for dredging ship detection in turbid water;

(3) To investigate the possibility of corroborating the impact of dredging on water turbidity, while simultaneously monitoring the number and distribution of vessels and water turbidity using time-series Landsat TM and MODIS images;

(4) To compare extrapolation and interpolation methods for estimating daily photosynthetically active radiation (PAR);

(5) To explore if the Three Gorges Dam positively affect the underwater light climate of *V. spiralis* and the food habitat of Siberian crane;

(6) To propose a conceptual framework for integrating a biomass simulation model for *V. spiralis* with remote sensing techniques and a geographical information system.

1.3 Study area

Considering the characteristic of individual research and the availability of material, the study was implemented at various spatial scales, from whole Poyang Lake, to the northern Poyang Lake, the Poyang Lake national nature reserve and Lake Dahuchi within the nature reserve.

Poyang Lake (**Figure 1.1**) is located between 115°47′-116°45′E, 28°22′-29°45′N at the southern bank of the Yangtze River. Its size fluctuates from less than 1000 km^2 in the dry season to approximately 4000 km^2 in the flood season. Its water level is determined by five confluent rivers (Raohe, Xinjiang, Fuhe, Ganjiang and Xiushui) and the Yangtze River together, with high water levels in summer and low in winter (Min 1995, Xu et al. 2001, Shankman et al. 2006). Poyang Lake plays significant roles in ecological conservation, and economic and social development (Huang 2006). Poyang Lake is an important international wetland, and has a rich biodiversity, with 102 species of aquatic plants and 122 species of fish (Chen et al. 2006b). It is one of the biggest bird conservation areas in the world, hosting millions of birds from over 300 species (Wu and Ji 2002).

Poyang Lake national nature reserve (**Figure 1.2**) is located between 115°55′ - 116°03′E, 29°05′ - 29° 15′N in the northwest of Poyang Lake (Wu and Ji 2002), and it was established in 1988 to conserve the endangered Siberian crane. The nature reserve includes nine lakes which are connected to the Poyang Lake during high water levels in summer but disconnect when water levels are low in spring, autumn and winter. Lake Dahuchi with area of about 30 km^2 plays crucial role for providing habitat for wintering Siberian crane.

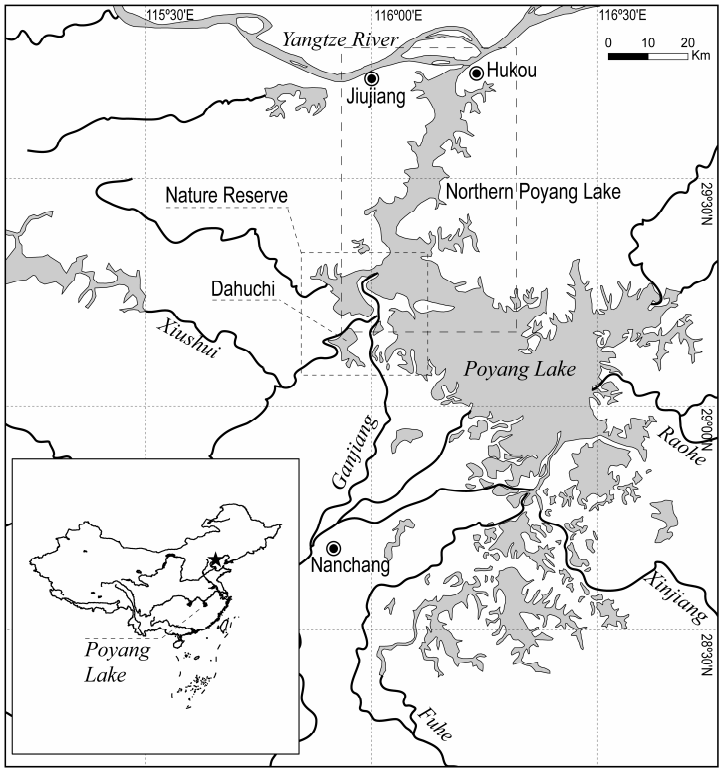

Figure 1.1. Location of Poyang Lake, northern Poyang Lake, Poyang Lake national nature reserve (Nature Reserve) and Lake Dahuchi.

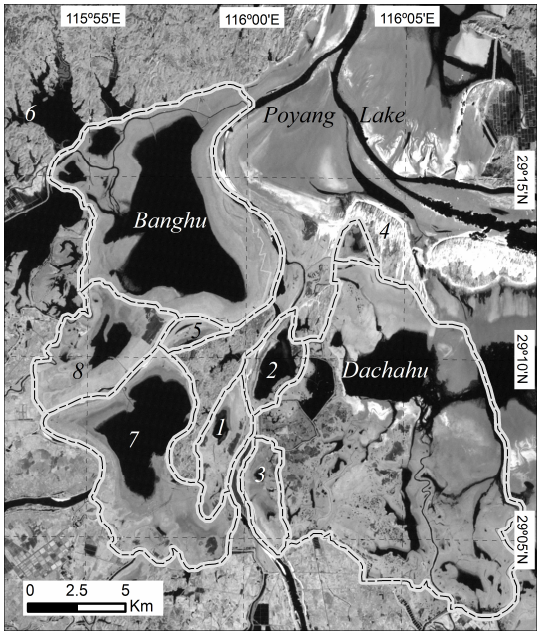

Figure 1.2. Landsat thematic mapper (TM) image (15 December 2004 when water level is low) of the nature reserve showing the lakes: 1, Changhuchi; 2, Zhonghuchi; 3, Xianghu; 4, Meixihu; 5, Zhushihu; 6, Sixiahu; 7, Dahuchi and 8, Shahu.

1.4 Thesis outline

Each chapter of this thesis, except for the introduction and the synthesis, has been prepared as an individual paper. These papers have been published or submitted to peer-reviewed journals or edited book. To maintain a consistent style through the thesis, the used abbreviations, units, graphs, tables, citations and referencing styles were unified, and they may be different from those of the original papers or book chapter. The structure of this thesis is as follows:

Chapter 1 states the research background, defines the study objectives, describes the study area and outlines the structure of the thesis.

In Chapter 2, two remote sensing data sources, MODIS and Landsat TM, are compared for estimating water clarity in the nature reserve.

Chapter 3 analyzes the performance of Landsat TM bands for ship detection in turbid water in northern Poyang Lake.

Chapter 4 explores the possibility to corroborate the strength of inferring dredging impact on water turbidity through simultaneously monitoring the number and distribution of vessels and water turbidity using time-series Landsat TM and MODIS images in the northern Poyang Lake.

Chapter 5 compares three extrapolation and interpolation methods for predicting daily photosynthetically active radiation within the nature reserve.

Chapter 6 presents a model simulating the photosynthetically active radiation reaching the top of canopy of *V. spiralis* and discusses how this could be affected by the change of water level in the Yangtze River induced by the Three Gorges Dam.

In Chapter 7, a conceptual framework for the integration of a simulation model of plant biomass of *V. spiralis* with remote sensing and a geographical information system is introduced.

Chapter 8 summarizes the results of Chapter 2 to 7, and discusses the interrelations of these chapters and the works in the future.

The literature used in each chapter shows some overlap, and is therefore combined in common literature list, which is placed after the last chapter.

CHAPTER 2

COMPARISON OF MODIS AND LANDSAT TM5 IMAGES FOR MAPPING TEMPO-SPATIAL DYNAMICS OF SECCHI DISK DEPTHS

Abstract

Landsat has successfully been applied to map Secchi disk depth of inland water bodies. Operational use for monitoring a dynamic variable like Secchi disk depth is however limited by the 16-day overpass cycle of the Landsat system and cloud cover. Low spatial resolution moderate resolution imaging spectroradiometer (MODIS) image captured twice a day could potentially overcome these problems. However, its potential for mapping Secchi disk depth of inland water bodies has so far rarely been explored. This study compared two image sources, MODIS and Landsat thematic mapper (TM), for mapping the tempo-spatial dynamics of Secchi disk depth in Poyang Lake national nature reserve, China. Secchi disk depths recorded at weekly intervals from April till October in 2004 and 2005 were related to 5 Landsat TM and 22 MODIS images respectively. Two multiple regression models including the blue and red bands of Landsat TM and MODIS respectively explained 83% and 88% of the variance of the natural logarithm of Secchi disk depth. The standard errors of the predictions were 0.20 and 0.37 m for Landsat TM and MODIS-based models. A high correlation (r = 0.94) between the predicted Secchi disk depth derived from the two models was observed. A discussion of advantages and contras of both sensors leads to the conclusion that MODIS offers the possibility to monitor water transparency more regularly and cheaply in relatively big and frequently cloud covered lakes as is with Poyang Lake.

Published as:

Guofeng Wu, Jan de Leeuw, Andrew K. Skidmore, Herbert H. T. Prins, and Yaolin Liu. *Comparison of MODIS and Landsat TM5 images for mapping tempo-spatial dynamics of Secchi disk depths in Poyang Lake national nature reserve, China*. International Journal of Remote Sensing, 2008, in press.

2.1 Introduction

Lake ecosystems provide multiple goods and services to society in commerce, aesthetics, tourism, recreation and biodiversity conservation (Jorgensen et al. 2005). The provisions of these benefits are to a great extent influenced by water quality, which is commonly monitored to assess the health of lake ecosystems.

Water clarity has often been used as an indicator of a lake's overall water quality for it correlates well with water quality (Li and Li 2004, Shaw et al. 2004). The Secchi disk is one of the most commonly used tools to measure water clarity (Duane Nellis et al. 1998, Kloiber et al. 2002a, Gan et al. 2004). However, this method may be costly for intensive sampling within water bodies in which water clarity fluctuates highly in time and space scale (Brezonik et al. 2002, Kloiber et al. 2002b, Hakanson and Boulion 2003).

Remote sensing offers possibility to infer water clarity from captured reflectance (Harma et al. 2001, Liu et al. 2003b, Li and Li 2004). This is because lake clarity is affected by algae, suspended sediment and dissolved organic matter within water column (Liu et al. 2003b, Swift et al. 2006). These components interact with photons of light and alter the spectral composition of down- and upwelling light which results in a flux emerging from the water surface that contains information on the composition of the water column (Li and Li 2004, Ma and Dai 2005, Pozdnyakov et al. 2005).

This potential of remote sensing was explored following the launch of the Landsat satellites in the 1970s, and Landsat images have frequently been used to assess water clarity, including Secchi disk depth. Lathrop and Lillesand (1986), for example, used the Landsat thematic mapper (TM) green band to estimate Secchi disk depth in southern Green Bay, WI, and central Lake Michigan, USA. Lathrop (1992) compared Secchi disk depth derived from Landsat TM images in Green Bay, Lake Michigan, Yellowstone Lake and Jackson Lake, WY. Giardino et al. (2001) used blue/green ratio of Landsat TM image to estimate Secchi disk depth in Lake Iseo, Italy. Kloiber et al. (2002a, 2002b) employed 13 Landsat Multispectral Scanner (MSS) and TM images over the period 1973–1998 to assess spatial patterns and temporal trends of Secchi disk depth in more than 500 lakes with surface areas >10 ha in Minneapolis and St. Paul, MN, USA. Nelson et al. (2003) developed a regression model between Secchi disk depth and Landsat TM blue/red ratio to estimate Secchi disk depth in 93 lakes in Michigan, U.S.A. Hellweger et al. (2004) applied Landsat TM red band to predict Secchi disk depth in New York Harbour. Zhang (2005) utilized a linear regression model and neural network respectively to predict Secchi disk depth from Landsat TM image in the Gulf and archipelago sea of Finland.

Landsat has thus successfully been applied to the mapping of Secchi disk depth, but has its limitations in operational use for regular monitoring. This is because water clarity is a highly dynamic variable, and its variability may not effectively be captured by a satellite with an about biweekly overpass. In many parts of the world frequent cloud cover further reduces the actual availability of cloud-free images to a level which makes Landsat unsuitable for monitoring purposes of a highly dynamic variable, like Secchi disk depth.

Moderate resolution imaging spectroradiometer (MODIS), with its medium spatial resolution, daily coverage, high sensitivity and cost-free distribution (Li and Li 2004, Miller and McKee 2004), would be more suitable to monitor such dynamics. However, this potential has rarely been explored in inland water bodies. For example, Lillesand

and Chipman (2001) mentioned using MODIS data to estimate Secchi disk depth of large lakes on a regional basis. The Secchi disk depths of Green Bay, Lake Michigan and eleven other lakes were estimated weekly to biweekly using MODIS blue/red spectral radiance ratio from July of 2001 (Lillesand 2004).

Although Landsat TM data has limitation of low temporal resolution and MODIS images hold potential in assessing water clarity, so far no reference was found comparing these two different data sources in detail. This study aims to develop models regressing the Secchi disk depths measured in the field with MODIS and Landsat TM5 images respectively, to compare the results from these two different image sources and to explore the possibility of MODIS for mapping tempo-spatial dynamics of Secchi disk depth as a substitute of Landsat TM in the Poyang Lake national nature reserve, China.

2.2 Materials and methods

2.2.1 Study area

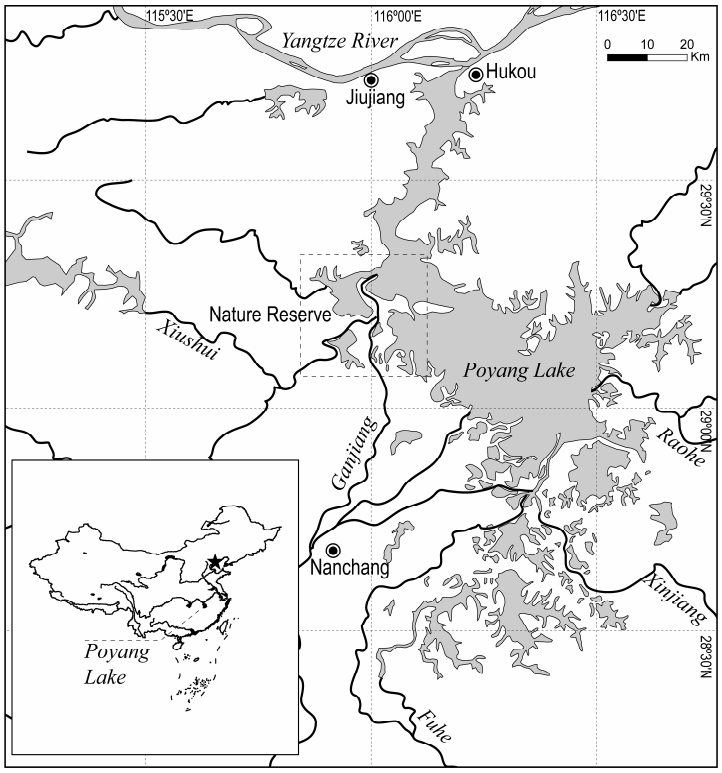

Figure 2.1. Map showing the locations of Poyang Lake and Poyang Lake national nature reserve (Nature Reserve).

Poyang Lake national nature reserve (**Figure 2.1**) is located between 115°55′-116°03′E, 29°05′-29°15′N in the northwest of Poyang Lake (Wu and Ji 2002). The reserve was established in 1988 to conserve the endangered Siberian crane which winters almost uniquely in this area. The water level fluctuates seasonally from low in winter to high in July and August. The extent of Poyang Lake varies accordingly from

about 4000 km^2 in summer to less than 1000 km^2 in winter. The nature reserve includes nine lakes which are connected to the Poyang Lake during high water levels in summer but disconnect when water levels are low in spring, autumn and winter (see **Figure 2.2**).

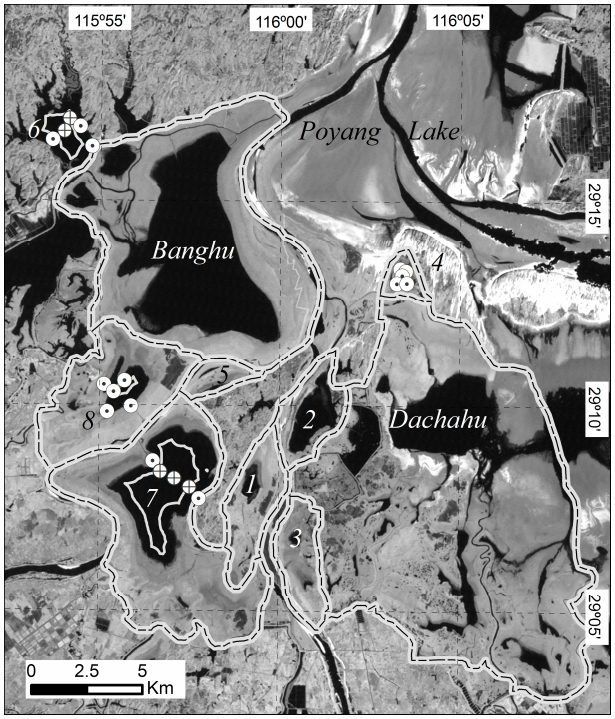

Figure 2.2. Landsat thematic mapper (TM) image (15 December 2004 when water level is low) of the nature reserve showing the lakes and locations of Secchi disk depth recording. Lakes: 1: Changhuchi; 2: Zhonghuchi; 3: Xianghu; 4: Meixihu; 5: Zhushihu; 6: Sixiahu; 7: Dahuchi; 8: Shahu. : Boundary of the nature reserve; : Buffer of 500 meters from lake shore. Secchi disk recording location located >500 ( ) and < 500 m ( ) from the lakeshore.

2.2.2 Secchi disk depth

In 2004 and 2005, Secchi disk depth was recorded by the Bureau of Jiangxi Poyang Lake National Nature Reserve and the International Crane Foundation in three lakes (Dahuchi, Shahu and Meixihu) within and one (Sixiahu) adjacent to the nature reserve. Sampling date, global positioning system (GPS) position and Secchi disk depth measured using a standard 20 cm Secchi disk were recorded at five locations (**Figure 2.2**) in each lake with about weekly intervals from April till October.

2.2.3 MODIS data

At present, two MODIS instruments onboard the US National Aeronautics and Space Administration (NASA) Terra and Aqua spacecraft platforms are operational for global remote sensing of the land, ocean, and atmosphere. MOD09/MYD09 is a seven-band surface reflectance product computed from MODIS-Terra/MODIS-Aqua level 1B

bands 1 to 7, centred at 645, 858, 470, 555, 1240, 1640 and 2130 nm respectively. The data have been corrected for the effect of atmospheric gases, aerosols and thin cirrus clouds and thus provide an estimate of the spectral reflectance as it would be measured at ground level in the absence of atmospheric scattering or absorption. MOD09GQK/MYD09GQK contains MODIS bands 1 and 2 at 250 m spatial resolution, while MOD09GHK/MYD09GHK stores MODIS bands 1 to 7 at 500 m spatial resolution (http://modis-land.gsfc.nasa.gov/surfrad.htm, accessed 20 September 2006).

Each of the spectroradiometers on the Terra and Aqua spacecrafts captures the whole earth twice a day. The potential number of daytime images between 1 April to 31 October (214 days) in 2004 and 2005 was 856. Most images were, however, of poor quality due to cloud cover or atmospheric conditions. We adopted the following procedure to select good quality images. First, we downloaded all the MOD09A1/MYD09A1, an eight-day composite of the 250 m surface reflectance data, of April till October during 2004-2005 from NASA's Earth Observing System (EOS) data gateway (http://edcimswww.cr.usgs.gov/pub/imswelcome, accessed 16th February 2006) and visually inspected their quality. Next, the MOD09A1/MYD09A1s represented by poor quality were discarded, assuming no better images were available for that period, and 44 MOD09A1 or MYD09A1s having moderate to good quality were retained. Then, for each MOD09A1 or MYD09A1, we consulted the online MODIS L1B 250 m quick looks to check the qualities of daytime images over our study area and selected the images with good quality. Finally, the corresponding MOD09GQK or MYD09GQK and MOD09GHK or MYD09GHK for the selected 22 images with good quality were downloaded from NASA's EOS data gateway.

The following pre-processing was implemented successively to each image. First, every image was projected into WGS 84/UTM zone 50N using nearest-neighbour resampling to preserve the original reflectance values. Then, a sub-image of the study area was clipped from the larger original image. Next, bands 3 and 4 were re-sampled from 500 to 250 m using nearest-neighbour interpolation and bands 1 to 4 were stacked into one image. Finally, land areas and small water bodies were removed using a binary mask derived from the Normalized Difference Water Index (NDWI), which effectively discriminates soil and vegetation from open water (McFeeters 1996).

2.2.4 Landsat TM images

From 1 April to 31 October in 2004 and 2005, in total 28 Landsat TM5 images covering the study area were captured, 19 of which were of moderate and good quality. Five good quality Landsat TM images of 5 May, 22 June, 24 July, 9 August and 28 October 2004 were obtained from the Chinese Remote Sensing Satellite Ground Station. Each image was pre-processed as follows: Atmospheric correction was carried out according to the cosine approximation model (COST) described by Chavez (1988, 1996), Chen et al. (2004), Chander and Markham (2003) and Chander et al. (2004). Topographic maps at scale 1:50,000 were used to register the atmospherically corrected image to the Beijing 54/Gauss-Kruger projection using a first-order polynomial and nearest-neighbour resampling. The root mean square error (RMSE) for positional accuracy was within half a pixel. The projected image was re-projected to WGS 84/UTM zone 50N also applied to the MODIS data. Land areas and small water bodies were removed using a binary mask created through visual interpretation of an unsupervised classification of the TM image.

2.2.5 Selection of sampling points

These sampling and selection procedures resulted in a dataset of MODIS, Landsat TM data and Secchi disk depth recordings schematically shown in **Figure 2.3**. Above it was explained that Secchi disk depth was recorded at 20 locations. **Figure 2.2** shows that, during low water level, the four lakes were disconnected and several Secchi disk depth locations came within a few hundred meters from the shore. Investigating the relation between MODIS data and Secchi disk depth assumes that MODIS pixels consist of open water only. Inclusion of upshore lands in a MODIS pixel would contaminate the spectral signature. This is a realistic risk given that the spatial resolutions of blue and green bands are 500 m. To reduce the risk of contamination, we used the boundaries of lakes at low water level derived from the TM image of 15 December 2004 and removed all Secchi disk sampling locations within 500 m offshore from further analysis. This reduced the number of sampling locations used in the analysis of the MODIS data from 20 to five, two in Sixiahu and three in Dahuchi. For the analysis of the relation between Secchi disk depth and Landsat TM we selected all ten sampling locations in the same lakes.

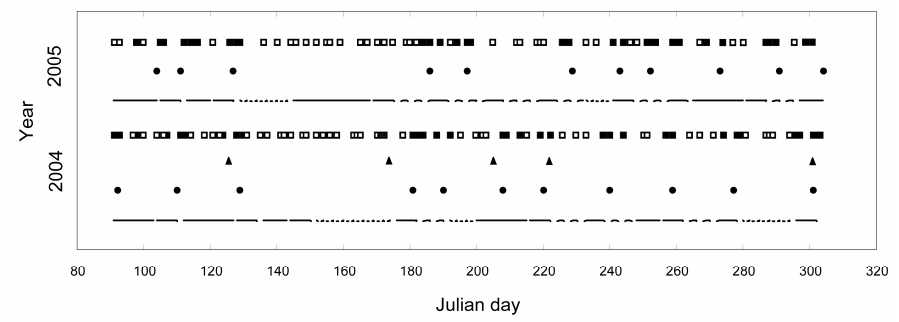

Figure 2.3. Summary of the quality of the available moderate resolution imaging spectroradiometer (MODIS) data (poor:⋯⋯; moderate:- - -; good:——), and the dates of the selected MODIS (●) and Landsat thematic mapper (TM) (▲) data, as well as the dates of Secchi disk depth records used (■) and not used (□) in this analysis.

Table 2.1. Statistics describing variability in Secchi disk depth (SDD, m) measurements and reflectance values (%) of the blue, green and red bands of 22 moderate resolution imaging spectroradiometer (MODIS) and 5 Landsat thematic mapper (TM) images.

	MODIS (n = 71)				*Landsat TM (n = 25)*			
	SDD	*Blue*	*Green*	*Red*	*SDD*	*Blue*	*Green*	*Red*
Maximum	2.84	0.1229	0.2091	0.2341	2.16	0.0598	0.0957	0.1525
Minimum	0.06	0.0074	0.0311	0.0090	0.32	0.0195	0.0292	0.0228
Average	0.97	0.0525	0.0964	0.0800	1.17	0.0362	0.0470	0.0547

We next related the Secchi disk depth records to the spectral information of MODIS and Landsat TM images respectively. The measurements of Secchi disk depths did not always concur with the overpasses of the available images and a difference of up to six days was accepted. The MODIS and Landsat TM pixel values of these locations could still be affected by floating aquatic vegetation. We used NDWI to identify suspect pixels and retained only the data with NDWI values > 0, corresponding to open water (Fraser 1998b). **Table 2.1** shows the statistics of Secchi disk depth and

visible bands of MODIS and Landsat TM images.

2.2.6 Statistical analysis

Graphical display of the relation between Secchi disk depth and the individual MODIS and Landsat TM bands revealed non-linear relationships which could be overcome through logarithmically transforming Secchi disk depth. We next searched simple and multiple regression models best fitting the relation between the natural logarithm of Secchi disk depth and the individual bands or band ratios while exploring linear, logarithmic, inverse, quadratic, cubic, power, compound, S-curve, growth and exponential regression models.

The selected best fitting regression models were inverted and applied to four pairs of MODIS and Landsat TM images with concurrent or close to concurrent overpass dates to create distribution maps of Secchi disk depth. We used the following process to investigate as to how well the predictions from two satellite systems agreed for each pair of images: First, we obtained Secchi disk depths and green and infrared (IR) band values of 59 randomly selected sampling points from maps derived from MODIS and Landsat TM images respectively. Then, we removed the sampling points with NDWI ≤ 0 from the following analysis. Finally, the correlation between Secchi disk depths of the two maps for the remaining sampling points was calculated.

2.3 Results

Figure 2.4 depicts the fluctuations of field-measured Secchi disk depths at central positions of Dahuchi and Sixiahu from 1 April (Julian day 92 respectively 91) to 31 October (Julian day 305 respectively 304) in 2004 and 2005. Generally, Secchi disk depth was low (several centimetres) in winter and early spring, increased in late spring, maintained higher values (up to 3 metres) in summer, and declined in autumn. These seasonal trends appear to be regular, turbid water between October and May of next year, and transparent water from June till September.

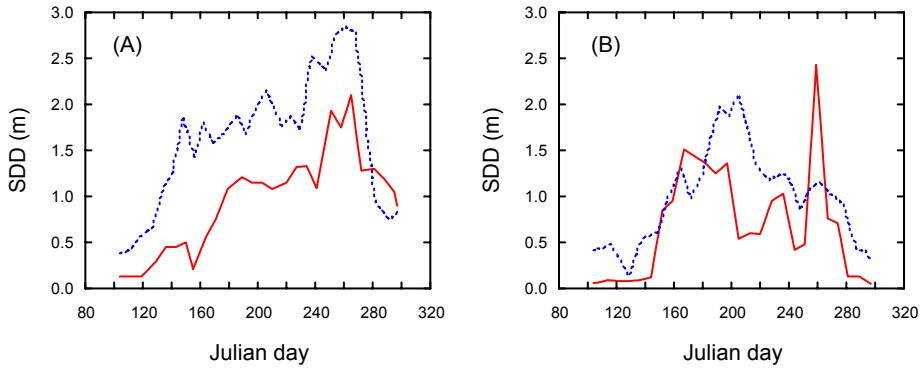

Figure 2.4. Secchi disk depth (SDD) recorded in Dahuchi (——) and Sixiahu (- - - -) in 2004 (A) and 2005 (B).

Figure 2.5 shows the relation between individual visible bands of MODIS and Landsat TM and the natural logarithm of Secchi disk depth (ln(SDD)). All bands correlate negatively with ln(SDD). The red and green bands had better correlations with ln(SDD) than the blue band. The variance of ln(SDD) was best explained by the red band for

MODIS images and the green band in case of the Landsat TM images.

Table 2.2 lists the best fitting multiple regression models describing the relation between the natural logarithm of Secchi disk depth and MODIS and Landsat TM bands. The forward selection procedure included in both cases the red and blue bands in the model. The red band had a negative sign for both MODIS and Landsat TM. The blue band had a negative sign in case of Landsat TM but was positively related in case of MODIS. The two models explained 88% and 83% of the variation of the natural logarithm of Secchi disk depth with estimated standard error (*s.e.*) of 0.37 and 0.20 m respectively. *F*-tests showed that the two regression models both were statistically significant at $P = 0.001$. The multiple correlation coefficients derived from the two models, $R_{MODIS} = 0.94$ and $R_{TM} = 0.91$, were not significantly different (*z*-test for two correlation coefficients, $z = 0.11$, $P = 0.91$). A variance ratio test revealed that the MODIS-based model had a significantly higher variance than the Landsat TM-based model ($F = 3.42$; *d.f.* = 70, 24; $P < 0.002$). **Figure 2.6** describes the relation of the natural logarithm of measured Secchi disk depth against the predicted one from the best fitting models.

Table 2.2. Selected best fitting regression models between the natural logarithm of Secchi disk depth (ln(SDD)) and the blue and red bands of moderate resolution imaging spectroradiometer (MODIS) and Landsat thematic mapper (TM) images (*s.e.*: standard error).

Image	*Regression model*	R^2	*s.e.*	*F*	*P*	*n*
MODIS	ln(SDD) = 0.474 + 15.240 * blue – 21.130 * red	0.88	0.37	249.0	<0.001	71
Landsat TM	ln(SDD) = 1.133 – 10.533 * blue – 13.805 * red	0.83	0.20	60.51	<0.001	25

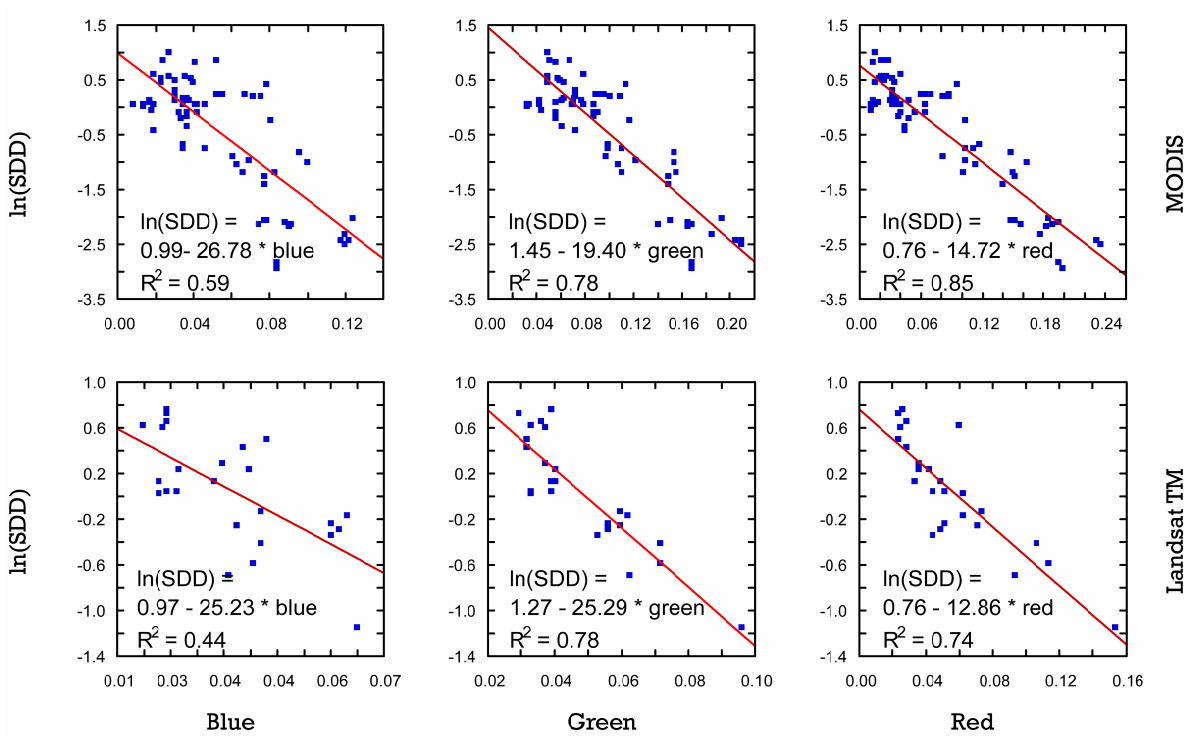

Figure 2.5. Scatter plots and regressions describing the relation between the natural logarithm of Secchi disk depth (ln(SDD)) and the reflectance of three visible bands of moderate resolution imaging spectroradiometer (MODIS) and Landsat thematic mapper (TM).

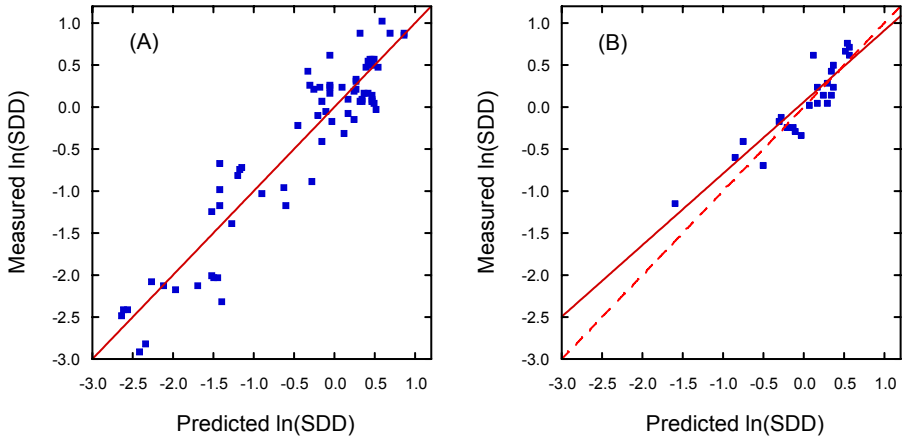

Figure 2.6. Scatter plots describing the natural logarithm of measured and predicted Secchi disk depth for moderate resolution imaging spectroradiometer (MODIS) (A) and Landsat thematic mapper (TM) (B).

We inverted the two selected best fitting regression models and applied them to four pairs of MODIS and Landsat TM images with concurrent or close to concurrent overpass dates. The resulting distribution maps of Secchi disk depth were shown in **Figure 2.7**.

Figure 2.8 compares the Secchi disk depth of sampling points from both maps to investigate how well the predictions by two satellite systems agreed. The selection procedure of sampling points from original 59 ones using NDWI method resulted in different sample sizes for the four pairs of MODIS and Landsat TM images. The agreement of the predictions made by the MODIS and Landsat TM data differed considerably between the four periods. The correlation (**Figure 2.8**), which was high when both satellites overpassed on the same day (r = 0.94), declined significantly (regression: F= 52.82; *d.f.* = 1, 2; P = 0.018) with increased time difference between overpasses of the satellites (**Figure 2.9**).

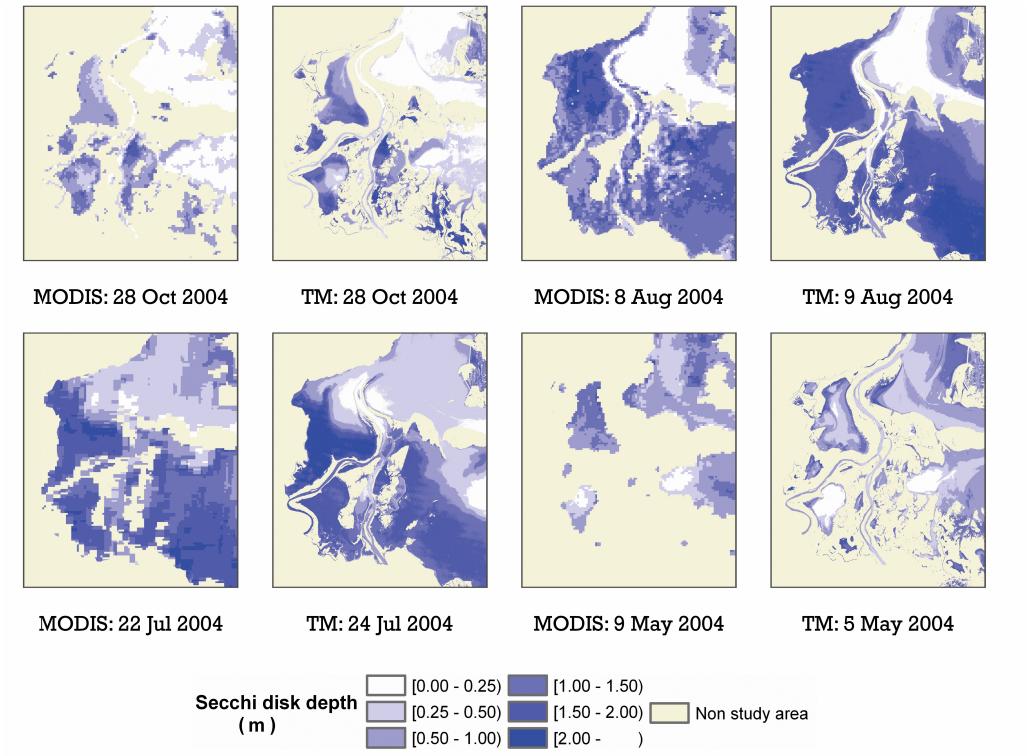

Figure 2.7. Comparisons of predicted Secchi disk depths from four pairs of moderate resolution imaging spectroradiometer (MODIS) and Landsat thematic mapper (TM) images with concurrent or close to concurrent overpass dates.

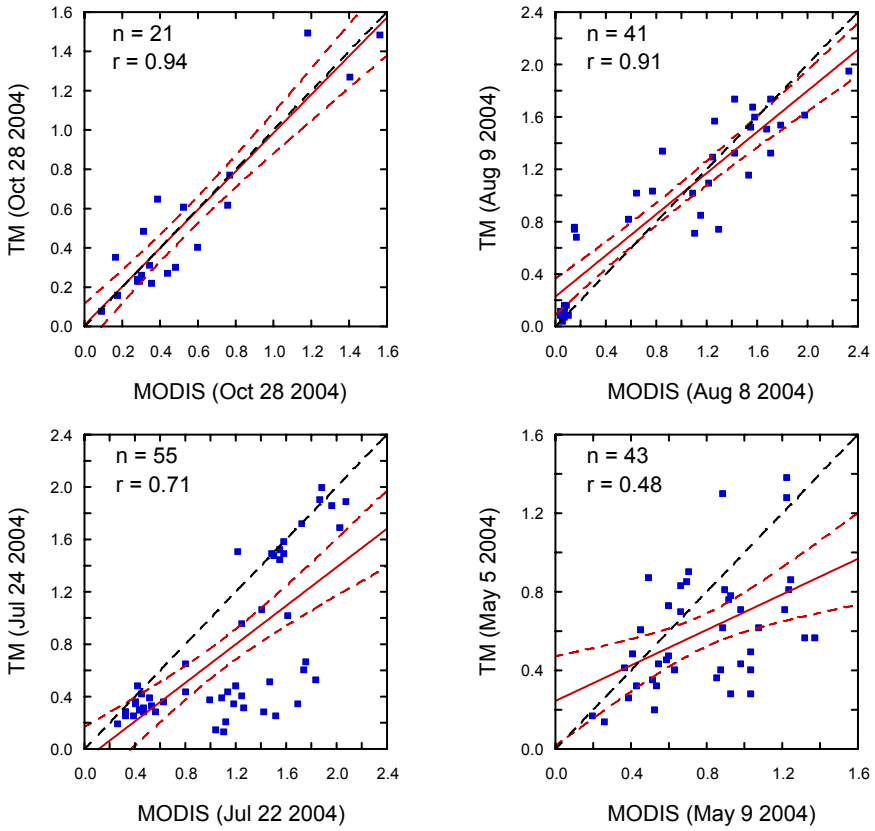

Figure 2.8. Scatter plots revealing the agreement of Secchi disk depths (m) predicted from Landsat thematic mapper (TM) and moderate resolution imaging spectroradiometer (MODIS) images with concurrent or close to concurrent overpass dates. Interrupted lines indicate 95% confidence intervals.

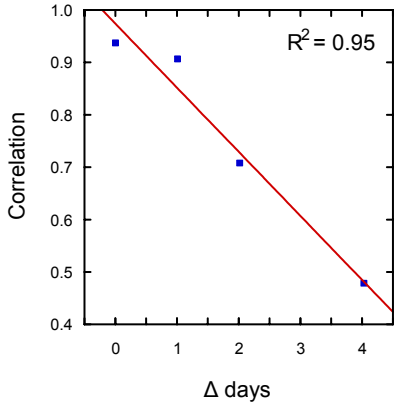

Figure 2.9. Relation between the correlation of the Secchi disk depths predicted from the moderate resolution imaging spectroradiometer (MODIS) and Landsat thematic mapper (TM) image and the time lapse between their overpasses (Δ days).

Poyang Lake is in the humid sub-tropical zone. We summarized the quality of Landsat TM images covering Poyang Lake national nature reserve from 2000 to 2005 (**Figure**

2.10) and found that the quality of 40% (55 scenes) of the total potential images (137 scenes) was good or moderate, 49% (67 scenes) poor and 11% (15 scenes) missing. The yearly average number of images with good or moderate quality was nine.

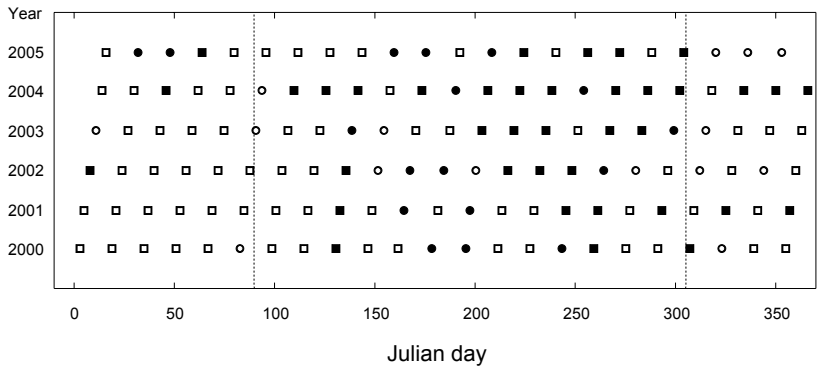

Figure 2.10. Statistics of the quality of Landsat thematic mapper (TM) image over Poyang Lake national nature reserve (good: ■; moderate: ●; poor: □; no data: ○) from 2000 to 2005 (Summarized from http://www.rsgs.ac.cn/english.html). The region between two vertical broken lines indicates the time period from April to October.

2.4 Discussion

This study demonstrated that water clarity could be mapped reliably using time series of Landsat TM and MODIS images. We reported that Landsat TM blue and red bands explained 83% of the variance of the natural logarithm of Secchi disk depth. This level of explained variance fits within the range of R^2 values of 0.72 to 0.98 reported in previous studies on the relation between Landsat TM image and Secchi disk depth or its natural logarithm and the estimated standard error is lower than the reported values (See **Figure 2.3**). However, all of these investigators, except Lillesand (2004), employed a single image, Secchi disk depth from one water body and with maximum two-day time difference between Secchi disk measurement and satellite overpass. Lillesand (2004) obtained an R^2 of 0.85 when using multiple images with concurring satellite overpass and Secchi disk depth recording. The R^2 declined from 0.85 to 0.82 and 0.75 when enlarging the maximum time difference between satellite overpass and Secchi disk depth recording from zero to three and seven days respectively. The result reported in this study thus stands out very well when considering that they were based on multiple (five) Landsat TM scenes which did not concur with the dates of Secchi disk depth recording. Moreover, our results confirm that reliable monitoring of Secchi disk depth is possible, not only for single date images but also for time series of Landsat TM data.

The red band was negatively related to ln(SDD) both for MODIS and Landsat TM data. The blue band was surprisingly related positively in case of MODIS and negatively for the Landsat TM. Others have related ln(SDD) to the green band (Lathrop and Lillesand 1986) or ratio of the blue and red band (Lillesand 2004). The red band was the single best predictor in our case. This could be the result of the fact that light attenuation in our study area appears to be primarily determined by sediment, which is resuspended between October and May at low water level due to wind action.

Table 2.3. Description of our model and some published regression models relating Secchi disk depth (SDD) to satellite image bands: B = blue, G = green, R = red and Δ day means the time lapse between satellite overpass and SDD recording.

Author(s)	*Sensor*	*Model*	R^2	*n*	*s.e.*	*Sampling universe*	*Satellite scenes*	*Δ day*
Wu et al.	TM	ln(SDD) = 1.133 – 10.533 * B – 13.805 * R	0.83	25	0.20	Two lakes	5	Max 3 days
	MODIS	ln(SDD) = 0.474 + 15.240 * B – 21.130 * R	0.88	71	0.37		22	Max 6 days
Kloiber et al. (2002a, 2002b)	TM	ln(SDD) = a* (B/R) + b * B + c	0.72~0.93	20	0.28~0.34	Many lakes	1	Max 1 days
Lillesand (2004)	TM	ln(SDD) = a + b * (B/R)	0.85	-	-	Many lakes	Many	Same day
	plus	ln(SDD) = a + b * (B/R)	0.82	-	-		Many	Max 3 days
	ETM+	ln(SDD) = a + b * (B/R)	0.75	-	-		Many	Max 7 days
	MODIS	B/R	0.79	50	0.33		One	-
Lathrop & Lillesand (1986)	TM	ln(SDD) = – 8.38 – 6.00 * ln(G)	0.98	9	1.05	One lake	1	Same day
		ln(SDD) = – 5.36 – 4.75 * ln(G)	0.91	6	1.12			
Hellweger et al.(2004)	TM	ln(SDD) = – 1.71 – 2.90 * ln(R)	0.85	21	-	-	-	-
Lavery et al. (1993)	TM	SDD = 0.74 – 0.05 * R + 1.80 * (B/R)	0.81	-	0.40	One estuary	1	Same day
Allee & Johnson (1999)	TM	SDD = (1.6 – 0.62) * R + 1.27 * R2 – 0.87 * R^3	0.96	30	-	One reservoir	1	Max 2 days
Giardino et al. (2001)	TM	SDD = 8.01 * (B/G) – 8.27	0.85	4	0.45	One lake	1	Same Day
Lathrop (1992)	TM	G/B = 0.687 * $SDD^{-0.192}$	0.82	-	-	One lake	1	Same day
		R/B = 0.443 * $SDD^{-0.411}$	0.83	-	-			
		G/B = 0.842 * $SDD^{-0.202}$	0.94	-	-			
		R/B = 0.654 * $SDD^{-0.450}$	0.94	-	-			

-: no data; ETM+: Landsat enhanced thematic mapper; MODIS: moderate resolution imaging spectroradiometer; *s.e.*: standard error; and TM: Landsat thematic mapper

We also reported that a combination of the red and blue MODIS bands explained 88% of the variance of the natural logarithm of Secchi disk depth, while the red band alone explained 85% of this variance. So far, few studies explored the relation between MODIS and Secchi disk depth in freshwater lakes, apart from Lillesand (2004) who reported that the blue over red band ratio of MODIS explained 79% of the variance of Secchi disk depth in Green Bay, Lake Michigan and eleven other lakes. The limited application of MODIS so far is probably related to the relatively large pixel size, which makes it suitable only for relatively large lakes. Our best model had a pixel size of 500 m since it also used the blue band. The model using the red band alone could be an alternative to be considered for somewhat smaller lakes, since its performance was almost as good as the model including the red and blue bands.

In this study we also reported that the multiple correlation coefficients derived from the models were not statistically significant different. It is tempting to use this statistic to compare and draw conclusions on the performance of the MODIS- and Landsat TM-based model. We argue, however, that such comparison cannot be used to draw conclusions on the performance of methods or sensors, because the results were obtained from different data sets. In this study, for instance, the results reported for Landsat TM was obtained using a dataset of five images while the MODIS analysis included 22 images. The range of the dependent variable (Secchi disk depth) differed between the two analyses; it was larger in case of MODIS (0.06 – 2.84 m) than Landsat TM (0.32 – 2.16 m).

Using the variance ratio test is an interesting way to compare the standard errors of the developed models based on MODIS and Landsat TM images. Similarly it does not allow, however, inferring that Landsat TM is performing better than MODIS, because the two regression models were obtained from two different data sets. The higher variance of the MODIS-based model could thus be the result of having another dataset, rather than pointing at a weaker performance of the MODIS.

Although the two models predicted Secchi disk depth well from MODIS and Landsat TM images respectively, there is still room for improvement. While we used the COST method, other methods for atmospheric correction of the Landsat TM images might improve modelling. Additionally, only 25 and 71 sampling points were used for developing Landsat TM- and MODIS-based model respectively. Increased sampling size might result in more accurate and robust models.

An advantage of Landsat over MODIS is its 30 m pixel size, which allows detection of water quality parameters over relatively smaller freshwater systems than the 250 m pixel size of MODIS. An important benefit of using Landsat TM and MSS images to assess water clarity is their ability of providing historical information, for Landsat data have been collected regularly since the early 1970s. Although the Landsat TM satellite has been successfully used for water clarity assessment, it also has limitations. First, lakes with higher Secchi disk depth return less signal reflectance from the water column to the Landsat TM sensor, thus, Secchi disk depth could not be well estimated (Li and Li 2004). A second important constraint is its 16-day orbital repeat cycle which limits the frequency of coverage over any given location. This frequency might be too low for a rapidly changeable variable such as water transparency. This limitation becomes even more significant over areas with frequent cloud cover (Lillesand 2004). In our study area, we found that the yearly average number of Landsat TM images with good or moderate quality over 2000 to 2005 was only nine. Landsat TM may thus not be very suitable for monitoring short term trends in water clarity in frequently cloud covered regions (Kloiber et al. 2002a). MODIS onboard the US NASA Terra and Aqua

spacecraft platforms has several advantages over Landsat TM, such as its daily and near-daily coverage (Lillesand 2004), its better spectral sensitivity (Li and Li 2004), and its cost-free distribution. Its relatively low spatial resolution (250 m for red and IR bands, and 500 m for blue and green bands) restricts its application to larger water bodies.

On the basis of the comparison of Secchi disk depth predicted from Landsat TM and MODIS data as well as a discussion of advantages and contras of both sensors, considering the areas of lakes and the frequent cloud cover occurring within the nature reserve, we concluded that MODIS is the better choice and could be considered as a substitute for Landsat TM for mapping the tempo-spatial dynamics of Secchi disk depth within Poyang Lake national nature reserve, China.

CHAPTER 3

PERFORMANCE ANALYSIS OF LANDSAT TM BANDS FOR DREDGING SHIP DETECTION IN TURBID WATER

Abstract

The visible and near infrared bands of Landsat have limitation for detecting ships, especially in turbid water. The potential of TM middle infrared bands for ship detection has so far not been investigated. This study analyzed the performance of the various Landsat TM bands for detecting dredging ships in the turbid water of the northern Poyang Lake, China. A colour composite of principle components 3, 2 and 1 of TM image was used to visually identify 81 dredging ships. The reflectance ratio of each ship and its adjacent water was calculated for every band. A z-score and related p value were used to assess the ship detection performance of the six Landsat TM bands. The reflectance ratio was related to water turbidity to analyze how water turbidity affected the capability of ship identification. The results revealed that the TM bands 1 to 4 showed limitation especially in turbid water, while bands 5 and 7 hold great potential in ship detection. The significant correlations between reflectance ratio and water turbidity in bands 1 to 4 could explain the limitations of bands 1 to 4; while water turbidity has no significant impact on the reflectance of bands 5 and 7, which could explain why the bands 5 and 7 provided stronger capacity compared with bands 1 to 4 in ship detection.

Submitted as:

Guofeng Wu, Jan de Leeuw, Andrew K. Skidmore, Yaolin Liu and Herbert H. T. Prins. *Performance analysis of Landsat TM bands in dredging ship detection in turbid water*. In reviewing.

3.1 Introduction

Dredging is an important economic activity with significant impacts on the environment. The potential of remote sensing for monitoring dredging impact on water turbidity has been long recognized. Dredging impacts are typically inferred from the increased water turbidity patterns revealed by remote sensing images (e.g., Merry et al. 1988, Jorgensen and Edelvang 2000). Wu et al. (2007b), however, argued that it remained difficult to infer dredging impacts from remotely sensed water turbidity patterns alone, because the increased water turbidity could result from natural variation. They suggested that the plausibility of inference of dredging impact would be corroborated when the observed water turbidity patterns could be associated to the presence of ships. Thus, ideally a remotely sensed dredging impact assessment system would combine water turbidity assessment and ship detection.

Basically two remote sensing techniques have been employed for ship detection. Firstly, the potential of optical remote sensing has been explored since the launch of Landsat in the 1970s. McDonnel and Lewis (1978) demonstrated the possibility to detect ships of 100 m length using Landsat MSS. Burgess (1993) applied Landsat thematic mapper (TM) and SPOT data to identify smaller ships. McDonnel and Lewis (1978) suggested that water turbidity might complicate and possibly inhibited ship detection while decreasing the signal-to-noise ratios of the visible and near infrared bands of Landsat MSS. In addition, optical remote sensing has a limited potential in operational monitoring since it does not work at night and in the presence of clouds. As a consequence, a second technique, Synthetic Aperture Radar (SAR) with capacity to image day and night under most meteorological conditions (Winokur 2000), is the state of the art technique for ship detection (Crisp 2004). For example, Liu et al. (2003a) used ERS SAR to monitor illegal fishing ships, Tunaley (2004) employed RADARSAT-2 SAR to detect ships, and Tello et al. (2006) applied spaceborne SAR to assist authorities in monitoring ship traffic. However, Zhang et al. (2006a) reported limitations of SAR in identifying smaller ships in inland waters.

Dredging impact assessment based on the association between ships and water turbidity patterns requires the simultaneous monitoring of ships and water turbidity. Simultaneity is necessary because both the location of ships and water turbidity patterns might change rapidly. Which remote sensing system(s) would be the most appropriate to achieve this simultaneous monitoring of ships and water turbidity? Greidanus (2006) concluded that SAR was most suitable for ship detections. However, SAR has no capability in water turbidity assessment due to its strong absorption by water. Optical remote sensing has been employed successfully to map water turbidity (e.g., Fraser 1998a, Gan et al. 2004, Vignolo et al. 2006). However, it is difficult to combine SAR with optical remote sensing simultaneously, because the overpass time of the platforms carrying these sensors is not synchronous. Simultaneity would be achieved easily when deriving the information of ships and water turbidity from the same sensor system. In this view, it is interesting to reconsider the capability of traditional optical remote sensing systems for ship detection.

Landsat TM has two additional bands in the middle infrared, which are probably less influenced by water turbidity. The potential of these middle infrared bands for ship detection has so far not been investigated. This paper analyzes the performance of the six Landsat TM bands and explores how the water turbidity influences their performance for detecting dredging ships in the northern Poyang Lake, China.

3.2 Materials and methods

3.2.1 Study area

Poyang Lake (**Figure 3.1**), the largest freshwater lake in China, is located between 115°47′-116°45′E, 28°22′-29°45′N at the southern bank of the Yangtze River. Intensive sand dredging for construction purpose started around 2001 (Zhong and Chen 2005). Recent reports (e.g., Zhong and Chen 2005, Fok and Pang 2006) suggest that dredging has a negative impact on this ecosystem. Since 2003 hundreds of dredging ships have been found between Hukou and Sand Hill in the northern Poyang Lake. Due to these intensive dredging activities, the water turbidity in this region decreased from Secchi disk depths of 1.5 m in the past to less than 0.5 m at present (Wu et al. 2007b).

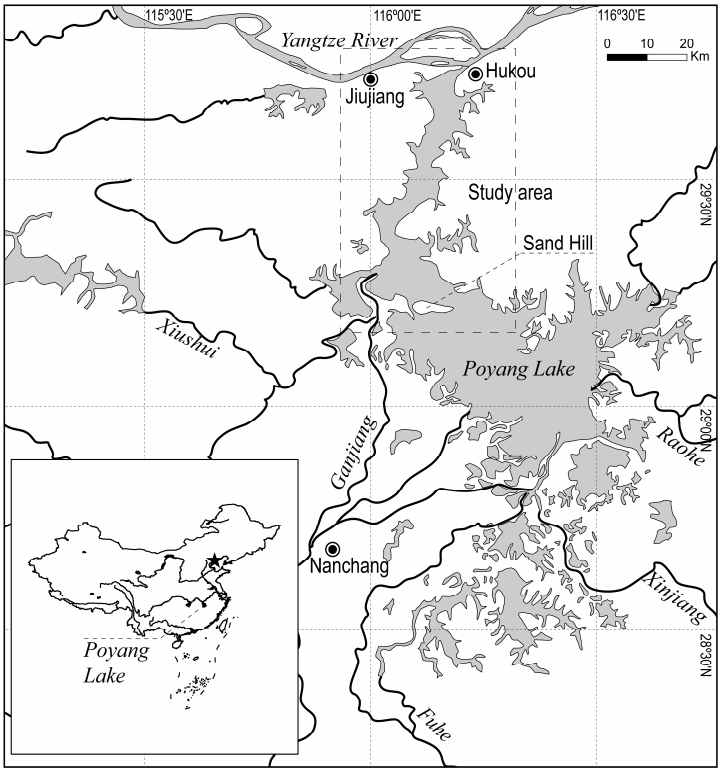

Figure 3.1. Map showing Poyang Lake and the study area – the northern Poyang Lake.

3.2.2 Landsat TM image

One Landsat TM image (path 121/row 40) of 30 July 2006 was obtained from the Chinese Remote Sensing Satellite Ground Station. The cosine approximation model (COST) described by Chavez (1988, 1996) and Chen et al. (2004) was applied to atmospherically correct the image. Topographic maps of 1:50,000 were employed to register the image to the Beijing 54/Gauss-Kruger projection using a first-order polynomial and nearest neighbour approach. The root mean square error (RMSE) for positional accuracy was within half a pixel. Land areas and small water bodies were

removed using a binary mask created through visual interpretation of an unsupervised classification of image. Only bands 1 to 5 and 7 with 30 m resolution were used in this study.

3.2.3 Sampling

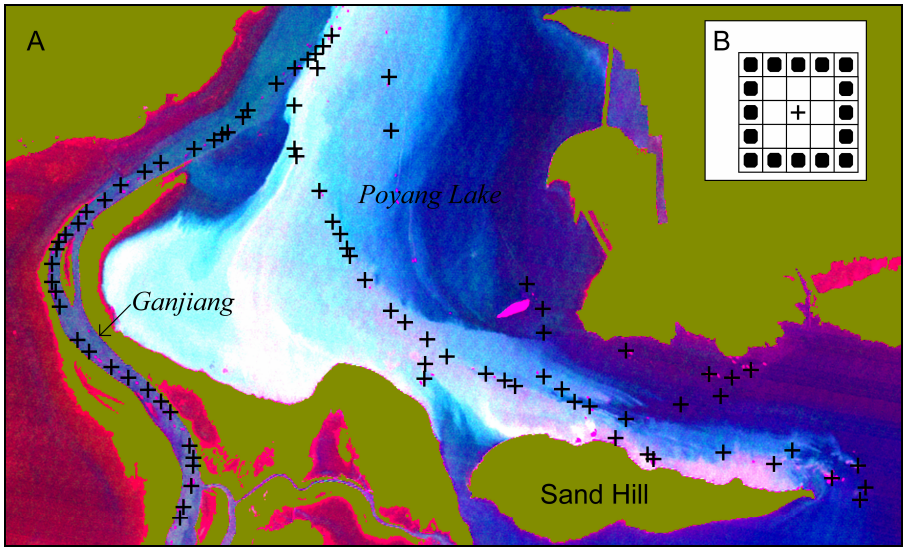

Figure 3.2. A: Colour composite of principal components 3, 2 and 1 of Landsat TM image showing the location of selected ship (+) in Ganjiang River and the northern Poyang Lake; B: Sixteen water pixels (●) around each selected ship used to represent the adjacent water.

During field visit to Poyang Lake we noted that barges transporting sand passed by in regular order, the one following the other with one to few hundred meters between individual ships. In order to enhance the visibility of such eventual objects, we subjected the water areas of the northern Poyang Lake and Ganjiang River to a principal component analysis. A colour composite of components 3, 2 and 1 of part of study area (**Figure 3.2** A) reveals around 180 regular spaced linearly arranged objects, which we believe to represent ships. We selected randomly 81 of these objects, and used the brightest pixel of each object to represent one ship. Then we selected sixteen pixels (**Figure 3.2** B) around each selected ship to represent the adjacent water while avoiding selection of other ships or land. Finally, the reflectance rates of these ship and their adjacent water pixels were extracted from the image for further analyses.

3.2.4 Secchi disk depth

Wu et al. (2007a) developed a regression model describing the relation between the natural logarithm of Secchi disk depth and the blue and red bands of a time-series of five Landsat TM images of 2004. The model explained 83% of the variance of the natural logarithm of Secchi disk depth. We applied this model to calculate the Secchi disk depth of water in the northern Poyang Lake and Ganjiang River.

3.2.5 Statistical analysis

The potential of Landsat TM bands for ship detection is related to the contrast in reflectance of the pixels with ships and their adjacent water. We used the reflectance ratio of ship and its adjacent water as the variable to quantify this contrast.

The reflectance ratio of ship to its adjacent water was calculated using the reflectance of ship and the average reflectance of its corresponding sixteen water pixels for each band. Multivariate analysis of covariance (MANCOVA) was used to test for significant differences in reflectance ratios among the six bands while considering water turbidity (Secchi disk depth) as a covariate.

Following rejection of the null hypothesis of equal reflectance ratio for the various bands, MANCOVA *post-hoc* Bonferroni *t*-test was used to test the significant mean difference of reflectance ratios for all pairs of Landsat TM bands. Next, to each band, we calculated the *z-score* of ratio mean from one. The *z-score* describes the divergence of reflectance ratios from one. The magnitude of the *z-score* thus expresses how well a band contrasts the ships from their surrounding water. The *p* value derived from the z-score can be interpreted as the probability of not identifying a ship when using a ratio greater than one as the classification rule. Therefore it was used to assess the ship detection performance of the six Landsat TM bands.

We then returned to the MANCOVA to test for the homogeneity of slopes of the regression between reflectance ratio and water turbidity. Following rejection of the hypothesis of equal slope we performed *t*-test of the slope of regression to test whether slope deviated from zero in order to analyze how water turbidity influenced the performance of ship detection in each band. All statistical analyses were performed in Statistica 6.0 or Microsoft Office Excel 2003.

3.3 Results

Table 3.1 describes the mean and standard deviation of the reflectance for 81 selected ships and their adjacent water pixels for the six Landsat TM bands. The reflectance of water is low with low variability in the middle infrared bands 5 and 7, while it is higher with relatively high standard errors in other bands, especially in the visible bands. The difference in reflectance between the bands for pixels with ships is less pronounced. The difference in reflectance between pixels with and without ship increases from the visible towards the near and middle infrared bands.

Table 3.1. Statistics describing the means and standard deviations of the reflectance (%) of ships and their adjacent waters for the six Landsat TM bands (n = 81).

Band	*Water*		*Ship*	
	Mean	*s.d.*	*Mean*	*s.d.*
TM 1	0.0677	0.0140	0.0721	0.0133
TM 2	0.0869	0.0197	0.0930	0.0185
TM 3	0.0920	0.0308	0.1110	0.0263
TM 4	0.0460	0.0199	0.0877	0.0263
TM 5	0.0264	0.0099	0.0920	0.0255
TM 7	0.0249	0.0081	0.0796	0.0199

The ships we studied did not occupy a whole pixel; such pixels as a consequence are mixtures of signals from ships and water. Significant linear relationships between

ships and their adjacent water (**Figure 3.3**) were observed for bands 1 (R^2 = 0.90), 2 (R^2 = 0.89), 3 (R^2 = 0.89), 4 (R^2 = 0.53), 5 (R^2 = 0.26) and 7 (R^2 = 0.26) at a significant level of 0.001.

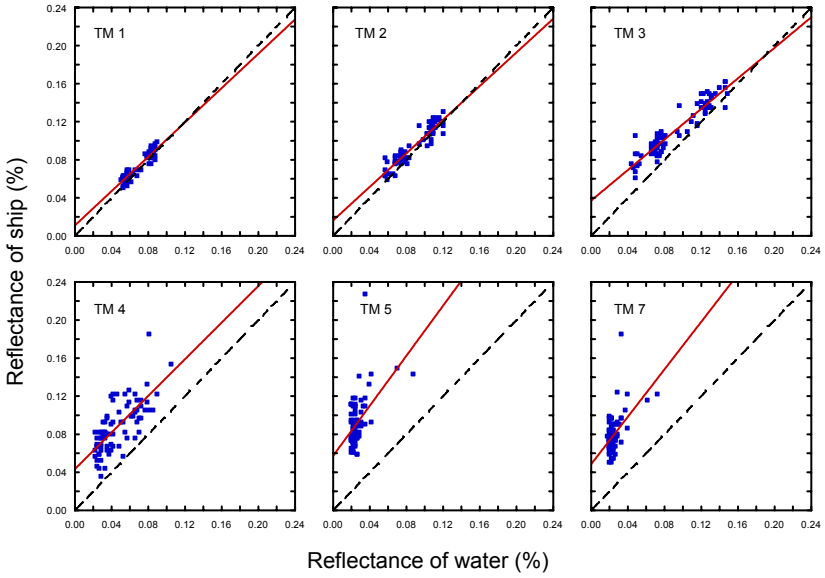

Figure 3.3. Scatter plots describing the reflectance correlations between ship and water for the six Landsat TM bands (n = 81).

The results in **Table 3.1** thus suggest that the contrasts between ships and their adjacent waters differ for the various bands. The MANCOVA results in **Table 3.2** reveal that the reflectance ratio of pixels with and without ships is significantly related to the TM bands, the Secchi disk depth of the waters and the interaction between these two variables.

Figure 3.4 shows the histograms and derived normal frequency distributions of the reflectance ratios of pixels with and without ship for the six TM bands. MANCOVA *post-hoc* Bonferroni corrected *t-tests* reveal that the means of these ratios differ significantly at α = 0.01 for all pairs of bands apart from the combinations of visible bands 1, 2 and 3.

Table 3.2. MANCOVA table describing the relation of Landsat TM band, Secchi disk depth (SDD) and the interaction between these two with the reflectance ratio of pixels with and without ship.

Term	*d.f.*	*F*	*P*
TM Band	5	119.076	<0.01
SDD	1	7.751	<0.01
Interaction	5	12.800	<0.01

A reflectance ratio of one indicates lack of contrast between pixels with and without ships. The results in **Figure 3.4** reveal that the frequency distribution of reflectance ratios for bands 1 to 3 almost centres on one; while that a ratio of one is located in the

tails of the frequency distributions for bands 5 and 7 by contrast. The *z-scores* in **Table 3.3** confirm the results in **Figure 3.4**. The *p* values reveal that the ratios below one occur frequently in the visible and near infrared bands 1 to 4, and that the middle infrared bands 5 and 7 by contrast have extremely low probabilities of ratios below one. These results indicate that the middle infrared bands discriminate ships better than the visible and near infrared bands.

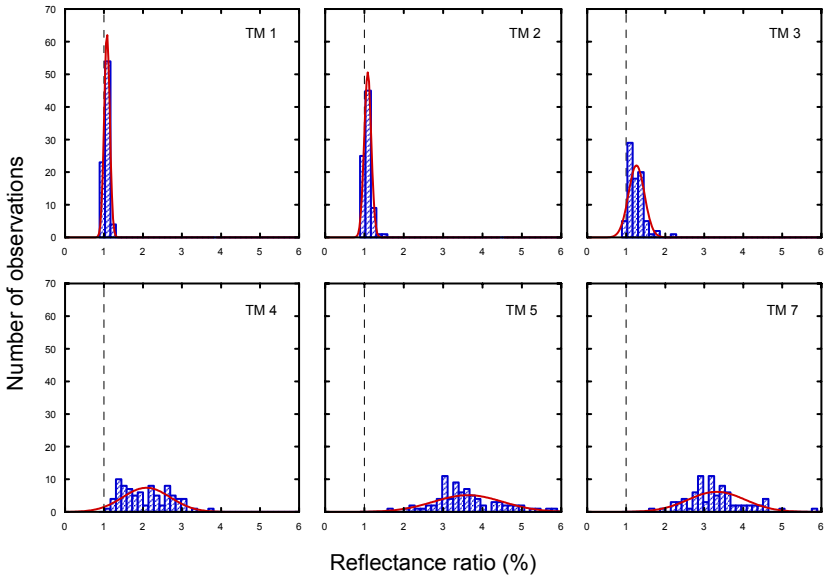

Figure 3.4. Histograms and normal frequency distributions of the reflectance ratios of pixels with and without ship for the six TM bands (n = 81).

The results of MANCOVA test for homogeneity of slopes in **Table 3.4** reveal a general slope of 0.2625 for the relation between reflectance ratio and water turbidity. This slope holds for band 7. The slopes of bands 1 to 3 do not significantly differ from this general slope. Bands 4 and 5, however, have significantly higher and lower slope respectively.

Table 3.3. Statistics describing reflectance ratios of ships and adjacent waters for the six Landsat TM bands (n = 81).

Band	*Mean*	*s.d.*	*z-score*	*P*
TM 1	1.0722	0.0720	-1.0028	0.1587
TM 2	1.0797	0.0889	-0.8965	0.1841
TM 3	1.2573	0.2035	-1.2644	0.1038
TM 4	2.0792	0.6071	-1.7776	0.0375
TM 5	3.6147	0.8772	-2.9807	0.0014
TM 7	3.3010	0.7304	-3.1503	0.0008

Figure 3.5 displays positive relation between reflectance ratio and water turbidity in bands 1 to 4, and negative one in bands 5 and 7. The results of null hypothesis in **Table 3.4** reveal that the relation is significant in bands 1 to 4, but not significant in bands 5 and 7. These results indicate that the performance of ship detection for bands 1 to 4 is significantly influenced by water turbidity, but not for bands 5 and 7.

Table 3.4. MANCOVA coefficients for Landsat TM band, Secchi disk depth (SDD) and their interaction term.

Variable	*Coefficient*	*s.e.*	*t*	*P*
Intercept	1.9376	0.0519	37.3419	<0.0005
TM 1	-0.9244	0.1160	-7.9673	<0.0005
TM 2	-0.9488	0.1160	-8.1776	<0.0005
TM 3	-0.9994	0.1160	-8.6132	<0.0005
TM 4	-0.6869	0.1160	-5.9201	<0.0005
TM 5	1.9498	0.1160	16.8044	<0.0005
SDD	0.2625	0.0943	2.7841	<0.01
*TM 1*SDD*	-0.1432	0.2109	-0.6792	0.4973
*TM 2*SDD*	-0.0786	0.2109	-0.3826	0.7096
*TM 3*SDD*	0.3830	0.2109	1.8164	0.0699
*TM 4*SDD*	1.4140	0.2109	6.7057	<0.0005
*TM 5*SDD*	-0.8143	0.2109	-3.8618	<0.0005

Table 3.5. Statistics describing two sided *t*-tests for the slope of the regression between reflectance ratio and water turbidity (Secchi disk depth) for the six Landsat TM bands (H_0: $\beta = 0$, n = 81).

Band	*slope*	*s.e.*	*t*	*P*
TM 1	0.1193	0.0305	3.9170	<0.0005
TM 2	0.1840	0.0354	5.1908	<0.0005
TM 3	0.6456	0.0597	10.8098	<0.0005
TM 4	1.6765	0.2077	8.0734	<0.0005
TM 5	-0.5518	0.4006	-1.3774	0.1723
TM 7	-0.4984	0.3328	-1.4973	0.1383

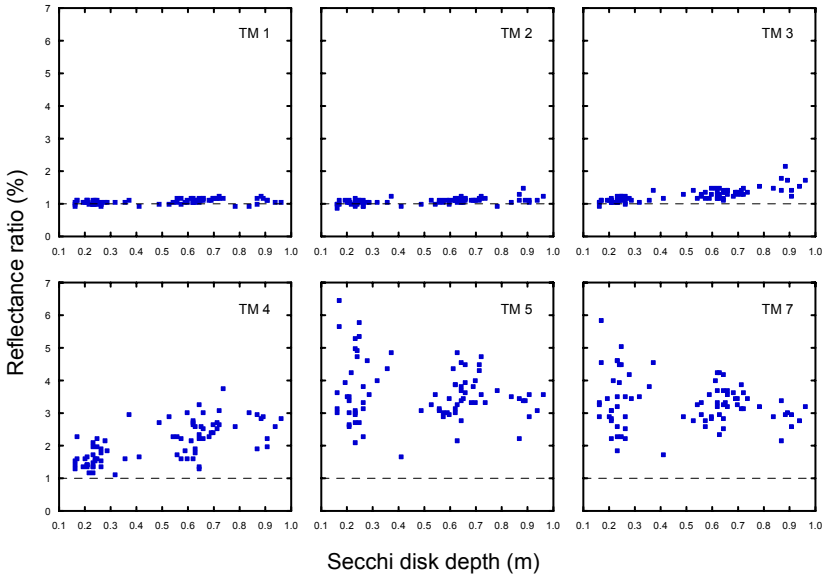

Figure 3.5. Relation of the reflectance ratio of ship and the adjacent water against water turbidity (Secchi disk depth) for the six Landsat TM bands (n = 81).

We used one reflectance ratio threshold of 1.5 to automatically identify ships from bands 5 and 7 of Landsat TM image. One small region with high ship density in our study area is displayed in **Figure 3.6**. From this figure highly consistent results are observed through the comparison of ship information from the colour composite of principal components 3, 2 and 1, bands 5 and 7 of Landsat TM image.

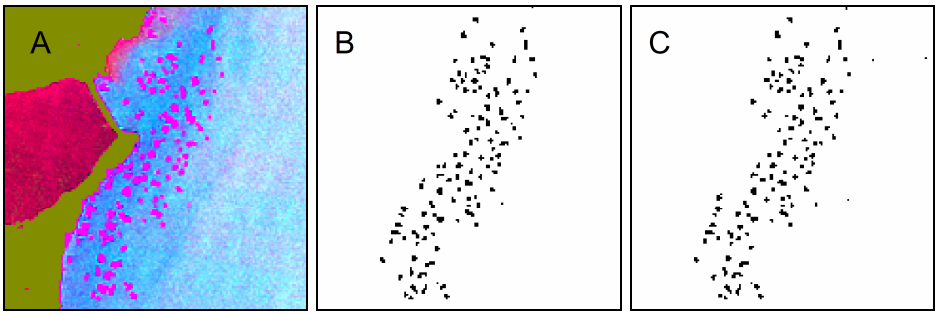

Figure 3.6. Comparison of ship information from the colour composite (A) of principal components 3, 2 and 1, bands 5 (B) and 7 (C) of Landsat TM image.

3.4 Discussion

In this study, we have shown that the middle infrared bands 5 and 7 of Landsat TM effectively discriminated dredging ships from the surrounding water, while the visible and near infrared bands 1 to 4 poorly discriminated the ships. These results differ from those of Burgess (1993) who concluded that Landsat TM red (band 3) and near infrared (band 4) bands were the most useful for ship detection in marine clear water environments. To our knowledge, this is the first evidence that the Landsat TM middle infrared bands hold potential for ship detection in turbid water.

Why do the middle infrared bands discriminate ships from turbid water, while the visible and near infrared bands are not effective? It is well known that the reflectance of water, irrespective of turbidity, is extremely low in the middle infrared bands 5 and 7, since these bands are located close to the strong water absorption peaks at approximately 1.4 and 1.9 um (Richards and Jia 2006). Turbid water, however, has higher reflectance in the visible and near infrared bands compared with middle infrared bands due to multiple scattering of radiation by suspended silt (Gupta 2003). We observed that the ships, which may or may not hold sands, have a much higher reflectance in the middle infrared bands. The reflectance of dry or wet sand is high in the middle infrared bands, and becomes low in the near infrared bands, even approaching that of turbid water (Sabins 1997). This results in a lower reflectance ratio for the visible and near infrared bands of the spectrum, but higher reflectance ratio for the middle infrared bands.

Our results revealed that water turbidity influenced the detectability of ship in the visible and near infrared bands, but not in the middle infrared bands. This observation is consistent with the result of McDonnel and Lewis (1978) who argued that the capacities of visible and infrared bands of Landsat MSS image in detecting ships were limited by turbid water.

Strong positive relationships between water turbidity and Landsat TM visible or near infrared band values have been reported by many studies (Lathrop and Lillesand 1986, Lathrop 1992, Zhao et al. 2003, e.g., Hellweger et al. 2004). We observed that the

reflectance of ships was significantly and positively related to those of their adjacent water in these bands (**Figure 3.3**). Thus we infer that the reflectance ratio between ships and their adjacent waters would reduce with the increasing water turbidity. This may explain why the potential of ship detection in the visible and near infrared bands is influenced by water turbidity. Although there are significant relations between ships and their adjacent waters in the middle infrared bands, these relations are really weak. Most importantly, the middle infrared bands have no clear relations with water turbidity due to strong absorption by water. Thus, water turbidity has no impact on the performance of ship detection in the middle infrared bands of Landsat TM.

3.5 Conclusion

In this study, we analyzed the performance of the Landsat TM visible, near and middle infrared bands for detecting dredging ships in the turbid water of the northern Poyang Lake, China. The principal results obtained can be summarized as: the Landsat TM visible and near infrared bands showed limitation especially in turbid water, while the middle infrared bands hold great potential in ship detection; and that water turbidity has no significant impact on the reflectance of the middle infrared bands could explain why the middle infrared bands provided stronger capacity compared with the visible and near infrared bands in ship detection.

SAR has been frequently and successfully applied to detect ships because it can be applied day and night under most meteorological conditions. However, SAR does not allow simultaneous ship detection and water turbidity assessment. Although Landsat TM images are often hampered by cloud cover, it is possible to detect ships, even in turbid waters. We thus recommend using the middle infrared bands of Landsat TM for operational ship monitoring in turbid water.

CHAPTER 4

CONCURRENT MONITORING OF VESSELS AND WATER TURBIDITY ENHANCES STRENGTH OF EVIDENCE IN REMOTELY SENSED DREDGING IMPACT ASSESSMENT

Abstract

Remotely sensed assessment of dredging impacts on water turbidity is straightforward when turbidity plumes show up in clear water. However, it is more complicated in turbid waters as the spatial or temporal changes in turbidity might be of natural origin. The plausibility of attributing turbidity patterns to dredging activities would be greatly enhanced when demonstrating association between dredging infrastructure and water turbidity. This study investigated the possibility to strengthen inference of dredging impact while simultaneously monitoring vessels and water turbidity in the northern Poyang Lake, China, where dredging was first introduced in 2001 and rapidly extended onwards. Time-series of Landsat TM and MODIS images of 2000-2005 were used to estimate the distribution and number of vessels as well as water turbidity. MODIS images revealed a significant increase in water turbidity from 2001 onwards. Landsat TM image analysis indicated a simultaneous increase in the number of vessels. Regression analysis further showed a highly significant positive relationship (R^2 = 0.92) between water turbidity and vessel number. Visual interpretation of ship locations led to the conclusion that clear upstream waters developed turbidity plumes while passing the first cluster of vessels. We concluded that dredging caused the increase in water turbidity, and simultaneously monitoring the water turbidity and vessels enhanced the strength of evidence in remotely sensed dredging impact assessments.

Published as:

Guofeng Wu, Jan de Leeuw, Andrew K. Skidmore, Herbert H. T. Prins, and Yaolin Liu. *Concurrent monitoring of vessels and water turbidity enhances the strength of evidence in remotely sensed dredging impact assessment*. Water Research, 2007. 41(15): 3271-3280.

4.1 Introduction

Poyang Lake is the largest freshwater lake in China. Its high water quality makes it an important international wetland, allowing its ecosystem to provide significant benefits to society (Chen et al. 2006b). Intensive dredging and supplying this sand to the Chinese construction industry started around 2001 (Zhong and Chen 2005). Recent reports (Zhong and Chen 2005, Fok and Pang 2006) suggest that the dredging has had negative impacts on the local ecosystem. Thus far, it remains unclear for the responsible authorities how widespread the dredging is and how intensively it affects the lake environment.

Dredging is an economic activity with pronounced environmental impacts (Pennekamp et al. 1996). It stirs up sediment, releases solutes and thus alters the physical, chemical and biological properties of the aquatic environment (e.g., Wildish and Thomas 1985, Nayar et al. 2003, Hossain et al. 2004). Dredging also removes the sediment and changes the topography of the bottom of the lake. These may negatively affect the products and services delivered by aquatic ecosystems, including submerged aquatic vegetation, fish, good-quality water, recreation and the potential for nature conservation.

Awareness about the side effects of dredging resulted in a demand to monitor its impacts. Dredging increases water turbidity. Therefore, turbidity is one of the general predictors used to assess the impact of dredging (e.g., Lewis et al. 2001, Spencer et al. 2006). Traditionally, *in situ* measurements are used to assess dredging impact by detecting the spatial patterns and comparing the states before and during or after the dredging operation of water turbidity (e.g., Bonvicini Pagliai et al. 1985, Munawar et al. 1989). However, this method is costly when it is required to assess the spatial or temporal extent of impacts.

Remote sensing offers a possibility to assess the dredging impact on water turbidity over spatial or temporal scales. However, such impacts cannot be detected directly but are inferred from remotely sensed turbidity patterns (e.g., Merry et al. 1988). Jorgensen and Edelvang (2000), for example, used CASI data to estimate suspended matter concentration in a dredging-related sediment plume. Sipelgas et al. (2006) mentioned that near-real-time moderate resolution imaging spectroradiometer (MODIS) was appropriate for monitoring suspended particulate matter distributions whilst dredging in the Paldiski South Harbour.

Indeed, it is easy to infer dredging from remotely sensed turbidity patterns when a plume of turbid water appears in a clear water environment, because the plume describes the impacted area while the tip localizes the dredging vessel. However, in turbid waters, it is much more difficult to assess the impact of dredging, as sediment plumes (if detectable) are not as easily recognizable as in clear water. Moreover, highly turbid waters do not necessarily imply dredging impacts, because the high turbidity could reflect natural variability as well.

Thus, it would be a challenge to improve the ability to discern dredging impacts in waters with high and variable turbidity. Osenberg et al. (1994) exploring techniques to assess environmental impacts from field assessments, remarked that it was challenging to isolate effect from the noise introduced by natural variability in a system. Schmitt et al. (1996) argued that it was difficult to demonstrate the effects of environmental impacts with traditional scientific approaches, which rely solely on experiments with replicated treatments. In order to overcome these problems, an

alternative before-after (BA) design approach that compares the states of the environment before and after an impact, or before-after control-impact (BACI) design, comparing control and impact sites, was used. So far, such study designs have, to our knowledge, not been employed to infer the dredging impacts from remote sensing images.

Dredging impact assessment may be difficult when using remote sensing-based water turbidity products alone, because the evidence of increased turbidity does not necessarily imply that it was caused by dredging. The presence of dredging vessels forms an additional piece of evidence, and thus may enhance the strength of the argument that remotely sensed patterns of increased water turbidity are attributable to dredging activities.

Information on vessel location typically is obtained from *in situ* observations. However, vessels may also be detected by remote sensing. Traditional dredging typically involves a cluster of vessels, including at least one dredging platform and several barges used for transporting the sand or dredge spills. We are not aware of the applications where remote sensing has been used specifically to map dredging vessels, but several techniques have been explored for ship detection. Medium-resolution optical satellite imagery has been used to localize vessels. For example, McDonnel and Lewis (1978) demonstrated the possibility to detect vessels of approximately 100 m length from Landsat MSS imagery (75 m spatial resolution), and Burgess (1993) used Landsat TM (30 m spatial resolution) and SPOT (20 m spatial resolution) to identify vessels of smaller sizes. These applications mainly focussed on marine clear water. However, McDonnel and Lewis (1978) suggested that high water turbidity complicated and possibly inhibited ship detection. In addition, radar has been successfully applied to identify and localize vessels (e.g., Van Genderen et al. 1998, Greidanus et al. 2004, Tunaley 2004) by virtue of its ability to image day and night under most meteorological conditions (Winokur 2000).

This paper investigates the possibility to corroborate the strength of inferring dredging impact on water turbidity, while simultaneously monitoring the number and distribution of vessels and water turbidity using time-series Landsat TM and MODIS images in the northern Poyang Lake.

4.2 Materials and methods

4.2.1 Study area

Poyang Lake (115°47′-116°45′E, 28°22′-29°45′N) is located on the southern bank of the Yangtze River (**Figure 4.1**). Its size fluctuates from less than 1000 km^2 in the dry season to approximately 4000 km^2 in the flood season. The lake receives water from five rivers (Raohe, Xinjiang, Fuhe, Ganjiang and Xiushui) and drains into the Yangtze through a channel in the north.

Poyang Lake is an important international wetland, and delivers significant environmental services such as floodwater storage. The lake has a rich biodiversity, with 102 species of aquatic plants and 122 species of fish (Chen et al. 2006b). It is one of the biggest bird conservation areas in the world, hosting millions of birds from over 300 species. The lake is particularly important to the conservation of the endangered Siberian crane (Li et al. 2005), as more than 95% of its world population congregate here during the winter (Wu and Ji 2002).

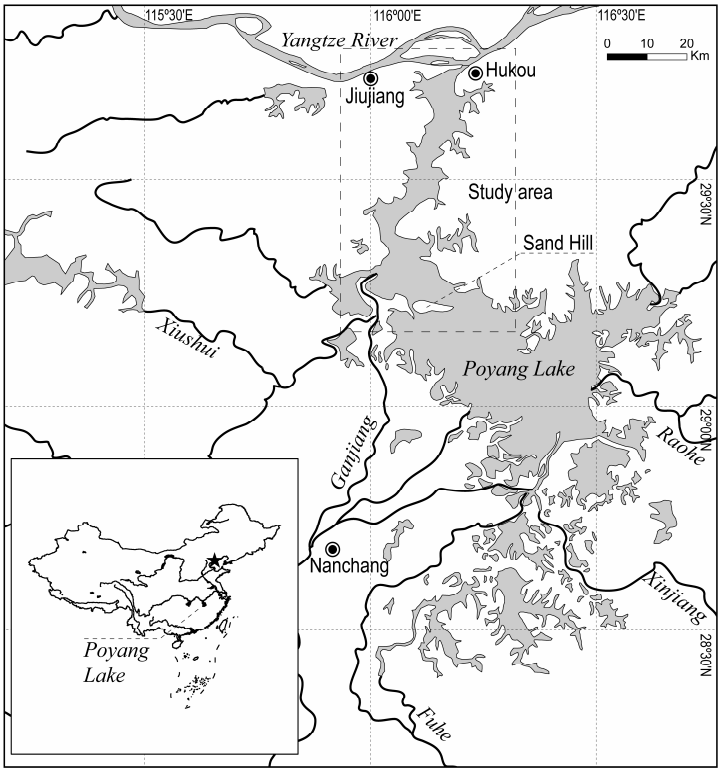

Figure 4.1. Map showing Poyang Lake and the study area – the northern Poyang Lake.

4.2.2 Dredging activities in the northern Poyang Lake

Figure 4.2. Clusters of dredging platforms and barges in the northern Poyang Lake (Data source: http://www.cjstbc.com/caisha/index.asp, accessed 16 October 2006).

Zhong and Chen (2005) attributed the intensification of dredging in Poyang Lake to a combination of factors. Firstly, dredging moved into Poyang Lake after it was banned from the Yangtze in 2001. Secondly, dredging further increased due to the rapidly rising demand for sand in order to support construction in the lower Yangtze River

economic zone. Finally, benefits to the local economy are likely to have persuaded the local government to allow and possibly promote dredging in this lake. Nowadays, hundreds of vessels (**Figure 4.2**) are found between Hukou and Sand Hill in the northern Poyang Lake.

4.2.3 MODIS images

Time-series of good-quality MODIS products (MOD09GQK or MYD09GQK and MOD09GHK or MYD09GHK) from June to October of 2000-2005 were downloaded from NASA's EOS data gateway (http://edcimswww.cr.usgs.gov/pub/imswelcome, accessed 16 October 2006). Images were projected into the WGS 84/UTM zone 50N using nearest-neighbour resampling in order to preserve the original reflectance values. A sub-image of the study area was cut from the larger original. Next, bands 3 and 4 were resampled from 500 to 250 m using nearest-neighbour resampling and bands 1-4 were stacked into one image. Finally, land areas and small water bodies were removed using a binary mask created through visual interpretation of the unsupervised classification of the MODIS image of 4 October 2004.

4.2.4 Landsat images

Seven good-quality Landsat TM scenes (path 121/row 40) of 2 September 2001, 20 August 2002, 23 August 2003, 9 August 2004, 28 October 2004, 12 August 2005 and 31 October 2005 were obtained from the Chinese Remote Sensing Satellite Ground Station. Atmospheric correction was carried out according to the cosine approximation model (COST) described by Chavez (1988, 1996) and Chen et al. (2004). Topographic maps of 1:50,000 were used to register the atmospherically corrected image to the Beijing 54/Gauss-Kruger projection using a first-order polynomial and the nearest neighbour approach. The root mean square error (RMSE) for positional accuracy was within half a pixel. The projected image was re-projected to the WGS 84/UTM zone 50N in order to remain consistent with the projection of MODIS images. The sub-image covering the study area was cut from the re-projected image. Considering the difference in water levels between summer and autumn, two mask layers created through visual interpretation of unsupervised classification of two TM images (captured on 23 August 2003 and 28 October 2004) were used to remove land areas and small water bodies. In addition, one Landsat ETM+ image taken on 23 September 2000 covering the study area was downloaded from the Earth Science Data Interface (http://glcfapp.umiacs.umd.edu/index.shtml, accessed 16 October 2006).

4.2.5 Predicting Secchi disk depth using MODIS images

Wu et al. (2007a) developed a regression model describing the relationship between the natural logarithm of Secchi disk depth and the MODIS red and blue bands. This model explained 88% of the variance of the logarithm of Secchi disk depth. We inverted this model to predict Secchi disk depth from MODIS images from June to October of 2000-2005. We then used the MODIS image of 24 July 2001 to create one region (**Figure 4.3**) covering the main channel, and obtained all the Secchi disk depth values within this region from the developed maps. For each image, these values were averaged to obtain an average Secchi disk depth estimate for the northern Poyang Lake.

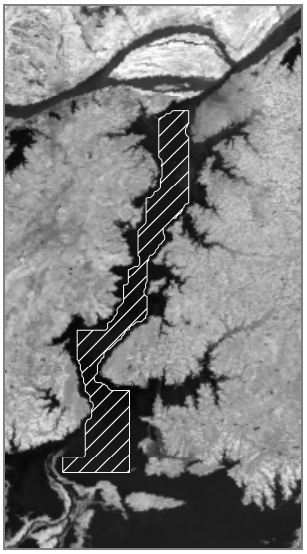

Figure 4.3. MODIS image (24 July 2001) showing the region selected for calculating average Secchi disk depth in the northern Poyang Lake.

4.2.6 Detecting Secchi disk depth and vessels using Landsat TM images

Wu et al. (2007a) developed a regression model describing the relation between the natural logarithm of Secchi disk depth and the Landsat TM blue and red bands. This model explained 83% of the variance of the natural logarithm of Secchi disk depth. We applied this model to the seven aforementioned pre-processed Landsat TM images in order to produce maps describing the spatial variation of Secchi disk depth.

During a field visit to Poyang Lake, we noted that barges transporting the sand passed by in regular order (i.e. one following the other, separated by a distance of one to a few hundred metres). Vessels were easily recognizable in Landsat TM imagery, as they manifested themselves as a sequence of linearly arranged dots. While exploring six Landsat TM bands, we noted that the barges were well discriminated by band 7, a short wave infrared band (2.08 - 2.35 um) with strong water absorption and strong reflectance of soil and rock (http://web.pdx.edu/~emch/ip1/bandcombinations.html, accessed 16 October 2006). The following processes were used to detect and count vessels from each Landsat TM image. We used unsupervised classification to classify band 7 into ten classes. A visually established threshold was used to discriminate platforms and barges from water. The resulting binary image was transformed into polygons with vector format, and the number of polygons was considered to represent the number of vessels.

4.2.7 Analyzing concurrence of change in water turbidity and number of vessels

An increase in water turbidity does not necessarily imply dredging, because it could be caused by other factors such as wave, wind or rainfall. Dredging would become a much more likely cause when the increase in water turbidity would concur with the increase in the number of vessels. To investigate this we used regression analysis to test the relationship between the number of vessels estimated from the Landsat TM images and the seasonal average of Secchi disk depth within the selected region from 2000 to 2005.

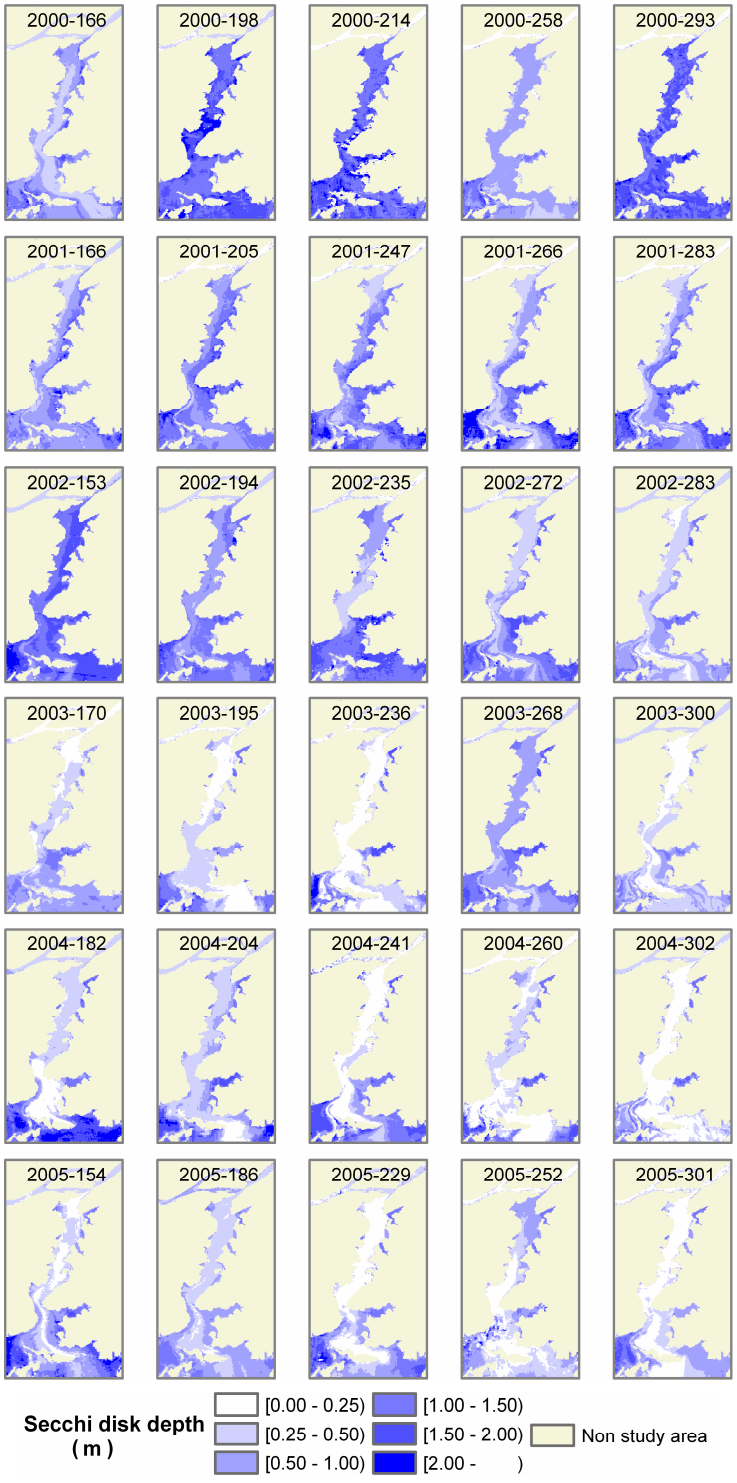

Figure 4.4. Maps showing Secchi disk depth predicted from MODIS imagery from June to October in 2000, prior to the arrival of dredging, and from 2001 to 2005 when dredging activities intensified.

4.3 Results

The time-series maps in **Figure 4.4** derived from MODIS images show a declining trend of Secchi disk depth in the period between June and October from 2000 to 2005. Secchi disk depth fluctuated between 0.5 and 1.5 m in 2000. In 2001 and 2002, the average value declined below 1 m, while during 2003-2005, it dropped below 0.5 m.

Figure 4.5 displays the variation of Secchi disk depth in the northern Poyang Lake from 2000 to 2005. The following regression model explained 56% of the variation of Secchi disk depth:

$$SDD = 1.7/(1+\mathrm{e}^{-0.9098+0.0014*D})$$

where SDD represents Secchi disk depth and D the day number since 1 January 2000. The slope of this regression equation differs significantly from zero (b = 0.0014, *s.e.* = 0.00029, *d.f.* = 29, t = 4.79, P < 0.001). Hence we rejected the null hypothesis which states that there is no change, and accepted the alternative, namely a significant decline in Secchi disk depth.

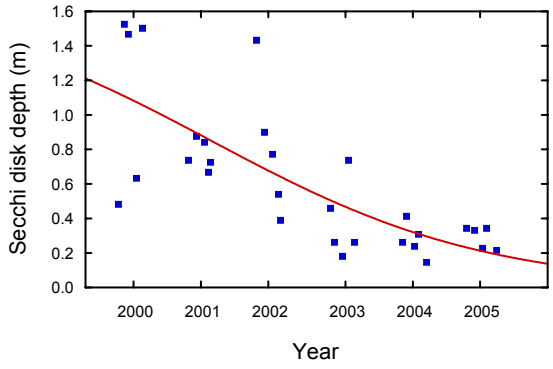

Figure 4.5. Plot showing the variation of Secchi disk depth from 2000 to 2005.

The maps in **Figure 4.6** depict the spatial and temporal variation of Secchi disk depth and dredging infrastructure derived from Landsat TM images from 2001 to 2005. Comparing these maps, we noted that the distribution of vessels was restricted to the main channel from Ganjiang River to Hukou in the first two years (2001-245 and 2002-232), while from 2003 onwards (2003-235, 2004-222 and 2005-224) vessels were also concentrated in the region north of Sand Hill. A seasonal pattern of vessel distribution becomes apparent when comparing the maps in summer (2004-222 and 2005-224) with those in autumn (2004-302 and 2005-304). The maps show that dredging was restricted to the deeper main channel of the northern Poyang Lake in autumn, presumably because low water prohibited dredging in the shallow waters north of Sand Hill. The maps from 2001 to 2005 confirm the aforementioned increasing trend in water turbidity, by virtue of the MODIS images. Finally, the maps also show that dredging occurred in the lower part of Ganjiang. The discharge of sediment from here undoubtedly contributed to water turbidity in the northern Poyang Lake.

Figure 4.7 displays two more detailed pictures of the distribution of water turbidity and vessels in the lower Ganjiang and the area north of Sand Hill in the summer of 2003 and 2004. Poyang Lake drained into the Yangtze during these two dates, and the flow of water was from the southeast to the northwest. The figure revealed that the clear waters flowing from the southeast developed turbid plumes when passing the

first cluster of vessels in the region north of Sand Hill.

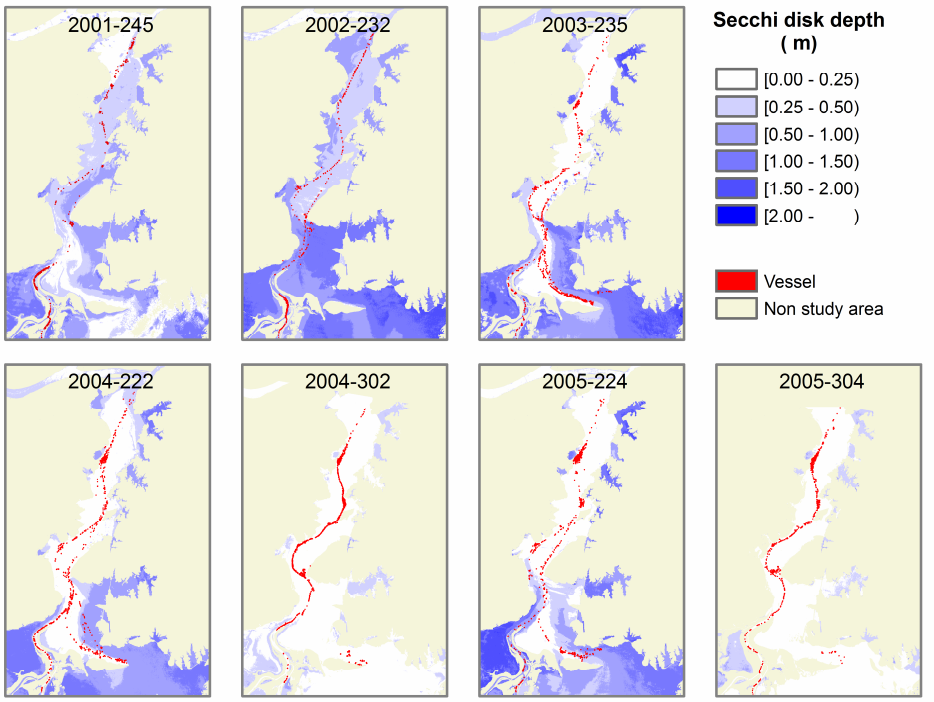

Figure 4.6. Time-series maps showing the distribution of Secchi disk depth and vessels during summer and autumn from 2001 to 2005 in the northern Poyang Lake and Ganjiang.

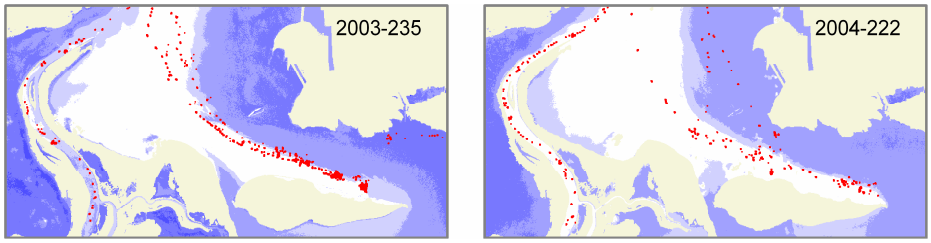

Figure 4.7. Maps showing the association between water turbidity and distribution of dredging vessels in the region north of Sand Hill.

Figure 4.8 shows the number of vessels estimated from Landsat TM images in the northern Poyang Lake and Ganjiang. From the Landsat ETM+ image of 23 September 2000, very few vessels were detected. The vessel number grew to about 140 in 2001, and it reached about 230, 430 and 450 in 2002, 2003 and 2004, respectively. About 380 vessels were estimated in 2005, a little less than that in 2004.

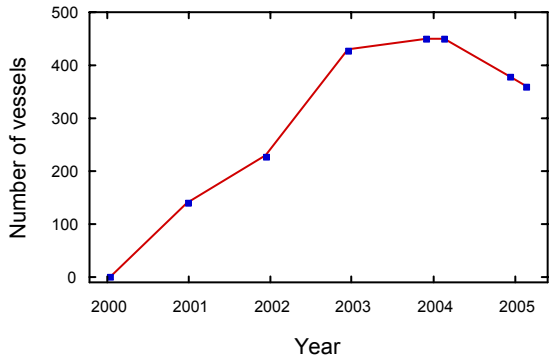

Figure 4.8. Number of vessels in the northern Poyang Lake and Ganjiang during summer and autumn (2000 to 2005).

The regression (**Figure 4.9**) between the average annual Secchi disk depth estimated from MODIS images and the number of vessels derived from Landsat TM images was highly significant (R^2 = 0.92, F (1, 4) = 60.38, P < 0.005).

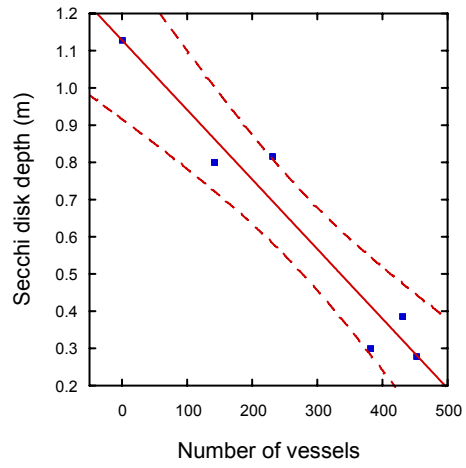

Figure 4.9. Relation between the average annual Secchi disk depth and number of vessels for six consecutive years (2000 to 2005), including 95% confidence interval with dashed lines.

The Landsat TM image of 15 December 2004 taken at low water level (**Figure 4.10**) shows the dented main channels in Ganjiang and the region north of Sand Hill. We note that the distribution of these irregular patterns coincided with the location of the cluster of dredging vessels displayed in **Figure 4.7**.

4.4 Discussion

In this study, the results based on time-series of MODIS images indicated a significant increase in water turbidity of the northern Poyang Lake. Remote sensing has frequently been employed to map dredging-related water turbidity patterns (e.g., Merry et al. 1988, Jorgensen and Edelvang 2000, Sipelgas et al. 2006). Thus far, it has rarely been applied to monitoring dredging-induced change in water turbidity in inland waters over long time spans. Our results indicated that multi-temporal MODIS data offer potential for operational monitoring of change in turbidity of inland waters.

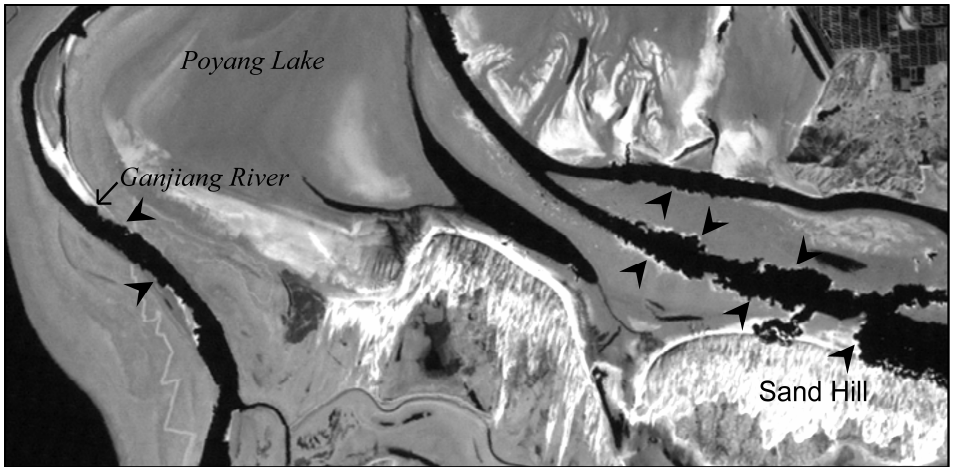

Figure 4.10. Landsat TM image of 15 December 2004 showing irregular dented pattern in the main channels (illustrated by black arrows) of Ganjiang River and the region north of Sand Hill. Note that the black areas represent open water.

Secchi disk depth prediction based on the visible part of the spectrum revealed the changed water turbidity, but did not reveal its cause. Therefore, how can we ascertain whether dredging rather than other processes caused the increase in turbidity? Arguments for this rely on the remotely sensed detection of vessels, for which Landsat TM band 7 was used. Wu et al. (Chapter 2) concluded that the middle infrared bands 5 and 7 of Landsat TM better discriminated vessels from their surrounding waters than the visible and near infrared bands.

Did the procedures used in this study reliably count the number of vessels? While counting the number of vessels, we assumed that every vessel would be reflected by at least one distinct pixel. This assumption would be no longer tenable when vessels were too small to be detected by Landsat TM. The length and width of barges are in the order of 30 and 10 m and above, and the size of dredging platforms is around 60 by 20 m (estimated by Jan de Leeuw during a field visit in July 2006 and corroborated by local people). We consider it unlikely to miss vessels due to their size, because McDonnel and Lewis (1978) reported good detection of ships having a width with one-third of the size of an MSS pixel. A more likely occurrence is the underestimation of the number of vessels, which might occur when vessels were close to each other and they could not be separated as individual objects. We consider it likely that the vessel count reported in this study underestimated rather than overestimated the true number of vessels.

What arguments did the results offer to support the claim that water turbidity increased because of dredging? We firstly reported that the increase in number of vessels coincided with and was significantly related to the increase in water turbidity. A strong and significant relation does however not prove causation. The negative relation between number of vessels and water turbidity could be the result of boats whirling up sediment in shallow waters. Such ship-related resuspension would particularly occur in shallow lakes, like Poyang. **Figure 4.7** reveals lines of vessels moving through turbid water. These follow the deeper central channel of Poyang Lake and Ganjiang, and most likely represent vessels loaded with cargo. Another line of vessels passes through clear water above shallower part of the lake. If ship-related

resuspension played a role, we would expect increased water turbidity in the shallower part of the lake. Such effect is, however, not apparent in **Figure 4.7**. We therefore conclude that vessel related resuspension does not explain the increased turbidity in the northern Poyang Lake.

Rejecting the significant relation between number of dredging-related vessels and water turbidity as evidence of dredging impact rises the question of whether other reasons could explain the strong increase in the number of vessels revealed by the Landsat TM images. It is, in this context, remarkable that the vessels did not travel further to the south than Sand Hill and the lower part of Ganjiang, which appear to be their final destinations. There is no reason apart from dredging as to why vessels would commute to and from these places. We identified this pattern in all images and therefore argue that the recorded increase in the number of vessels corresponds to platforms and barges associated with dredging activities, rather than boats travelling to and from ports along Poyang Lake and its tributaries.

One argument indicating the presence of dredging was the fact that the areas where vessels clustered during high water coincided with the areas where scars were visible in the sediments exposed during low water. Such scars do not naturally occur, and dredging is the only process that logically explains their presence. As such, these scars provide convincing proof of dredging occurring north of Sand Hill and in Ganjiang. However, dredge scars can only be detected in lakes where sediments are occasionally dry.

Another argument was the observation that clear waters upstream turned turbid when passing the first cluster of ships. This observation provided the most direct and convincing argument that the recorded vessels cause changes in water turbidity. This technique, which contrary to dredge scar detection can be used in wider range of environments, relies on the concurrent mapping of vessels and water turbidity.

Together, observations on the spatial and temporal association of vessels with turbidity corroborate the statement that dredging caused an increase in water turbidity. The evidence extracted from the MODIS and Landsat TM images thus complement and confirm each other. MODIS images provided more detailed information on water turbidity, and reported the increasing trend after 2000, while Landsat TM images revealed information on vessels and more details on the association between these and water turbidity. Together, these two remote sensing platforms strengthened the argument that the increased water turbidity resulted from dredging. When taken alone, Landsat and MODIS images would not have yielded such results, because MODIS imagery does not allow for the detection of vessels due to its low spatial resolution, whereas Landsat TM cannot regularly monitor water turbidity due to frequent cloud cover in this region (Wu et al. 2007a).

The argument in favour of dredging impact was based on the detection of vessels. Why use Landsat TM imagery when SAR is the state-of-the-art technique in vessel detection? SAR has the virtue of being able to be applied day and night under all meteorological conditions. However, in the case of dredging impact monitoring, one may wish to use synchronic information on vessel location and water turbidity. A single Landsat TM scene offers the possibility to map vessels and water turbidity concurrently. This would be much harder to realize when combining SAR and optical remote sensing from two separate platforms, because the location of ships and water turbidity patterns might change rapidly, and it is not easy to obtain simultaneously captured SAR and Landsat TM images. Landsat TM imagery has the possibility to concurrently monitor vessels and water turbidity, and it is for this reason that we

advocate the use of Landsat TM images for dredging impact assessment.

Many studies (Lubke et al. 1984, Nayar et al. 2003, e.g., Hossain et al. 2004, Zhong and Chen 2005, Spencer et al. 2006) have reported the impacts of dredging on aquatic ecosystems, including the effects of increased water turbidity, for instance, on aquatic plants and animals, and also noise, pollution, etc. Poyang Lake is an important base of aquatic products. Zhong and Chen (2005) expressed that the noise, oil pollution, turbidity and decreased habitat caused by dredging could seriously affect the propagation, growth and subsistence of fish in the lake. Poyang Lake is also one significant habitat of several rare animal species, such as the Baiji, the Chinese sturgeon, the White sturgeon and the Yangtze finless porpoise. Fok and Pang (2006) reported that the populations of the Yangtze finless porpoise and Baiji have rapidly decreased with the rapid growth of fisheries boating, traffic and dredging activities in Poyang Lake.

Poyang Lake is reputed as the most important habitat of wintering waterfowl in East Asia. More than 95% of total Siberian crane population winter here, and their main food are the tubers of the submerged aquatic vegetation species, *Vallisneria spiralis L.* (Wu and Ji 2002). The increased water turbidity may decrease the available light for photosynthesis of *V. spiralis*, and consequently cause a decrease or disappearance of the food source of Siberian cranes.

In addition, the dredging activities close to Poyang Lake national nature reserve, which was established in 1988 to conserve the Siberian cranes (Wu and Ji 2002), resulted in partial collapse of the banks of Ganjiang (cited from Chinese newspaper), which has grasslands important to grazing waterfowl. All these resultant consequences could decrease the habitat of wintering Siberian cranes and other waterfowl. We also found that the toothed main channels in Ganjiang and regions to the north of Sand Hill (**Figure 4.10**), and their distribution are consistent with that of intensive dredging vessels. Therefore, we conclude that dredging modified the topography of the lake or river bottom, which provided us with another piece of valuable evidence of the dredging impact on this lake.

4.5 Conclusion

In this study, we investigated the possibility to corroborate the strength of inferring dredging impact on water turbidity while simultaneously monitoring the number and distribution of vessels and water turbidity using time-series Landsat TM and MODIS images. The principal results obtained can be summarized as follows:

(1) Time-series MODIS images revealed a significant increase in water turbidity from 2001 onwards.
(2) Time-series Landsat TM images described a simultaneous increase in the number of vessels with increasing water turbidity.
(3) Regression showed a highly significant positive relation between the number of vessels and water turbidity.
(4) We discussed the ship-related resuspension, final destinations of vessels and coincidence of vessel clusters with irregular dented patterns of turbid plume development when clear waters upstream passed the first vessel cluster; hence we confirmed that dredging caused the increase in water turbidity.
(5) Simultaneously monitoring water turbidity and vessels enhances the strength of evidence in remotely sensed dredging impact assessment.

We argue that there is reason for concern about the possible environmental impacts

on the ecology of Poyang Lake given the experiences on dredging impacts from abroad and recent concerns expressed in the Chinese media. So far, the nature and magnitude of these ecological impacts remain unknown. We suggest that it would be worthwhile to explore these possible impacts in order to develop scientific knowledge to support the decisions that need to be made by the responsible authorities, as they need to balance the pros and cons of dredging when deciding how to rationally manage this unique lake ecosystem.

CHAPTER 5

COMPARISON OF THREE EXTRAPOLATION AND INTERPOLATION METHODS FOR PREDICTING DAILY PHOTOSYNTHETICALLY ACTIVE RADIATION (PAR)

Abstract

Photosynthetically active radiation (PAR) is an important factor determining the growth and productivity of plants, and the accurate information of PAR is indispensable for simulating the growth and productivity of plants. This study aimed to compare three extrapolation and interpolation methods for predicting daily PAR reaching the earth surface over the Poyang Lake national nature reserve, China. The daily global solar radiation records at Nanchang meteorological station and daily sunshine duration measurements at nine meteorological stations around Poyang Lake were obtained for achieving the objective. Extrapolation methods of PAR derived from measured and predicted global solar radiation at Nanchang station and three stations (Yongxiu, Xingzi and Duchang) nearby the nature reserve were carried out, respectively. Meanwhile, the triangulated irregular network (TIN) and inverse distance weighted (IDW)-based interpolation method were implemented as well. The validation result using the PAR measured at Dahuchi Conservation Station (n = 105) revealed that: (1) the interpolation method achieved the best prediction of PAR (R^2 = 0.89, *s.e.* = 1.02, F = 830.02, P < 0.001) in all tested methods; (2) the extrapolation method from Nanchang station got moderate result (R^2 = 0.88, *s.e.* = 1.07, F = 745.29, P < 0.001); (3) the extrapolation method from Yongxiu station also produced acceptable prediction (R^2 = 0.87, *s.e.* = 1.14, F = 669.76, P < 0.001); however, (4) the extrapolation methods from Xingzi and Duchang station were not suitable for this specific site for their biased predictions. Considering the assumptions and principles supporting the extrapolation and interpolation methods, we concluded that the interpolation method produce more reliable result than the extrapolation methods and hold the greatest potential in all tested methods to be applied over the whole nature reserve.

Submitted as:

Guofeng Wu, Jan de Leeuw, Andrew K. Skidmore, Yaolin Liu and Herbert H. T. Prins. *Comparison of three extrapolation and interpolation methods for predicting daily photosynthetically active radiation (PAR) over the Poyang Lake national nature reserve, China.* In reviewing.

5.1 Introduction

Photosynthetically active radiation (PAR) is an important factor determining the growth and productivity of plants. It has been used frequently as an input variable in models for simulating the growth and productivity of plants (Yang et al. 2004, Wilson and Meyers 2007, e.g., Kobayashi and Iwabuchi 2008). Long-term and accurate records of PAR are required to implement these models. Such records, however, are not commonly available as PAR is not measured routinely.

In the absence of PAR record, a variety of methods have been explored to predict PAR. One of the commonly used approaches is to derive PAR from global solar radiation at sites with solar radiation records, while assuming that PAR is a fraction of global solar radiation. According to Doorenbos and Pruitt (1984), Zhang and Qin (2002), Mottus et al.(2001) and Moon (Cited by Zhang and Qin 2002), the proportion of PAR in global solar radiation varied between 35 to 50% depending on weather and climatic conditions. However, accurate records of global solar radiation reaching the earth surface are only available for a few sites because the cost of required instruments or maintenance and calibration of solar radiation sensors are high (Hunt et al. 1998). Therefore, various physical, statistical or stochastic methods are employed to predict global solar radiation at sites without radiation records.

Physical methods comprise radiative transfer models, and take the physical interaction between solar radiation and atmosphere into account, such as Rayleigh scattering, radiative absorption by ozone and water vapour, and aerosol extinction (Wong and Chow 2001, Muneer et al. 2007). For their complexities, such methods are difficult to use by non-experts (Tymvios et al. 2005). Statistical methods are based on empirical relations between the transmittance of incident solar radiation and meteorological variables (Liu and Scott 2001). They derive radiation from meteorological variables including sunshine duration (Wong and Chow 2001, Almorox and Hontoria 2004), cloud cover (Hunt et al. 1998, Muneer and Gul 2000), temperature (Rivington et al. 2005, Paulescu et al. 2006), precipitation (Liu and Scott 2001, Rivington et al. 2005), air humidity (Yang and Koike 2002) or their combination (El-Metwally 2004, Trnka et al. 2005). Some researchers (e.g. Rivington et al. 2005, Trnka et al. 2005) obtained highest precision while using sunshine duration. Stochastic methods (Cooter and Dhakhwa 1996, Hansen 1999) incorporate the aspects of physical and statistical methods, and are more flexible in combining stochastic processes such as cloud movement (Craggs et al. 1999). They could be helpful in exploring possible or theoretical model scenarios over a long time period (Iziomon and Mayer 2002), but cannot generate data matching the actual weather condition at particular time period (Liu and Scott 2001).

Two methods are generally applied to predict the radiation at unobserved locations from those at observed locations, such as meteorological stations. The extrapolation method uses the recorded or calculated radiation at a nearby site as the value at a unobserved site if the distance between the two sites falls below a certain value (Suckling 1985, Hunt et al. 1998). When a network of meteorological stations is existent, spatial interpolation methods, such as geometric interpolation and geostatistics, could be applied. For example, Barr et al. (1996) used inverse-distance-squared weighting (a geometric interpolation method) and Kriging (a geostatistics method) method to predict solar radiation on the Canadian prairies, and Rehman and Ghori (2000) and Tiba (2001) applied Kriging to derive spatial distribution of radiation in Saudi Arabia and Brazilian Northeast.

Increasingly, there is an interest to model productivity of aquatic ecosystems. The availability of PAR or associated records is, however, even sparser in this environment. Moreover, aquatic ecosystems might have weather conditions differing from those of the surrounding terrestrial ecosystems. It remains questionable, therefore, whether extra- or interpolation from nearby land-based climate stations results in accurate prediction of PAR over lake environments.

This study aims to compare three extrapolation and interpolation methods for predicting daily PAR over lakes from global solar radiation or sunshine duration recorded at nearby meteorological stations.

5.2 Materials and methods

5.2.1 Study area

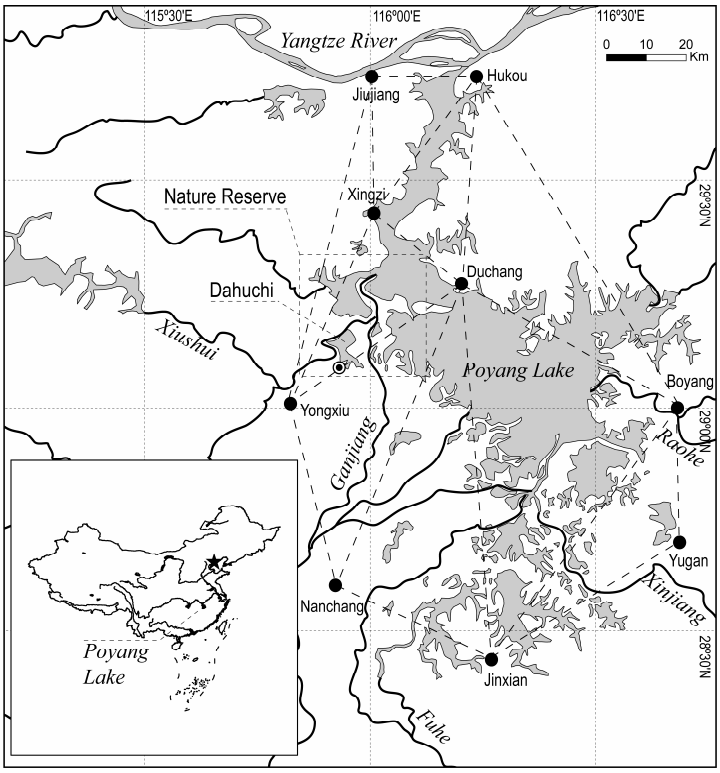

Figure 5.1. Locations of Poyang Lake, Poyang Lake national nature reserve, Lake Dahuchi, Dahuchi Conservation Station (◉) where PAR was measured, and nine meteorological stations (●) around Poyang Lake. The triangulated irregular network (TIN) of nine meteorological stations was used to predict daily PAR over the nature reserve.

The research was carried out in Poyang Lake national nature reserve (**Figure 5.1**). The reserve is located between 115°55′ -116°03′ E, 29°05′ -29° 15′ N in the northwest of Poyang Lake, and generally it is a flat terrain with several hills of around 50 m high (Wu and Ji 2002). It was established in 1988 to conserve the Siberian cranes,

and is one of the most important areas in the world for wintering waterfowl species, including 95%, 60% and 50% of the world population of Siberian crane, White-naped crane and Swan Goose, respectively (Wu and Ji 2002, Li et al. 2005).

5.2.2 Meteorological data

Daily global solar radiation is only recorded at Nanchang among the nine meteorological stations around Poyang Lake (**Figure 5.1**). We obtained daily sunshine duration from 2000-2006 at these stations. Meanwhile, daily global radiation at Nanchang meteorological station for the same period was acquired.

In addition, PAR at the top of Dahuchi Conservation Station (**Figure 5.1**), which just lies at the edge of Lake Dahuchi, was recorded with five minute interval from 6 July to 12 August and from 6 September to 10 November 2006 using a LI-190SA quantum sensor and a LI-1400 data logger (http://www.licor.com) for validating the results derived from the methods described below.

5.2.3 Extrapolation and interpolation methods

We predicted daily PAR over the nature reserve using the following three methods:

(1) Extrapolating from measured global solar radiation

The nature reserve is located around 55~75 km from the Nanchang meteorological station, which is the closest station with global solar radiation records to the nature reserve. Given this distance and the contrast between lake and urban environment, we considered that the radiation record at Nanchang might not reflect the radiation variation over the nature reserve. For validating this assumption, we supposed a fraction of 45% of PAR in global solar radiation according to Doorenbos and Pruitt (1984), Zhang and Qin (2002) and Moon (Cited by Zhang and Qin 2002), and used this proportion to predict daily PAR from daily global solar radiation at Nanchang station (Eq. 1). Then the predicted daily PAR was extrapolated to test its application potential over the nature reserve.

$$PAR = R * 0.45 \quad (1)$$

where *PAR* and *R* represent the daily PAR and global solar radiation on the earth surface, respectively.

(2) Extrapolating from predicted global solar radiation

Three meteorological stations (Xingzi, Yongxiu and Duchang) are closer to the nature reserve than Nanchang station (**Figure 5.1**). Solar radiation at these stations might more reasonably reflect that over the nature reserve. However, radiation measurements are lacking at these stations. Chen *et al*. (2006a) described a solar radiation model (Eq. 2), which explained 92% of the variation of radiation using sunshine duration at 86 meteorological stations in China.

$$R = R_{ext} * (0.001 * \Phi + 2.41 * 10^{-5} * H + 0.109 + 1.029 * \frac{S}{S_{ext}} - 1.216 * (\frac{S}{S_{ext}})^2 + 0.787 * (\frac{S}{S_{ext}})^3) \quad (2)$$

where S represents the daily sunshine duration on the earth surface, Φ and H represent the latitude and altitude of meteorological station, respectively, and R_{ext} and S_{ext} are extra atmosphere global solar radiation and potential sunshine duration,

which were calculated according to Wang (1999), considering the earth-sun distance, solar declination and latitude. We first validated the model using sunshine duration and solar radiation records from 2001 to 2006 at Nanchang station, and the result revealed a highly significant relation between the predicted and measured radiations (R^2 = 0.92, F = 26959.28, n = 2191, P < 0.0001). The model was then applied to predict daily global solar radiation from sunshine duration, and further calculated daily PAR using Eq. 1 in the three stations. Finally the derived daily PAR at these meteorological stations was extrapolated to the nature reserve, respectively.

(3) Interpolating from predicted global solar radiations

Spatial interpolation derives spatially continuous prediction of meteorological data from spatially discrete locations within a network of meteorological stations (Dobesch et al. 2007), We thus explored whether this method could provide more accurate result compared with the extrapolation methods. We first predicted the daily global solar radiations and PARs at the meteorological station using Eq. 2 and 1, respectively. Then, a triangulated irregular network (TIN) (Longley et al. 2001) with nine meteorological stations as TIN nodes was created, and TIN-based inverse distance weighted (IDW) method (Lancaster and Salkauskas 1986) (Eq. 3) was applied to interpolate the predicted PARs at the meteorological stations.

$$PAR_i = \left(\frac{PAR_1}{dis_{i1}^2} + \frac{PAR_2}{dis_{i2}^2} + \frac{PAR_3}{dis_{i3}^2}\right) / \left(\frac{1}{dis_{i1}^2} + \frac{1}{dis_{i2}^2} + \frac{1}{dis_{i3}^2}\right) \quad (3)$$

where PAR_i is the PAR on the earth surface at location i, PAR_1, PAR_2 and PAR_3 are the PARs at nodes (meteorological stations) 1, 2 and 3 forming a face of the TIN, and dis_{i1}, dis_{i2} and dis_{i3} are distances from location i to the three nodes, respectively.

We then used the daily PAR measured at the Dahuchi Conservation Station to validate the results derived from the above-mentioned methods. Agreement between the predicted and measured values was described by the intercept, slope and coefficient of determination (R^2) of the regression line of the predicted against measured values, and standard error (*s.e.*) of the prediction. The differences of correlation coefficients for all pair of regressions were tested, the null hypothesis tests of intercept equal to zero and slope equal to one were carried out, and the standard errors of the predictions were compared. Based on these tests and comparisons, we evaluated the performances of these methods and further determined the optimal method for predicting daily PAR over the nature reserve.

Finally, the daily PAR over Lake Dahuchi within the nature reserve was predicted using the optimal method and its seasonal pattern was summarized briefly.

5.3 Results

The TIN of nine meteorological stations around Poyang Lake is shown in **Figure 5.1**, and it covers the whole nature reserve.

The scatter plots of the measured PAR at Dahuchi Conservation Station against predicted PAR derived through all tested methods (**Figure 5.2**) show good agreements.

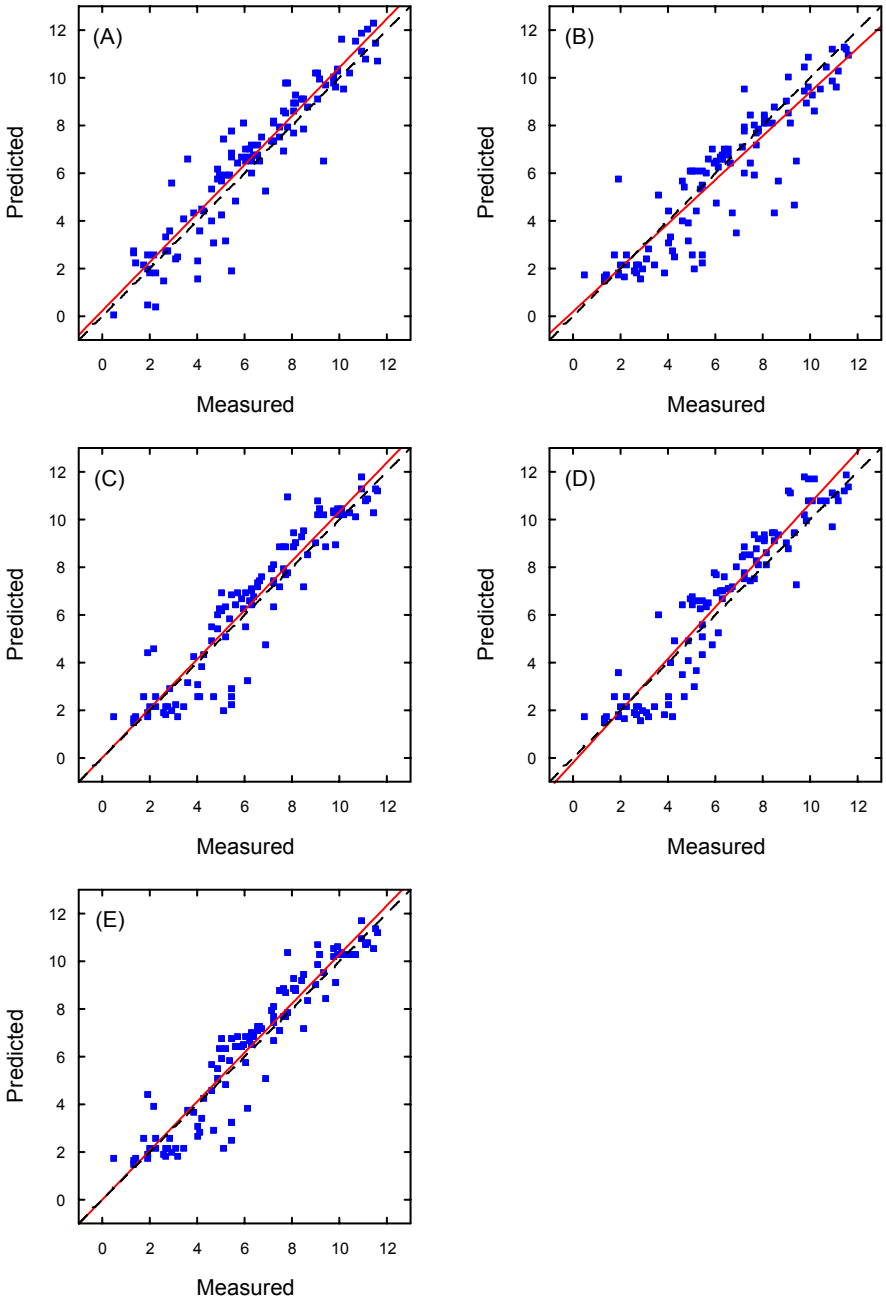

Figure 5.2. Scatter plots of daily PAR (MJ m $^{-2}$ day $^{-1}$) measured at Dahuchi Conservation Station against predicted PAR derived through extrapolation of global solar radiation measured at Nanchang (A) and predicted at Xingzi (B), Yongxiu (C) and Duchang (D), and interpolation of PARs predicted at these three meteorological stations (E) (n = 105).

The statistics describing the regression between measured and predicted PAR for all methods are listed in **Table 5.1**. Little difference was observed except that the extrapolation of radiation from Xingzi (B) showed somewhat poorer performance.

Table 5.1. Statistics describing the regression of measured PAR at Dahuchi Conservation Station against predicted PAR derived through extrapolation of global solar radiation measured at Nanchang (A) and predicted at Xingzi (B), Yongxiu (C) and Duchang (D), and interpolation of PARs predicted at these three meteorological stations (E) (n = 105).

	R^2	*s.e.*	*F*	*P*
(A)	0.88	1.07	745.29	< 0.001
(B)	**0.80**	**1.28**	**429.32**	**< 0.001**
(C)	0.87	1.14	669.76	< 0.001
(D)	0.89	1.06	868.43	< 0.001
(E)	0.89	1.02	830.02	< 0.001

Table 5.2 shows the result of difference tests of correlation coefficients for all pair of regressions. We found that only the correlation coefficient of the extrapolation method from Xingzi (B) was significantly different from those of other methods at significant level of 0.1 or 0.05, which confirmed the above observation that the extrapolation of radiation from Xingzi (B) showed somewhat poorer performance. This means that, from the point of view of R^2, all methods got similar results except (B).

Table 5.2. Difference tests (*P* value) of correlation coefficients for all pair of regressions. (A), (B), (C), (D) and (E) denote the extrapolation and interpolation methods same as in Table 5.1.

	(B)	*(C)*	*(D)*	*(E)*
(A)	**0.0471**	0.7750	0.7573	0.7573
(B)	**-**	**0.0886**	**0.0221**	**0.0221**
(C)	-	-	0.5521	0.5521
(D)	-	-	-	1

The result of null hypothesis tests of intercept equal to zero and slope equal to one for the regression lines (**Table 5.3**) revealed that the intercepts of all methods were not significantly different from zero, while the slopes of extrapolation methods from Xingzi (B) and Duchang (D) were significantly different from one at significant level of 0.1 and 0.05, respectively. This indicates that both extrapolations of solar radiation from Xingzi and Duchang station got biased predictions.

Table 5.3. Null hypothesis tests of intercept equal to zero and slope equal to one for regressions between the predicted and measured PARs. (A), (B), (C), (D) and (E) denote the extrapolation and interpolation methods same as in Table 5.1.

	Intercept			*Slope*		
	a±*s.e.*	*t*	*P*	*b*±*s.e.*	*t*	*P*
(A)	0.23±0.26	0.9085	> 0.1	1.02±0.04	0.5350	> 0.1
(B)	**0.20±0.30**	**0.6493**	**> 0.1**	**0.92±0.04**	**1.7926**	**< 0.1**
(C)	0.02±0.27	0.0620	> 0.1	1.03±0.04	0.7678	> 0.1
(D)	**-0.19±0.25**	**0.7528**	**> 0.1**	**1.09±0.04**	**2.3416**	**< 0.05**
(E)	0.01±0.24	0.0258	> 0.1	1.01±0.04	0.7616	> 0.1

Considering the standard error of prediction for the methods without prediction bias,

we found that interpolation method (E) got a smaller standard error, while extrapolation methods from Nanchang (A) and Yongxiu (C) with the moderate and larger one, respectively (**Table 5.1**).

Synthetically comparing and analyzing the intercept, slope, coefficient of determination and standard error of all predictions, we considered that the spatial interpolation method (E) got the best prediction of PAR at Dahuchi Conservation Station in all tested methods, while the extrapolation of global solar radiation measured at Nanchang (A) achieved moderate result and the extrapolation of global solar radiation predicted at Yongxiu station (C) obtained unbiased result as well. However, the extrapolation of global solar radiation predicted at Xingzi (B) and Duchang (D) station were less appropriate for their biased predictions.

The daily PAR over Lake Dahuchi from 2001 to 2006 (**Figure 5.3**) was predicted using the interpolation method (E). The seasonal pattern of daily PAR was higher in summer and lower in winter. Meanwhile, its daily variation was observed clearly for different weather conditions.

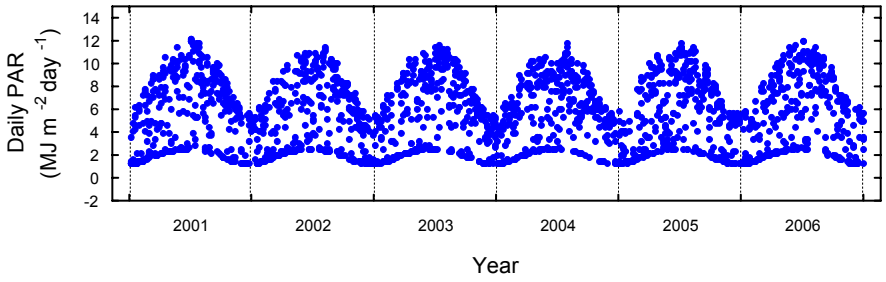

Figure 5.3. Daily PAR predicted using spatial interpolation method over Lake Dahuchi.

5.4 Discussion

In this study, we reported that the extrapolation of solar radiation measured at Nanchang station could explain 88% of variation of PAR at Dahuchi Conservation Station. The relatively short distance between Nanchang and the nature reserve possibly contributes to their similarity in solar radiation. This result is contrary to our assumption that the radiation record at Nanchang might not realistically reflect the variation of radiation over the nature reserve. It corresponds to the result of Hunt et al. (1998) who reported that it would be preferable to use the measured data from the neighbouring station if the distance between sites was less than 390 km. However, this does not mean that the other parts in the nature reserve could also get the similar result, because the Dahuchi Conservation Station is closer to Nanchang station compared with other parts. The prediction accuracy might decline with the increasing distance to the monitoring station (Suckling 1985, Gallegos and Lopardo 1988, Trnka et al. 2005).

We supposed that extrapolation of PAR from the metrological stations closer to the nature reserve might achieve better prediction of PAR compared with that from Nanchang station. However, we found that extrapolation from Xingzi, Yongxiu and Duchang did not result in better predictions than from Nanchang. Moreover, the extrapolating results from different stations showed relatively high differences. We

argue, however, that such comparison cannot be used to draw conclusions that the PAR at Nanchang station could better describe the solar condition in our study area than that at Xingzi, Yongxiu or Duchang station. We thus considered that the accuracy of the solar radiation model (Eq. 2) might affect the predictions of PAR at these stations, which further influence the accuracy of extrapolation methods. Meanwhile, the difference of solar radiations in our study area and these stations induced by the local environments could also contribute to these relatively lower accuracies.

We also found the extrapolated daily PAR from Yongxiu station could better explain the variation of solar radiation at Dahuchi Conservation Station compared with that from Xingzi and Duchang station. Such result could be explained by the fact that the distance of the Dahuchi Conservation Station to Yongxiu station is close than to Xingzi and Duchang station. This indicates that the PARs at Xingzi and Duchang station could also describe more accurately the PAR variation over the places more close to them. So the validation should be carried out for determining which station could be more suitable for a given position.

The TIN and IDW-based spatial interpolation method got the best predictions of PAR in all tested methods. TIN restricts which three meteorological stations might mainly affect the radiation at a given point considering the distribution of all stations; while IDW is based on the spatial correlation of variables and predicts the values of variables at unobserved locations from those at observed locations. The combination of TIN and IDW thus could derive more accurate prediction of PAR compared with the extrapolation method, which only uses the data from one station. Therefore, from the angle of the assumptions and principles supporting these methods, we consider that the interpolation methods could produce more reliable results than the extrapolation methods over the nature reserve.

5.5 Conclusion

In this study, we compared three extrapolation and interpolation methods for predicting daily PAR over the Poyang Lake national nature reserve. The principal results obtained can be summarized as follows:

(1) The extrapolation method from directly measured solar radiation at Nanchang station could explain 88% of variation of daily PAR at Dahuchi Conservation Station, and achieved moderate result. However, the prediction accuracy for other parts within the nature reserve might decline with the increasing distance to Nanchang station;
(2) Although the extrapolation method from predicted solar radiation at Yongxiu station got relatively low prediction, it still could explain 87% of variation of daily PAR at Dahuchi Conservation Station. Its application over other parts within the nature reserve should be validated;
(3) The extrapolation methods from predicted solar radiation at Xingxi and Duchang station could not be applicable directly at Dahuchi Conservation Station for their biased predictions. But they could potentially describe the PAR variation in the places more close to them;
(4) The spatial interpolation method got the best prediction of daily PAR at Dahuchi Conservation Station, and held the greatest potential in all tested methods to be applied over the whole nature reserve.

CHAPTER 6

WILL THE THREE GORGES DAM POSITIVELY AFFECT THE UNDERWATER LIGHT CLIMATE OF *VALLISNERIA SPIRALIS L.* AND FOOD HABITAT OF SIBERIAN CRANE IN POYANG LAKE?

Abstract

Almost 95% of the entire population of the Siberian crane (*Grus leucogeranus*) winter in Poyang Lake, China, where they forage on the tubers of the submerged aquatic macrophyte, *Vallisneria spiralis L.* Three Gorges Dam on the Yangtze River may possibly affect the food source of the Siberian crane by affecting the light availability reaching the top of the *V. spiralis* canopy. In this study, the photosynthetically active radiation at the top of the *V. spiralis* canopy (PAR_{tc}) in Lake Dahuchi was modelled from 1998 to 2006, and the potential impacts of changes in water level and turbidity on the underwater light climate of *V. spiralis* and on the habitat of the Siberian crane were analyzed. PAR_{tc} was calculated from incident irradiance while the losses due to reflection at the water surface, absorption and scattering within the water column were taken into consideration. The results indicated significant differences in PAR_{tc} between years. Six years of water level and Secchi disk depth records revealed a seasonal switching of the lake from a turbid state at a low water levels in autumn, winter and spring to a clear state at a high water levels in summer. The highest PAR_{tc} occurred at intermediate water levels, which were reached when the Yangtze River forces Lake Dahuchi out of its turbid state in spring and the water becomes clear. The intended operation of the Three Gorges Dam, which will increase water levels in May and June, may advance the moment when Lake Dahuchi switches from turbid to clear. We suggest that this might increase production of *V. spiralis* and possibly improve the food habitat conditions for wintering Siberian crane in Poyang Lake.

Submitted as:

Guofeng Wu, Jan de Leeuw, Andrew K. Skidmore, Herbert H. T. Prins, Elly P. H. Best, Yaolin Liu. *Will the Three Gorges Dam positively affect the underwater light climate of Vallisneria spiralis L. and food habitat of Siberian crane in Poyang Lake?* In reviewing.

6.1 Introduction

Endemic species are vulnerable to extinction when environmental change affects their habitat. Thus, areas with high diversity of endemic species deserve attention in case of environmental change. Poyang Lake, a lake system connected to the Yangtze River of China, hosts significant proportions of the Yangtze finless porpoise (*Neophocaena phocaenoides asiaeorientalis*), swan goose (*Anser cygnoides*) and almost 95% of the entire world population of the endangered Siberian crane (*Grus leucogeranus*). The Siberian crane winter at this lake and forage on the tubers of the submerged aquatic macrophyte, *Vallisneria spiralis L.* (Wu and Ji 2002, Li et al. 2005).

The environmental conditions of Poyang Lake are rapidly changing due to economic development and hydro-engineering projects in the watershed within which it is situated. For example, dredging increased the water turbidity in the northern Poyang Lake (Wu et al. 2007b). The environmental conditions might also be influenced by operation of the Three Gorges Dam in the Yangtze River, which is scheduled for completion by 2009 (Wang 2002). These changes might affect the habitat of the Siberian crane (Liu and Xu 1994, Jiang and Huang 1997, Kanai et al. 2002, Wu et al. 2007b). However, these studies did not explore how the Three Gorges Dam might influence the food habitat of Siberian crane. We suggest that the Three Gorges Dam might affect the habitat of the Siberian crane as follows: (1) the Three Gorges Dam may affect the hydrology of Poyang Lake, (2) the changed hydrology may influence the tuber production of *V. spiralis* in Poyang Lake and (3) the changed tuber production may impact the foraging by the wintering Siberian crane. So far, however, there is no direct evidence to support this expectation, as little research has been reported on the ecology of the tuber-feeder food chain of Poyang Lake.

Is there evidence to support the premise that a changed tuber production would affect the foraging of tuber-feeders? Jonzen et al. (2002), Nolet et al. (2006) and Raymond et al. (2006) reported that tuber density of sago pondweed (*Potamogeton pectinatus*) affected the foraging of tundra swan (*Cygnus columbianus bewickii*) in Lake Lauwersmeer in the north of the Netherlands, and Sponberg & Lodge (2005) found that waterfowl in Lake Mattamuskeet, North Carolina, USA, gave up foraging when tuber density of wildcelery (*Vallisneria americana*) was below a certain threshold.

How would hydrology influence the photosynthesis and tuber production of *V. spiralis*? The growth and production of submerged vegetation is regulated by light intensity reaching its canopy, water temperature, CO_2 and nutrient availability (Best and Boyd 2001a, Best et al. 2001, Van Nes 2002). Light availability likely controls the growth and production of *V. spiralis* as it is highly variable in the waters with fluctuating water depth and clarity of Poyang Lake. The light response of *V. spiralis* has not been studied, but a light compensation point of 20-25 and 10 mol m^{-2} sec^{-1} was found respectively for the related *V. americana* (Madsen et al. 1991, Blanch et al. 1998). This corresponds to 1-2% of surface irradiance during sunshine, and agrees with the observation that *V. americana* maintains photosynthesis above 0.5% of surface irradiance (Korschgen and Green 1988). Tuber production requires a higher light intensity. Kimber et al. (1995) reported a threshold of 5-9% of surface irradiance for tuber production under temperate climatological conditions, which forms the lower limit of the 9% surface irradiance threshold cited for *V. americana* occurrence in temperate North-Florida (Dobberfuhl 2007).

How would the hydrology of the Yangtze River affect the hydrological conditions in

Poyang Lake, and, thus, indirectly, the tuber production of *V. spiralis*? The Yangtze River with five confluent rivers together control the water level in Poyang Lake (Min 1995, Xu et al. 2001, Shankman et al. 2006). The Siberian crane forage in lakes in deltas at the periphery of Poyang Lake. So far, no analysis has been made to investigate whether the Yangtze River influences the water level and clarity of these peripheral lakes.

A crucial question is whether the Three Gorges Dam will affect the hydrology in Poyang Lake. Addressing this question requires insight into the consequence of operating the Three Gorges Dam and its impact on the dynamics of the Yangtze River. Such an analysis has recently been reported by Wang et al. (2005). The Three Gorges Dam will be operated for flood control, power generation and navigation. The water level of the reservoir will alternate between 175 and 145 m in winter and summer, respectively. The discharge will be increased from January to April for power generation, while from May to June the water level of the reservoir will be lowered to create capacity for flood control. The discharge will be reduced from October to November to recharge the reservoir. Above we argued that the water level change of the Yangtze River might affect the production of *V. spiralis* while influencing the light regime. So far, it is not understood how the reported operation of the Three Gorges Dam and the induced water level change in the Yangtze River might influence the light regime of *V. Spiralis* in Poyang Lake.

This study presents a model simulating the photosynthetically active radiation (PAR) reaching the top of *V. spiralis* canopy and discusses how the changes in water level of the Yangtze River induced by operation of the Three Gorges Dam may affect the PAR in Lake Dahuchi.

6.2 Materials and methods

6.2.1 Study area

Poyang Lake, the largest freshwater lake in China, is located between 115°47′-116°45′E, 28°22′-29°45′N at the southern bank of the Yangtze River (**Figure 6.1**). It is receives runoff water from five river watersheds of Raohe, Xinjiang, Fuhe, Ganjiang and Xiushui, meanwhile connects to Yangtze River at Hukou, which serves as the only outlet for the lake. The Poyang Lake national nature reserve (115°55′ -116°03′ E, 29°05′ -29°15′ N) lies in the northwest corner of Poyang Lake, and was established in 1988 to conserve the Siberian crane (Wu and Ji 2002, Li et al. 2005). The current study was carried out in Lake Dahuchi within the nature reserve, which is connected to Poyang Lake during high water in summer, but is disconnected when water levels are low in spring, autumn and winter.

6.2.2 Water level and Secchi disk depth

Lake Dahuchi is surrounded by creek banks of 14 to 15 m. Its water level is controlled from September to April by a sluice gate, connecting Lake Dahuchi with the Xiushui River. During high water levels, Lake Dahuchi connects with Poyang Lake, and its water level is, thus, affected by the Yangtze River and the five confluent rivers. To evaluate how the water levels of the Xiushui River, Poyang Lake (Ganjiang station) and the Yangtze River (Hukou station) affect the water level in Lake Dahuchi, we explored tentative relationships between gage data.

Water level and Secchi disk depth have been measured in Lake Dahuchi by the

Bureau of Jiangxi Poyang Lake National Nature Reserve and by the International Crane Foundation since 1999. Daily water level was recorded using a water level gauge. Secchi disk depth was measured using a standard 20 cm Secchi disk at five locations at weekly intervals from April until October. Daily Secchi disk depths were derived through linear interpolation from the recorded values.

The water level and Secchi disk depth records in Lake Dahuchi were incomplete for 1998-2000 and 2002, and, therefore, the water level data from the nearby station in the Xiushi River were used to replace the missing water level data for Lake Dahuchi. A non-linear relation between Secchi disk depth (SDD) and water level (WL) was observed while exploring the recorded water level and clarity data, which was described by a Huisman-Olff-Fresco (HOF) model (Eq. 1) (Huisman et al. 1993):

$$SDD = c_1 /(1 + e^{c_2 - c_3 * WL}) \quad (1)$$

where c_1, c_2 and c_3 are constants. Eq. 1 was then used to predict Secchi disk depth to complete the gaps in the Secchi disk time series from 1998 to 2006.

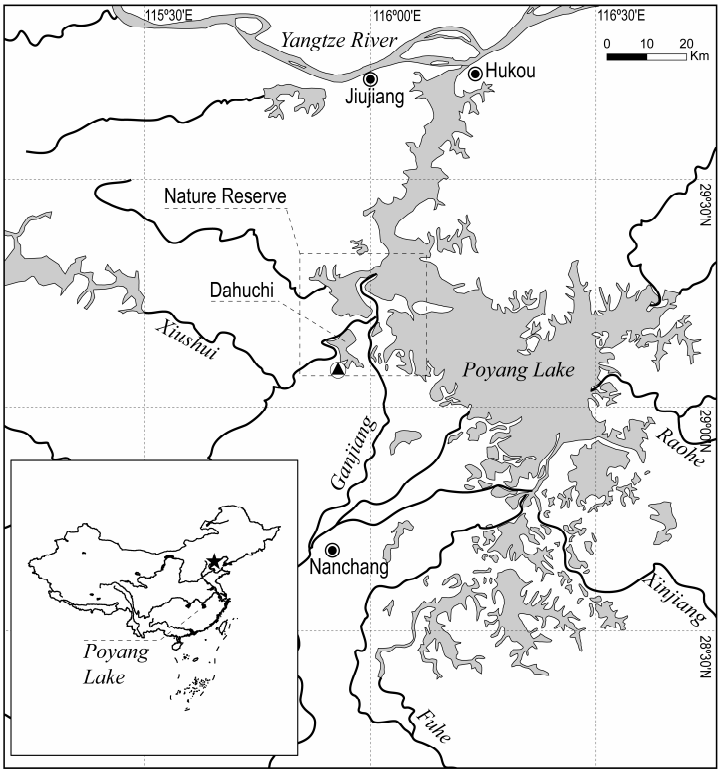

Figure 6.1. Location of Poyang Lake national nature reserve (Nature Reserve), Lake Dahuchi and Dahuchi Conservation Station (▲) in which daily photosynthetically active radiation (PAR) was measured.

6.2.3 Modelling photosynthetically active radiation (PAR)

The PAR reaching the top of *V. spiralis* canopy was estimated as follows. PAR at the

water surface (PAR_{+0}) was calculated from the global solar radiation recorded at Nanchang meteorological station (approximately 55 km from Lake Dahuchi), assuming that PAR accounts for 45% of the total global solar radiation (based on values of 50, 38 and 44% according to Doorenbos and Pruitt (1984), Zhang & Qin (2002) and Moon (Cited by Zhang et al. 2006b)). PAR at the top of the Dahuchi Conservation Station recorded from 6 July to 12 August and from 6 September to 10 November 2006 using a LI-190SA quantum sensor and a LI-1400 data logger (http://www.licor.com) served as a validation data set.

Subsurface PAR (PAR_{-0}) was calculated with Eq. 2, assuming a reflectance rate (k_r) of 4% according to Campbell & Aarup (1989) and Joshi (2005):

$$PAR_{-0} = PAR_{+0} * (1 - k_r) \quad (2)$$

Then the PAR at water depth d (PAR_d) was calculated according to Lambert-Beer's law (Eq. 3):

$$PAR_d = PAR_{-0} * e^{-k_{PAR} * d} \quad (3)$$

where the attenuation coefficient, k_{PAR} (m^{-1}), was derived from Secchi disk depth (SDD) records according to Eq. 4 (Poole and Atkins 1929):

$$k_{PAR} = a / SDD \quad (4)$$

where a is a constant, which may vary from case to case for different water types (Kirk 1994, Scheffer 1998). The value of a was determined using a LI-192SA quantum sensor and a LI-250A light meter (http://www.licor.com) to measure underwater PAR at various depths at 32 locations in Lake Dahuchi on 12 August and 16 October 2005. At the same time, the Secchi disk depth at each location was measured using a standard 20 cm Secchi disk. Then k_{PAR} was calculated according to Lambert-Beer's law (Eq. 5):

$$k_{PAR} = (\ln(PAR_{wd_1}) - \ln(PAR_{wd_2})) / (wd_1 - wd_2) \quad (5)$$

where PAR_{wd_1} and PAR_{wd_2} are PARs at water depths wd_1 and wd_2 (m) with $wd_2 > wd_1$. We estimated a while regressing K_{PAR} against SDD (**Figure 6.2**) according to Eq. 4 ($k_{PAR} = 1.133/SDD$, $R^2 = 0.98$, $F = 1836.495$, $n = 32$, $P < 0.005$). The standard error of the constant was 0.026, or 2% of the estimate.

Finally, PAR at water depth d and on the top of *V. spiralis* canopy (PAR_{tc}) was calculated according to Eq. 6 and 7 respectively, which integrate Eq. 2, 3 and 4:

$$PAR_d = PAR_{+0} * (1 - k_r) * e^{-(a/SDD) * d} \quad (6)$$

$$PAR_{tc} = PAR_{+0} * (1 - k_r) * e^{-(a/SDD) * (e_w - e_b - l)} \quad (7)$$

where e_w and e_b are water level and lake bottom elevation (m, National Vertical Datum 1985), respectively, and l is the height of the *V. spiralis,* which increases with the number of days since the first day of May (nd) according to a regression equation (Eq. 8) published by Wu & Ji (2002).

$$l = 9.94 * nd^{0.39} \quad (8)$$

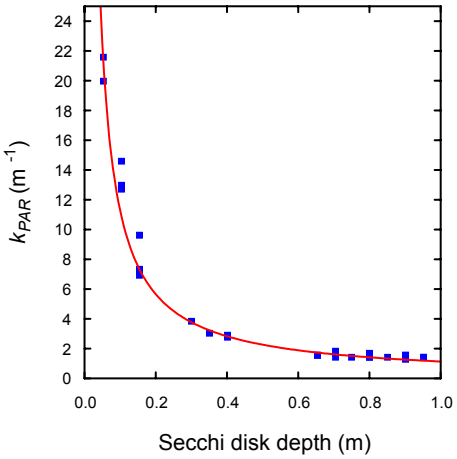

Figure 6.2. Relation between photosynthetically active radiation (PAR) attenuation coefficient (k_{PAR}) and Secchi disk depth.

6.2.4 Modelling PAR variation against water level

PAR_{tc} depends on the lake bottom elevation into which *V. spiralis* was rooted. In this study, the Eq. 7 and 8 were combined to simulate the temporal variation of PAR_{tc} for *V. spiralis* rooted at elevations of 12 and 12.8 m in Lake Dahuchi, respectively, which correspond to the least and most elevated boundaries of *V. spiralis* in this lake. Since *V. spiralis* forms tubers from July to September (Wu and Ji 2002), ANOVA was used to explore whether PAR_{tc} in this period differed between years.

The stepwise relation between water level and water turbidity might induce non-linearity in the relation between the PAR at a selected elevation and water level. Thus, by integrating the Eq. 1, 2, 3 and 4 into a new Eq. 9, PAR at a selected elevation *ele* (PAR_{ele}) in the lake can be calculated as a function of water level for exploring such non-linearity:

$$\begin{aligned} PAR_{ele} &= PAR_{+0} * (1 - k_r) * e^{-(a/(c_1/(1+e^{c_2 - c_3 * WL})))*d} \\ &= PAR_{+0} * (1 - k_r) * e^{-(a/(c_1/(1+e^{c_2 - c_3 * WL})))*(WL - ele)} \end{aligned} \quad (9)$$

6.3 Results

The seasonal variations of water levels of the Lake Dahuchi, Xiushui River, Poyang Lake (Ganjiang station) and Yangtze River (Huhou station) in 2004 and 2005 are shown in **Figure 6.3**. From mid-September to mid-May, the water levels in Lake Dahuchi were independent of those of the Xiushui River, Poyang Lake and the Yangtze River, and generally remained below about 14 m. More pronounced fluctuations of Lake Dahuchi between May and September showed a good correlation with the fluctuations in water levels of the Xiushui River (r = 0.84 and 0.94 in 2004 and 2005), Poyang Lake (r = 0.83 and 0.93 in 2004 and 2005) and the Yangtze River (r = 0.81 and 0.93 in 2004 and 2005). The water levels of the Yangtze River, Poyang Lake and the Xiushui River receded in September in both years, when the level of Lake Dahuchi deviated from those of the other systems. The Lake Dahuchi water level was slowly drawn down via a sluice to gradually expose shallow water food habitat to the foraging waterfowl from September onwards.

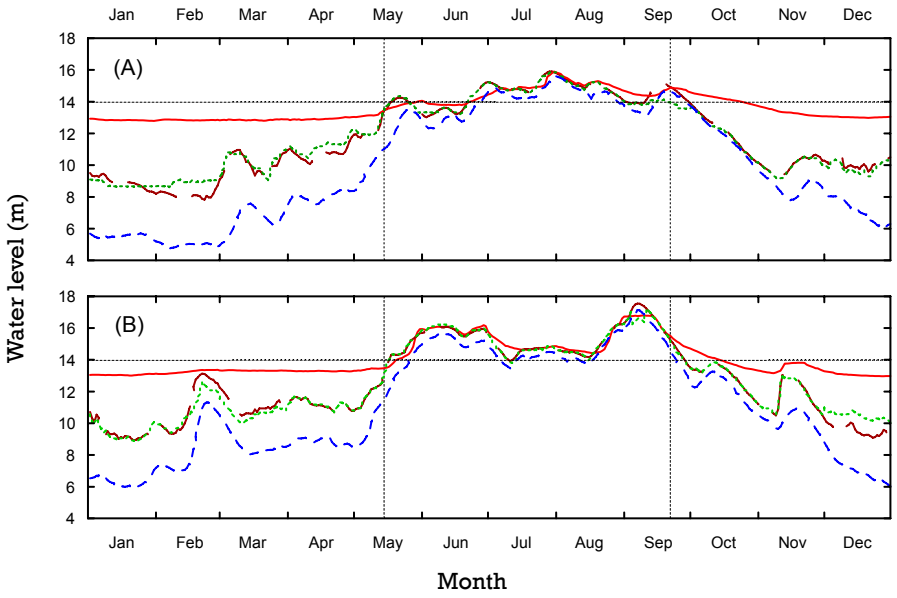

Figure 6.3. Water levels in Lake Dahuchi (——), Xiushui River (— —), Poyang Lake at Ganjiang (·····) and the Yangtze River at Hukou (- - - -) in 2004 (A) and 2005 (B). Vertical lines mark the onsets of water level in Lake Dahuchi being dependent and independent to that of Xiushui River in spring (about 14 May) and autumn (about 22 September) respectively.

The water level of Lake Dahuchi was linearly related to that of the Yangtze River at Hukou when the Yangtze River water level was higher than 14 m (**Figure 6.4**), but there was no relationship when the Yangtze River water level at Hukou was less than 14 m. In other words, Lake Dahuchi water levels below 14 m thus appears to be independent from that of the Yangtze River, while it is related above 14 m.

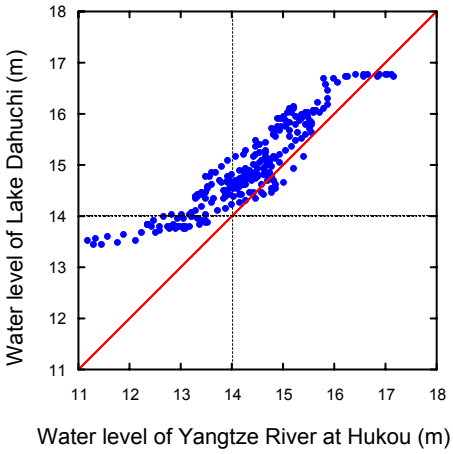

Figure 6.4. Relation between the water level of Lake Dahuchi and that of the Yangtze River at Hukou from 14 May to 22 September in 2004 and 2005.

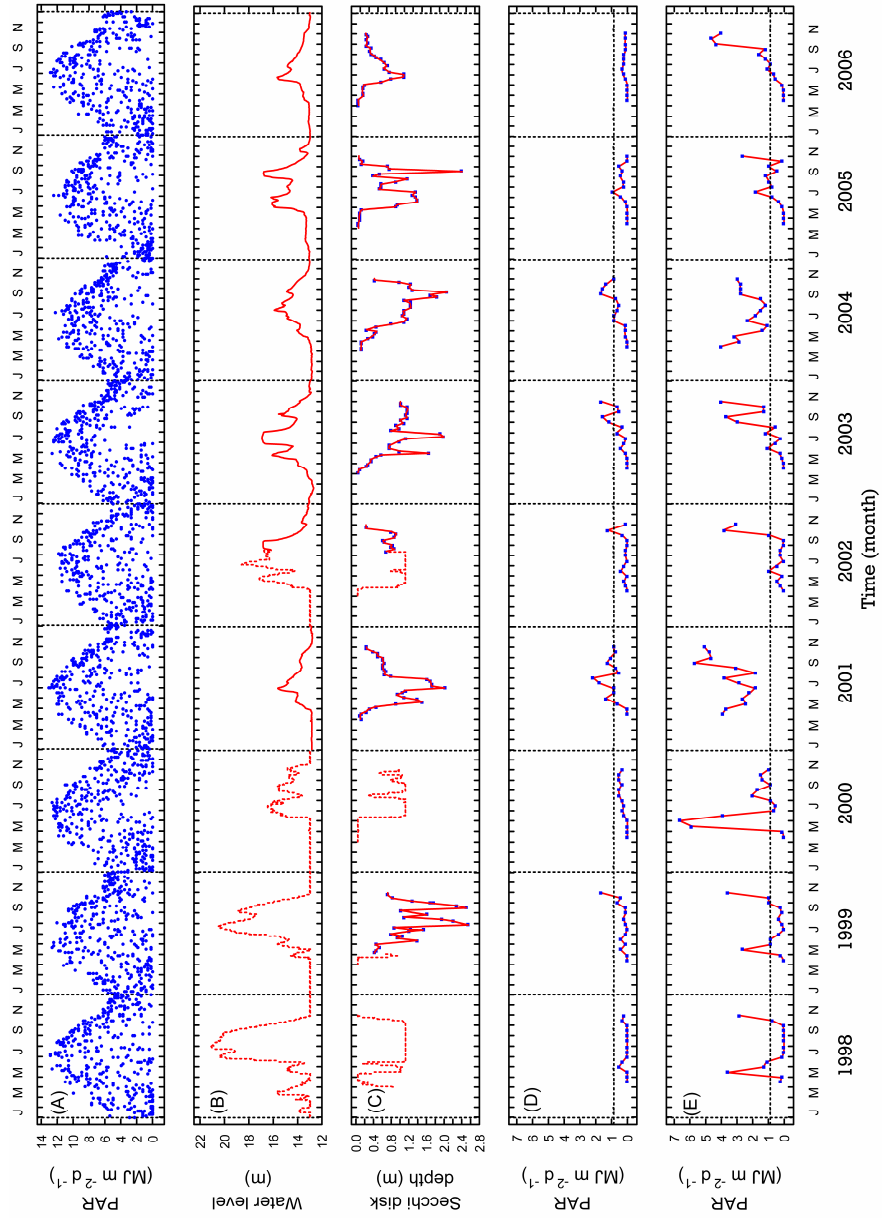

Figure 6.5. (A): estimated daily PAR at Nanchang station, (B): recorded daily water level in Lake Dahuchi (——) or Xiushui River (·····), (C): recorded (·), interpolated (——) or predicted (·····) Secchi disk depth, and (D) and (E): estimated daily PAR (averaged over two week periods) reaching the top of canopy of *V. spiralis* rooted at 12 and 12.8 m. Horizontal lines in (D) and (E) represent a limit of 9% surface radiation during sunshine period (Kimber et al. 1995, Dobberfuhl 2007) as being the threshold for tuber production in *V. americana*.

The daily PAR recorded in Nanchang meteorological station varied seasonally with the inclination of the sun and the variation in atmospheric conditions (**Figure 6.5** (A)). One-way ANOVA revealed that the PAR did not differ significantly between years (F = 1.728, $d.f.$ = 8, P = 0.08). Daily PAR extrapolated from Nanchang station predicted 88% of the variation of PAR at Dahuchi Conservation Station (F = 745.29, n = 105, P < 0.001). The prediction was unbiased as the intercept and slope of the regression did not differ significantly from zero (a = 0.23, $s.e.$ = 0.26, t = 0.909, $d.f.$ = 104, P = 0.39) and one (b = 1.02, $s.e.$ = 0.04, t = 0.535, $d.f.$ = 104, P = 0.59) respectively.

The water level from 1998 to 2006 (**Figure 6.5** (B)) revealed a seasonal pattern, from high in summer to low in winter. Summer water levels were high in 1998 and 1999 and low in 2001, 2004 and 2006.

The Secchi disk depth in Lake Dahuchi changed from almost or close to zero (turbid) at a water level below 13.5 m to around 1.1 m (clear) at a water level of 14.5 m (**Figure 6.6**). Water level (WL) explained 60% of the variation in Secchi disk depth (SDD) with the HOF model (SDD = $1.125/(1+e^{46.837 - 3.352*WL}$, F = 247.990, n = 155, P < 0.005). The low Secchi disk depth at a water level less than 13.5 m coincided with the period of lake recession between September - October and April - May of the following year (**Figure 6.5** (B)). From Figs. 5 and 6, it can be concluded that Lake Dahuchi switches from a turbid state between autumn and spring to a clear state in summer. The regression equation derived from the data shown in **Figure 6.6** was used to complete the Secchi disk depth record from 1998 to 2006 (called 'predicted') in **Figure 6.5** (C).

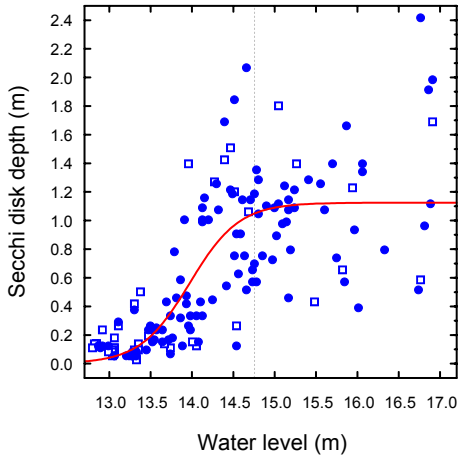

Figure 6.6. Relation between water turbidity (Secchi disk depth) and water level in Lake Dahuchi (• = measured in the field, ▫ = estimated from MODIS images (Wu et al. 2007a)).

Daily PAR (averaged over two week periods) reaching the top of the *V. spiralis* canopy rooted at an elevation of 12 m was generally low in spring and increased in summer and autumn (**Figure 6.5** (D)), while radiation reaching the top of the *V. spiralis* canopy rooted at an elevation of 12.8 m was considerably higher (**Figure 6.5** (E)). One-way ANOVA revealed that the annual PAR_{tc} from July to September differed significantly between years for plants rooted at elevations of 12 m (F = 92.07, $d.f.$ = 8, P < 0.001) and 12.8 m (F = 112.19, $d.f.$ = 8, P < 0.001), respectively. PAR levels at 12.8 m over this period remained continuously below the 9% irradiance threshold required for tuber production in the related species *V. americana* in 1998, 1999 and 2006, while for plants rooted at 12 m, this threshold was exceeded in 2001, 2003 and 2004 only.

The water level in Lake Dahuchi was extremely high from July to September in 1998 and 1999 (**Figure 6.5** (B)). PAR_{tc} was also reduced in both years **Figure 6.5** (D) and (E)), despite the fact that water was very clear in 1999 (**Figure 6.5** (C)). PAR_{tc} remained low as well when water levels were extremely low in 2005 and 2006.

The relationship between water level and water turbidity in Lake Dahuchi in **Figure 6.6** indicates that an increase in water level might increase rather than decrease the light availability at a certain elevation in the water column. Eq. 9 was thus used to calculate the PAR at various elevations as a function of water level (**Figure 6.7**). It turned out that for any elevation between 12 and 13 m, the available light intensity increased when the water level increased above 13.5 m, and peaked around 14.5 -15 m. For submerged vegetation with canopy at an elevation of 13 m, the PAR at a water level of 16 m is similar to that at water level of 13.5 m (about 5% of incident radiation); however, the available light intensity at an a water level of 14.5 m (about 17% of incident radiation) is three times higher. Thus, submerged aquatic vegetation canopies at elevations between 12 and 13 m receive less light than the requirement for tuber formation in the related *V. americana* at water levels less than 13.5 m. Increasing the water level increases the light intensity to levels surpassing the threshold for tuber production of *V. americana*.

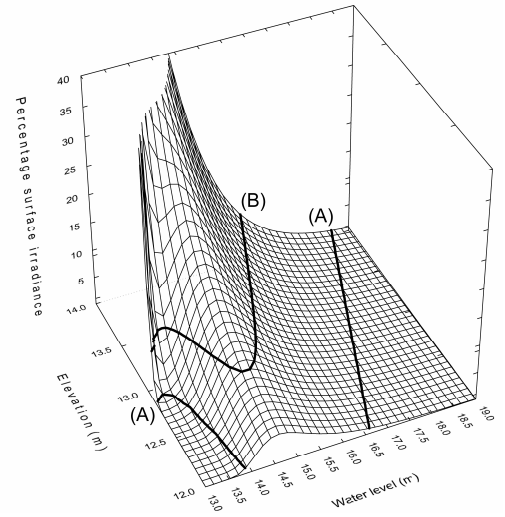

Figure 6.7. Percentage of surface irradiance reaching a lake bottom at a certain elevation as a function of water level. Light compensation point (1% surface irradiance, (A)) and threshold for tuber production (9% surface irradiance, (B)) reported for *V. americana* indicated by thick lines.

6.4 Discussion

This study revealed a strong seasonal and inter-annual fluctuation in PAR reaching the top of a *V. spiralis* canopy. These fluctuations were caused by variations in irradiance reaching the water surface, water level, attenuation within the water column, and height of the *V. spiralis* vegetation. Irradiance at the water surface varied strongly from day to day, but ANOVA revealed that it did not vary significantly between years. To what extent does the length of leaves influence the year to year variation in PAR_{tc}? Aquatic plant species elongate their leaves in response to low light intensities (Bowes et al. 1977, Cooling et al. 2001). The model used here (Eq. 8) does not account for such flexibility in leaf elongation, as it was based on observations from two years (1998 and 1999) with extremely high water levels. The predicted inter-annual variation in PAR reaching the top of canopy as shown in **Figure 6.5** can thus not be attributed to year to year variation in height of the *V. spiralis* vegetation, as we used the same model to

simulate the height for all years. We, thus, argue that the predicted inter-annual fluctuations in PAR reaching the canopy depend on fluctuations in water level and light attenuation within the water column. As light attenuation appeared in turn determined by water level, we conclude that water level exerts an overriding impact on the PAR reaching the canopy of *V. spiralis.*

We also reported a non-linear relation between water level and PAR at a given elevation in the lake water column. This non-linearity was caused by the sigmoid relation between water level and Secchi disk depth. Water with a high turbidity at a water level less than 13.5 m switched to a great clarity at a level above 14.5 m. The high turbidity at low water levels (below 13.5 m) is attributed to wave-induced sediment resuspension at the lake periphery, as is common in shallow lakes (Scheffer 1998). The increased clarity at elevated water levels above 14.5 m can be explained by reduced sediment resuspension since the lake fringe then overlays perennial grassland.

How would the combination of changes in water level and transparency influence the production of *V. spiralis*? Our results revealed that at water levels below an elevation of 13 m *V. spiralis* is exposed to light intensities below the compensation point reported for the related *V. americana*. We presume that this reflects the threshold of *V. spiralis*, as most submerged aquatic plants have compensation points close to 1 % of surface irradiance (e.g., Korschgen and Green 1988, Madsen et al. 1991, Blanch et al. 1998). The model presented here further suggests that water levels surpassing an elevation of 14 m are required to create the light conditions permitting tuber production. This suggestion is based on the assumption that the light requirement of *V. spiralis* for tuber formation is the same as that of the related *V. americana*, i.e., 9% of surface irradiance. Indeed we propose to further study the light requirements of *V. spiralis* regarding photosynthesis and reproduction.

We demonstrated that the water level of Lake Dahuchi tracked that of the Xiushui River, Poyang Lake and the Yangtze River at high water levels from May to September, which is the growing season of *V. spiralis*. We, thus, suggest that the levels of the Yangtze River and the inflows from the confluent rivers influence the production of *V. spiralis* through their impact on water level, clarity and light regime in Lake Dahuchi. Because the wintering Siberian crane forage on the tuber of *V. spiralis*, we, therefore, expect that the water regimes of the Yangtze River and the confluent rivers would be crucial for the productivity of the food source for the wintering Siberian crane.

Wang et al. (2005) reported that the Three Gorges Dam will change the water level of the Yangtze River in May and June. An advancement of the rise of the water level of the Yangtze River during the growth season of *V. spiralis* may force Lake Dahuchi out of its turbid state earlier and increase the light intensity reaching the canopy and the production of *V. spiralis.* On the other hand, a water level surpassing 14.5 m elevation would decrease the light intensity reaching the plant canopy. We anticipate, however, that the first possibility would occur more frequently than the second possibility, and conclude that the operation of the Three Gorges Dam is more likely to increase than decrease the light availability and productivity of *V. spiralis* on the short term. It remains difficult to assess the consequences of this for the Siberian crane, as we do not have accurate models to predict tuber biomass of *V. spiralis*, and do not know to what extent crane populations are limited by tuber biomass. However, as our results suggest that Three Gorges Dam is likely to improve the light conditions for biomass production we conclude that there is no reason to support the concerns that the Three Gorges Dam would negatively affect the production of food of Siberian crane.

Wang et al. (2005) also reported that the Three Gorges Dam will lower the bed of the Yangtze River due to increased erosion. Water levels in Shashi and Wuhan city are expected to recede by about 3 and 0.75 m, respectively, at a discharge of 30,000 $m^3 s^{-1}$ in the next 40 years. Such receding water levels may negatively impact the light availability and production of *V. spiralis*, but their impact would be difficult to assess since no prediction of the magnitude of such a water level recession on the Poyang Lake system exists.

The main finding of this research is the new insight that optimal light conditions for submerged vegetation are attained when water levels are pushed up by the Yangtze and other rivers. We suggest that this insight is crucial when aiming to predict the response of tuber forming macrophytes to hydrological change. In this respect it is interesting to note that hydrology will not only be affected by the Three Gorges Dam. A range of other large scale planning or ongoing engineering projects could influence the water levels of the Yangtze River and the confluent rivers of the Poyang Lake system as well. The South-to-North Water Transfer Project will reduce the discharge, and, thus, reduce the water level of the middle and lower Yangtze River (Cai et al. 2002). The hydrology of Poyang Lake will also be affected by reservoirs in its confluents (Song and Jin 2001). Water levels will be strongly influenced by the proposed Poyang Lake Control Project which aims to manage the lake level for multiple purposes (Xiong and Hu 2003). All these hydro-engineering projects might change the hydrology of Lake Dahuchi. We suggest that conservation of these wetlands and their fauna should be based on sound insights in their hydro-ecology.

CHAPTER 7

A CONCEPTUAL FRAMEWORK TO INTEGRATE A SIMULATION MODEL OF PLANT BIOMASS FOR *VALLISNERIA SPIRALIS L.* WITH REMOTE SENSING AND A GEOGRAPHICAL INFORMATION SYSTEM

Abstract

More than 95% of the world population of the endangered Siberian crane winter at Poyang Lake, China. They forage on the tubers of the submerged aquatic species, *Vallisneria spiralis L.*. The production of *V. spiralis* tubers depends on the local hydrological conditions. Ongoing and proposed engineering projects in the catchments of Poyang Lake and the Yangtze River might change the hydrology of the lake. It has been suggested that this might impact the production of *V. spiralis* tubers and thus affect the feeding habitat of Siberian cranes. In this paper, we propose a conceptual framework to integrate a simulation model of plant biomass for *V. spiralis* with remote sensing and a geographical information system. We discuss the possibility to employ VALLA, a plant growth model developed for the closely related *Vallisneria americana* to simulate the growth and biomass of *V. spiralis* tubers under various scenarios of water level and transparency. We also discuss the potential applications of remote sensing and geographical information system to measure hydrological variables required to drive the simulation model. We expect that the system, once implemented, could contribute to (i) evaluate the impact of possible hydrological changes in the future on submerged aquatic vegetation which attracts Siberian cranes (ii) enhance the ability to assess the impact of ongoing engineering projects and (iii) assess whether tuber feeding bird populations are constrained by the regional availability of food resources.

Published as:

Guofeng Wu, Jan de Leeuw, Elly P. H. Best, Jeb Barzen, Valentijn Venus, James Burnham, Yaolin Liu and Weitao Ji. *A conceptual framework for integrating a simulation model of plant biomass for Vallisneria spiralis L. with remote sensing and a geographical information system.* In Wetland and Water Resource Modeling and Assessment: A Watershed Perspective (Wei Ji, Editor), CRC Press / Taylor & Francis, USA, 13 December 2007.

7.1 Introduction

Submerged aquatic vegetation (SAV) forms a significant component of shallow lake and river ecosystems. It cycles nutrients, stabilizes flow, enhances water clarity, influences primary production, and protects the shores from erosion (Carr et al. 1997, Van Nes et al. 2003). Moreover, it provides an important food source for migratory birds. Bewick's swans (*Cygnus columbianus bewickii*), for instance, feed on the tubers of *Potamogeton pectinatus* in autumn in the Netherlands (Jonzen et al. 2002), while in Canada Trumpeter swans (*Cygnus buccinator*) forage on the tubers of *Potamogeton pectinatus* during spring (LaMontagne et al. 2003). Migratory North American waterfowl species in the tribe Athyini depend heavily upon tubers produced by a variety of SAV species (Korschgen 1989), and Siberian cranes (*Grus leucogeranus*) rely on the tubers of *Vallisneria spiralis L.* throughout the winter at Poyang lake, China (Wu and Ji 2002). Careful management of lake and river systems with SAV are therefore indispensable not only from the perspective of ecosystem health, but also for the conservation of migratory bird species.

Protected lake areas and backwater areas of rivers are not isolated water bodies, but are parts of larger watersheds. Natural or anthropogenic changes may influence these water bodies and, in turn, impact the growing conditions of SAV along with the availability of food for waterfowl. These changes can often be subtle. Van Vierssen et al. (1994), for example, described that SAV declined during the 1960s and 1970s in Lake Veluwe, the Netherlands, due to eutrophication caused by wastewater, and recovered following significant water quality improvement since the late 1980s. Harwell and Havens (2003) mentioned that elevated water levels and low water transparency during the late 1970s caused a decline in SAV density in Lake Okeechobee in south Florida. Similar changes in SAV abundance have also occurred in the Upper Mississippi River over fifty years (Jahn and Anderson 1986).

Poyang Lake (**Figure 7.1**), China, hosts an extremely high density of wintering birds, many of whom feed on *V. spiralis* tubers (Wu and Ji 2002). Large numbers of swans and virtually the entire world's population of Siberian cranes rely exclusively on this food source (Meine and Archibald 1996). *V. spiralis* tubers are also an important part of the diet of the endangered Swan Goose (Wu and Ji 2002). The production and availability of *V. spiralis* tubers depend on the local prevailing environmental conditions in both summer and winter. The environmental conditions, in turn, are not only influenced by the vegetation, birds, and activities of the local human community inside the protected areas, but also by the surrounding hydrological conditions. The Poyang Lake ecosystem is full of feedback systems operating among various biotic and abiotic factors (**Figure 7.2**). The hydrological conditions might also be changed due to ongoing and proposed engineering projects in the catchments of both Poyang Lake and the Yangtze River, as well as dredging as reported by Wu et al. (2007b).

Poyang Lake national nature reserve, designated with the highest conservation category in China, is the oldest protected area in Poyang Lake. It was established in 1988 to conserve the Siberian cranes, and places 5% of the total area of Poyang Lake under protected status. Proper management of this nature reserve requires the ability to forecast the impact of engineering projects on the productivity of *V. spiralis*. More importantly, the use of the nature reserve by tuber-feeding birds varies greatly among, as well as within, years (Kanai et al. 2002). Given the spatial scale of the entire Poyang Lake, models would be the only possible tool that could be used for predicting future impacts of multiple development projects over such a large and

heterogeneous landscape. In contrast, models required to develop this management tool are currently lacking in this region. Process-based shallow lake ecosystem models that incorporate hydrological variables and simulate SAV biomass would be ideally suited for such a purpose.

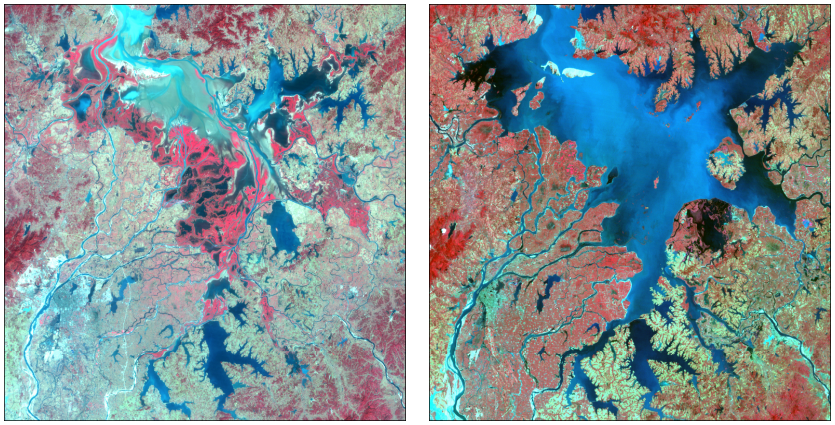

Figure 7.1. Landsat TM images of Poyang Lake. In dry season the water level is relatively low and numerous shallow lakes are disconnected from the main water body of Poyang Lake (Left image captured on 28 October 2004), while in summer all these lakes compose one large water body (Right image captured on 15 July 1989).

The nature reserve is composed of nine lakes encompassing approximately 224 km^2 (Wu and Ji 2002), while the entire Poyang Lake basin encompasses 4,500 km^2. It would be costly and difficult to measure the onsite environmental conditions in every lake within the reserve, much less among the various regions of the entire lake that cranes use (Kanai et al. 2002). Remote sensing (RS) techniques and geographic information system (GIS) might provide the means to quantify some of the variables required to drive the above-mentioned SAV biomass simulation models. In addition, a GIS could be used as a tool for the input, storage, retrieval, manipulation, analysis and output of these spatial data, and also serve as an intermediary for implementing the SAV biomass simulation models.

The objective of this paper is to propose a conceptual framework for the integration of a SAV biomass simulation model for *V. spiralis* with RS techniques and a GIS. After implementation, the system could be used to study the response of the growth of *V. spiralis* to changes in environmental conditions, and predict the density and mass of *V. spiralis* tubers in space and time. The potential roles of GIS and RS in this endeavour will be emphasized. The questions to be addressed and potential user communities will be outlined and discussed.

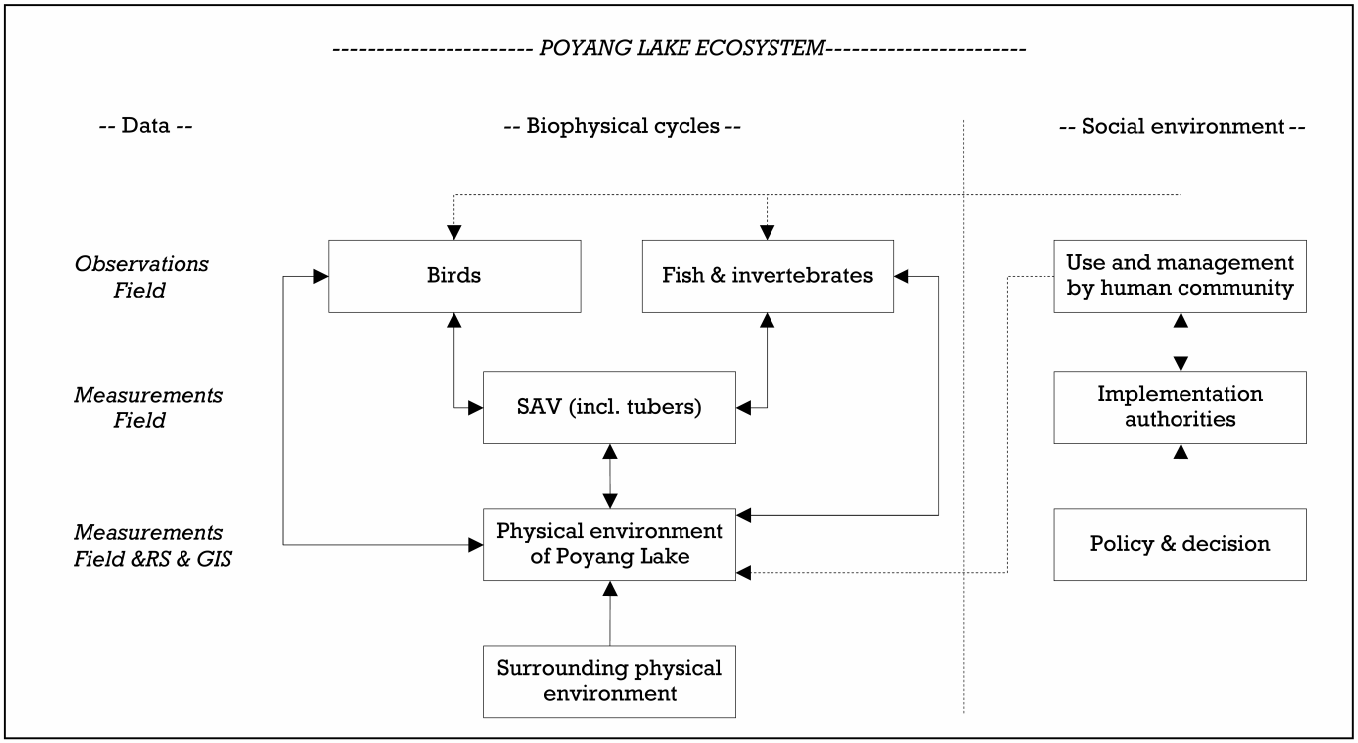

Figure 7.2. Hypothesized and important cause and effect interactions among environment, submerged aquatic vegetation and tuber-feeding birds in the Poyang Lake ecosystem, China. Solid lines: material flow; interrupted lines: activities and information flows; RS: remote sensing; GIS: geographical information system; SAV: submerged aquatic vegetation.

7.2 Ecology and production of *V. spiralis*

The production ecology of *V. spiralis* in Poyang Lake has been studied by Wu and Ji (2002). *V. spiralis* winters as tubers and seeds. It sprouts in April, flowers in June, reaches its maximum aboveground biomass in mid-September and fills its tubers from mid-July until shoots senesce in late October. Field measurements in 1999 indicated that aboveground plant biomass decreased from the shore to the centre of the lakes. The average shoot density close to the shore was about 50 to 70 stems/m^2, and individual fresh weight of each green shoot at maximum extent averaged about 12 g/stem. In areas with high tuber abundance, tuber density reached 10 to 70 tubers/m^2 with a biomass range of 6 to 45 g fresh weight/m^2. Wu and Ji (2002) concluded that water level, light intensity, temperature and chemical properties of the water influenced growth and production of *V. spiralis* most. The importance of water level was demonstrated by the observation that the *V. spiralis* population collapsed during the flood of 1998, when water levels were more than four meters higher than in normal years (Wu and Ji 2002).

7.3 SAV simulation models

Relationships between environmental variables and the biomass of SAV have been included in a variety of plant growth simulation models (Collins and Wlosinski (1989), Scheffer et al. (1993), Calado and Duarte (2000), Best and Boyd (2001b), Van Nes et al .(2003), Herb and Stefan (2003), Giusti and Marsili-Libelli (2005)). Some of these models are generic, such as Charisma (Van Nes et al. 2003), while others focus on one species, for example MEGAPLANT for *Potamogeton pectinatus L.* (Scheffer et al. 1993, Hootsmans 1994) and VALLA for *Vallisneria americana Michx.* (Best and Boyd 2001a).

All these models include descriptions of the seasonal growth cycle. The modelled plants may survive the winter as shoots or as wintering structures (tubers or seeds). Growth is initiated at a preset day, and from that moment onwards, each wintering structure transforms a fixed daily percent of its remaining biomass into the sprout. At a later preset day, aboveground biomass is transformed into belowground structures that survive the winter.

Environmental factors and vegetation characteristics influence growth. The macrophyte characteristics were modelled with different degrees of complexity. For example, Best and Boyd (2001a) considered different vertical layers within the shoot biomass, plant organs, and $\geq$1 tuber cohort sprouting per year, while Hootsmans (1994) took the formation of a second shoot into account.

Of particular relevance for our current case is VALLA (Best and Boyd 2001a), a model that has been developed for *V. americana*, a species closely related to *V. spiralis*, and can be run at climates varying from temperate to tropical. This model has been used to evaluate the feasibility for *V. americana* to recolonize rehabilitated navigation pools of the Illinois River, USA (Best et al. 2004). It has also been used for ecological risk assessment of planned changes in commercial navigation on the Upper Mississippi River (UMR) (Bartell et al. 2000). After recalibration for fast-flowing river conditions (Best et al. 2005), the model is currently being used to evaluate the tentative effects of changes in water level management in navigation pools of the UMR, USA, on the tuber availability for wintering waterfowl (including Tundra swans). The latter UMR case is similar to the current Poyang Lake case, in which a major goal is to evaluate the tuber availability for the Siberian cranes and other tuber-grazing waterfowl.

Field data published by Wu and Ji (2002) suggest that the species of *V. spiralis*

occurring in Poyang Lake is unclear. Wu and Ji (2002) also described the development cycle and showed the prevalent Poyang Lake *V. spiralis* species produces relatively small shoots and large tubers compared to the default *V. americana* species used for the latest recalibration of VALLA for the UMR. A clearer description of the Poyang Lake *V. spiralis* has been provided now, and new seeds are currently available, so the identification of the Poyang Lake *V. spiralis* species should be possible. Once VALLA is recalibrated for the Poyang Lake *V. spiralis* species, various scenarios of water level and transparency changes expected from development projects could be modelled and the impacts on the tuber production in Poyang Lake might be predicted. Other research on use of tubers by birds could then be incorporated into this model to predict changes to the carrying capacity of wintering waterfowl that feed on tubers.

7.4 Conceptual framework integrating SAV simulation model with RS and GIS

Typically models have been used to simulate the impact of changing environmental conditions on SAV, and it would be tempting to combine these growth simulation models with GIS to make predictions across spatially heterogeneous environments. Huang and Jiang (2002) distinguished three approaches to integrate environmental models with GIS: loose, tight and full coupling. Loose coupling relies on the transfers of data files between stand-alone GIS and environmental models. For tight coupling, the environmental models are usually embedded within a GIS, and the interactions between them depend on the parameter transfers. Full coupling is a full integration of environmental models within GIS, generally using an advanced programming language or GIS macro language.

We propose a conceptual framework (**Figure 7.3**) of loosely integrating VALLA with RS and a GIS for simulating the plant and tuber biomass of *V. spiralis*. This framework consists of three main components: GIS, RS and the SAV simulation model. RS and GIS will be used to estimate spatial distributions of important environmental variables that vary frequently and have not been recorded in the field, such as solar radiation reaching the water surface and water temperature. Additionally, the GIS is also used to input, store, retrieve, manipulate, analyze and output spatial variables and other spatial data, such as solar radiation, digital elevation model (DEM), light attenuation and spatial distribution of tuber biomass. The SAV simulation model imports the environmental variables from GIS, simulates the plant and tuber production of *V. spiralis,* and exports the results to GIS for analysis and visualization.

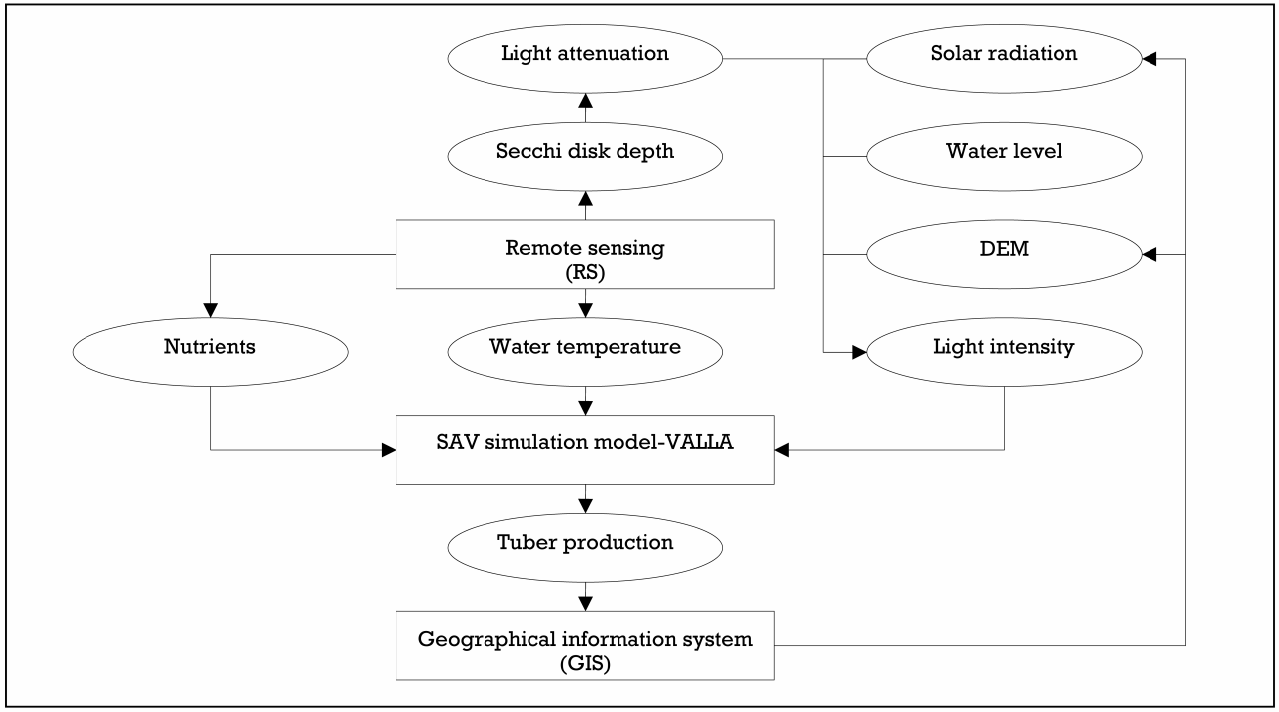

Figure 7.3. A conceptual framework integrating a SAV simulation model of *Vallisneria spiralis L.* with RS and a GIS. Solar radiation represents the global solar radiation reaching the water surface, and light intensity represents the light intensity reaching the canopy of SAV.

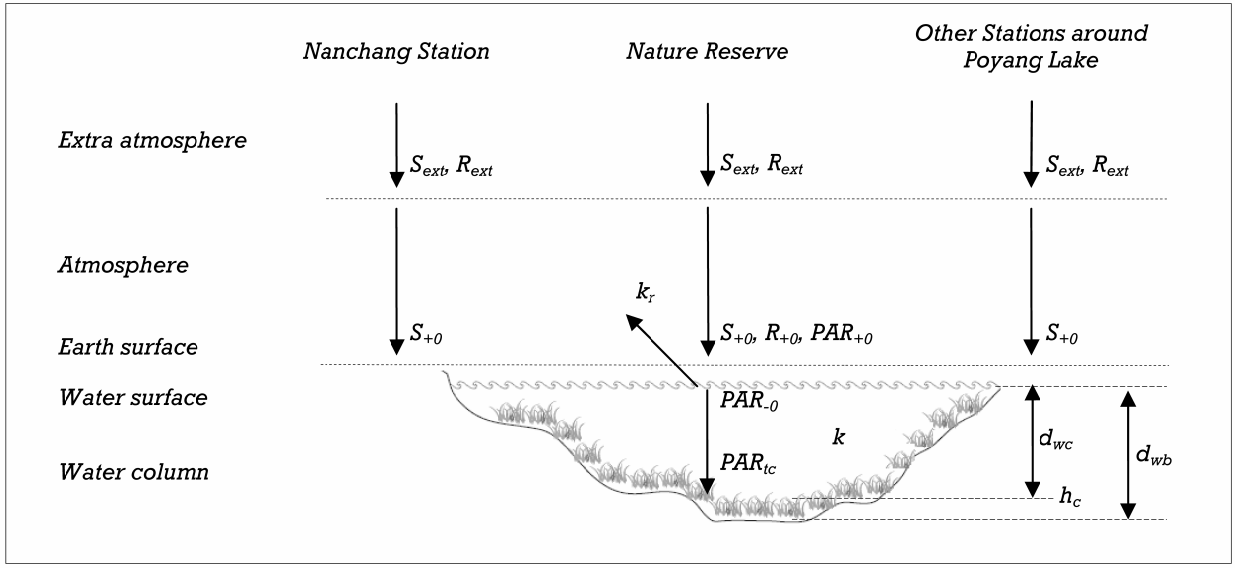

Figure 7.4. Model to calculate the light intensity reaching the canopy of SAV. R_{ext}: extra atmosphere global solar radiation; S_{ext}: extra atmosphere or potential sunshine hours; R_{+0}: global solar radiation reaching the earth or water surface; S_{+0}: measured or estimated sunshine hours on the earth or water sutface; PAR_{+0}: PAR reaching the earth or water surface; PAR_{-0}: PAR entering water body; PAR_{tc}: PAR reaching the canopy of SAV; k_r: reflection coefficient on water surface; k: light (PAR) attenuation coefficient in water column; d_{wb}: water depth; h_c: height of SAV; d_{wc}: height of water column above canopy.

7.5 Environmental variables and their measurements in Poyang Lake

SAV simulation models require input data such as light intensity reaching the canopy of the vegetation, water temperature and the concentrations of nutrients and CO_2. The spatial distribution of none of these variables has been measured in Poyang Lake. However, a number of associated variables which could be used to derive light intensity reaching the canopy, such as water level and Secchi disk depth (SDD), have been measured. These *in situ* measurements, however, have been collected for a few lakes only. Confronted with such problems the geoinformation technologies could be correlated with limited *in situ* sampling and be used to measure or infer environmental variables for large areas without *in situ* sampling.

The light intensity reaching the canopy of the *V. spiralis* is probably the most important variable to be measured since the availability of light is the primary factor controlling photosynthesis of SAV, a primary plant function that drives biomass growth, in most aquatic systems (Carr et al. 1997). Light at the canopy level is determined by the radiation reaching the water surface, reflection by the water surface, and penetration of the light through the water column to the canopy of SAV (**Figure 7.4**). Presently no reliable solar radiation estimates exist for Poyang Lake, and the closest station with such data, Nanchang is 65 kilometres away.

Measurements of sunshine hours (S_{+0}) are available for eight stations around Poyang Lake. We combined these data with a triangulated irregular network (TIN) and inverse distance weighting (IDW) interpolation method to interpolate sunshine hours over the lake. Chen et al. (2006a), analyzing the daily global radiation data and sunshine hours from 1994 to 1998 at 86 stations in China, reported that 92% of the daily global radiation could be explained by daily sunshine hours. We applied this model combined with sunshine hours derived through interpolation to estimate daily global solar radiation (R_{+0}) within the nature reserve. A possible alternative could be using the duration of cloud cover derived from low resolution satellite images to predict daily solar radiation (Kandirmaz et al. 2004). We are currently studying the possibility to predict solar radiation over Poyang Lake from hourly records of cloud cover recorded by the Chinese Fengyun-2C (FY-2C) geostationary meteorological satellite.

The radiation reaching the canopy depends on the light attenuation and depth of the water column (d_{wc}) above the canopy of SAV. The d_{wc} can be derived while using the DEM, measured water levels and vegetation height. Light attenuation (k) is related to SDD (**Figure 7.5**), a variable that has been recorded in three lakes within the nature reserve and one lake immediately adjacent to it since 1999. Lillesand and Chipman (2001) mentioned the potential of using low-resolution MODIS satellite data to estimate SDD of large lakes. Lillesand (2004) reported that 79% of variation of weekly to biweekly SDD of eleven inland lakes in Wisconsin could be explained by the ratio of the blue and red MODIS bands. Using the *in situ* SDD measurements collected in 2004 and 2005 within nature reserve, we developed a regression model between the natural logarithm of SDD and the blue and red bands of MODIS, and it also explained 88% of the SDD variation (Wu et al. 2007a). The SDD predicted from MODIS imagery could thus be used to complement information on water transparency for those lakes where measurements have not been taken. Moreover, it provides a synoptic overview of the variability in transparency within lakes.

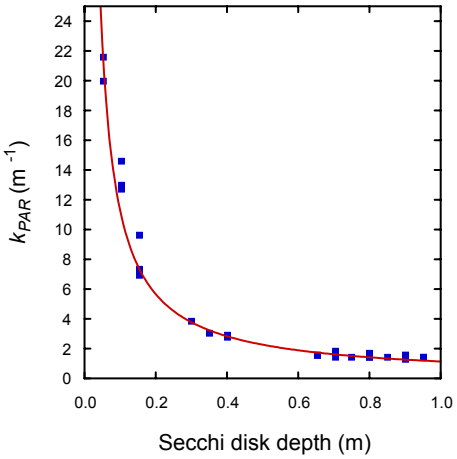

Figure 7.5. Relation between the attenuation of photosynthetically active radiation (K_{PAR}) and Secchi disk depth (R^2 = 0.98).

We implemented the combination of radiation estimates over the lake and SDD with other field based measurements to calculate the radiation reaching the canopy of vegetation, which could then be used as an input to a SAV simulation model coupled to a GIS.

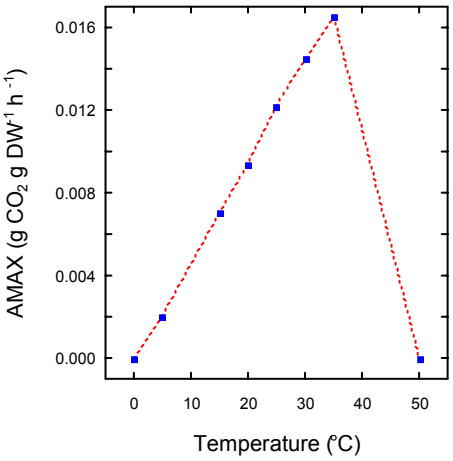

Figure 7.6. CO_2 assimilation capacity at light saturation (AMAX), based on data published by Best and Boyd (2001a).

Another important required variable is water temperature, as it has a pronounced influence on photosynthesis. Photosynthesis over the whole canopy is integrated from instantaneous CO_2 gross assimilation rates, and it is a function of absorbed light energy and the photosynthesis light response of individual shoots. As only a small portion of the total incoming solar radiation is used in photosynthesis, growth rates of individual shoots largely depend on the maximum rate of assimilation (AMAX). AMAX is the actual CO_2 assimilation rate at light saturation for individual shoots, which responds dynamically to varying water temperatures at different water depths. For the related species, *V. americana*, AMAX-to-temperature relations are given in **Figure 7.6**.

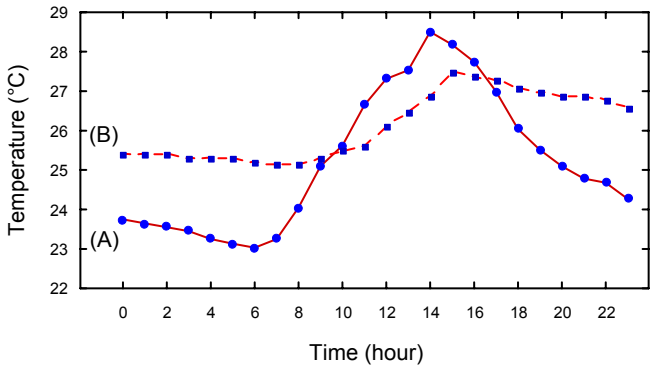

Figure 7.7. Average diurnal water temperature from August to September 2005 at water depths 0.5 (A) and 1 (B) m respectively in Poyang Lake.

Water temperatures show a diurnal progression, and its amplitude varies with different water depths, as can also be seen from **Figure 7.7**. Combining AMAX-to-temperature (**Figure 7.6**) and diurnal temperatures as observed over Poyang Lake (**Figure 7.7**), it is evident that neither daily average water temperatures from synoptic observations nor observations from polar-orbiting satellites capture diurnal CO_2 gross assimilation rates well. So it is necessary to obtain radiation and temperature data with higher temporal resolution (hourly).

At present, no record of seasonal variation of water temperature within the nature reserve exists. RS offers the possibility to measure surface water temperature. For example, Fox et al. (2005) employed SeaWiFS and AVHRR to estimate the spatial and temporal distributions of water temperature, while Handcock et al. (2006) studied the accuracy and uncertainty of water temperature estimates from the thermal-infrared band of ASTER, MODIS and Landsat ETM+ images.

Despite authors have successfully been able to use imagery from polar-orbiting satellites to estimate water temperatures, too few clear sky observations remain to satisfy our strict model requirements. This gap is due to the relatively low temporal resolution of the images. A challenge lies in the use of geo-stationary satellite data to estimate water temperature and insolation commensurate with the temporal and radiometric requirements of our objective. Fengyun-2C (FY-2C), a geo-stationary meteorological satellite operated by the General National Satellite Meteorological Center (NSMC) of China, observes a large part of Asia centred at 105 degrees east. Future work is focusing on the development of algorithms for estimating water (skin) temperature and solar irradiance from this relatively new sensor. Theoretically, temperature and radiation can be determined 24 times per day from FY-2C, but in practice fewer observations are available due to cloud cover. Based on these estimates, an attempt will be made to model underwater temperature and light conditions using an inductive modelling approach as the optimum water depth for the growth of *V. spiralis* is at 2 to 3 meters depth, and not at the surface (Chambers and Kalff 1987).

The temporal or spatial distribution of other environmental variables, such as total phosphorus and total nitrogen, have also been studied through RS by several researchers (Dewidar and Khedr 2001, Wang and Ma 2001), and their implementation possibilities in Poyang Lake could be explored in the future.

7.6 Questions to be addressed

A SAV simulation model coupled to a GIS as described above could be used to address important environmental questions, of which three major ones are summarized here.

First, plans are underway to change the hydrology of the Poyang Lake and the Yangtze River. Concern has been expressed that those hydrological changes could negatively affect *V. spiralis* production and therefore the feeding habitat of wintering Siberian cranes or other tuber-feeding waterfowl. To hydrological engineers and resource planners it would be useful to quantitatively evaluate the impact of future hydrological changes on biota, especially where endangered species are involved, as is the case at Poyang Lake (Wu and Ji 2002). Development plans could then be redesigned and expensive alterations, once infrastructure has been built, can be avoided.

Second, once engineering projects have been completed, it is important to evaluate the impacts of hydrological changes on the ecosystem in which the SAV plays an important role. With the Three Gorges Dam approaching completion, it is not yet understood how various potential water management scenarios from the dam may (or may not) affect SAV production at Poyang Lake, located downstream of the Three Gorges Dam. Predicting impacts from the Three Gorges Dam is difficult because there is a tremendous seasonal and year-to-year hydrological variability. Dredging is another activity changing the hydrology of Poyang Lake (Wu et al. 2007b). It has been suggested that it might influence the production of *V. spiralis,* but the exact impacts remain to be assessed. SAV-dominated ecosystems of Poyang Lake likewise respond to hydrological variability (International crane Foundation and Bureau of Poyang Lake national nature reserve, unpublished data). SAV simulation models, like VALLA, might augment our understanding of the system behaviour and allow us to assess the most important variables to monitor. A calibrated model predicting tuber biomass production, as affected by hydrology, will also enable us to distinguish between future changes in tuber biomass attributed to natural seasonal and year-to-year variations versus man-made hydrological changes.

A third application of a SAV simulation model could be to evaluate whether tuber feeding bird populations are constrained by the available food sources and in what years. Such an analysis can only be undertaken at the level of the catchments within which the birds reside. Application of GIS-based SAV models might ultimately enable conservationists to address such questions.

CHAPTER 8

SYNTHESIS

8.1 Introduction

Almost 95% of the world's population of Siberian crane (*Grus leucogeranus*) winter in Poyang Lake, where they forage on the tubers of the submerged aquatic macrophyte *Vallisneria spiralis L.* The growth and production of *V. spiralis* are regulated by the local hydrological conditions, which might not only be influenced by the local factors, but also be modified by the changed hydrology of the Yangtze River induced by the ongoing and proposed engineering projects. This study investigated the impact of the dredging activities in the northern Poyang Lake and the Three Gorges Dam in the Yangtze River on the water turbidity and water level of Poyang Lake, analyzed how these hydrological changes influenced the underwater light climate of *V. spiralis*, and discussed their potential impacts on the growth and productivity of *V. spiralis* and further on the food habitat of Siberian crane in Poyang Lake.

This chapter summarizes the main results and their interrelationships in this study, and addresses future works.

8.2 Main results and their interrelationships

(1) MODIS offers possibility to monitor water clarity regularly and cheaply in relatively big and frequently cloud covered lakes

The potential of remote sensing to assess the dynamics of water clarity has been explored since the launch of the Landsat satellites in the 1970s. Regular monitoring is, however, hampered by frequent cloud cover and low revisit time repeat. Moderate resolution imaging spectroradiometer (MODIS) could be more suitable to monitor such dynamics. However, this potential has rarely been explored in inland water bodies.

Chapter 2 compared two image sources, MODIS and Landsat thematic mapper (TM), for mapping the tempo-spatial dynamics of water clarity. Time-series *in situ* records of water clarity (Secchi disk depth) were related to five Landsat TM and twenty two MODIS images respectively. Two multiple regression models including the blue and red bands of Landsat TM and MODIS respectively explained 83% and 88% of the variation of the natural logarithm of Secchi disk depth. The standard errors of the predictions were 0.20 and 0.37 m for Landsat TM and MODIS-based models.

Compared with MODIS, Landsat TM provides finer spatial resolution and more historical information of water clarity; it has less signal reflectance from the water column and lower orbital repeat cycle. MODIS has several advantages over Landsat TM, such as its daily and near-daily coverage, better spectral sensitivity and cost-free distribution. On the basis of the comparison of water clarity predicted from Landsat TM and MODIS data as well as the advantages and contras of both sensors, it is concluded that MODIS could offer the possibility to monitor the dynamics of water clarity more regularly and cheaply in relatively big and frequently cloud covered lakes like Poyang Lake.

(2) Landsat TM mid-infrared bands hold potential in ship detection in turbid water

Simultaneous information of ship and water turbidity could improve the strength pf evidence of dredging impact assessments. Synthetic aperture radar (SAR) has been frequently and successfully applied to detect ships because it can be applied day and night under most meteorological conditions. It, however, does not allow synchronic

detection of vessels and water turbidity. The visible and near infrared bands of Landsat have limitation for detecting ships, especially in turbid water. Therefore, it is interesting to explore the capability of mid-infrared bands of traditional optical remote sensing systems for ship detection.

Chapter 3 analyzed the performance of the various Landsat TM bands for detecting dredging ships in the turbid water of the northern Poyang Lake, China. The result revealed that the TM bands 1 to 4 had limitation especially in turbid water, while bands 5 and 7 held great potential in ship detection. The significant correlations between reflectance ratio and water turbidity in bands 1 to 4 could explain the limitations of bands 1 to 4; while water turbidity has no significant impact on the reflectance of bands 5 and 7, which could explain why the bands 5 and 7 provided stronger capacity compared with bands 1 to 4 in ship detection. Therefore, it is recommended using the mid-infrared bands of Landsat TM for operational ship monitoring in turbid water.

(3) Simultaneously monitoring the water turbidity and vessels enhanced the strength of evidence in remotely sensed dredging impact assessments

Dredging is an economic activity with pronounced environmental impacts. Remotely sensed assessment of dredging impacts on water turbidity is straightforward when turbidity plumes show up in clear water. It is, however, more complicated in turbid waters as the spatial or temporal changes in turbidity might be of natural origin. The plausibility of attributing turbidity patterns to dredging activities would be greatly enhanced when demonstrating the association between dredging infrastructure and water turbidity.

Chapter 4 investigated the possibility to strengthen inference of dredging impact while simultaneously monitoring vessels and water turbidity in the northern Poyang Lake, China. One MODIS-based water clarity model was developed in Chapter 2, and it was applied to derive the historical change of water clarity from 2000 to 2005 in northern Poyang Lake. Chapter 3 reported that the mid-infrared bands of Landsat TM 5 images hold potential in ship detection in turbid water. Therefore, time-series Landsat TM images were used to estimate ship from 2000 to 2005. MODIS images revealed a significant increase in water turbidity from 2001 onwards, while Landsat TM image analysis indicated a simultaneous increase in the number of vessels. Regression analysis further showed a highly significant positive relationship ($R^2 = 0.92$) between water turbidity and vessel number.

On the basis of discussion of ship-related resuspension, final destinations of vessels and coincidence of vessel clusters with irregular dented patterns and turbid plume development when clear waters upstream passing the first vessel cluster, it is confirmed that dredging caused the increase in water turbidity. Therefore, the study revealed that simultaneously monitoring water turbidity and vessels enhanced the strength of evidence in remotely sensed dredging impact assessments.

The increased water turbidity caused by dredging may decrease the available light for photosynthesis of *V. spiralis*, and consequently may cause a decrease or disappearance of the food source of Siberian cranes.

Chapter 2 and 3 provided necessary methods for deriving historical information of water clarity and ships, which contributed to the conclusion that the dredging resulted in the decline of water clarity in the northern Poyang Lake.

(4) Spatial interpolation method hold more potential in predicting the spatial distribution of solar radiation than extrapolation methods

Photosynthetically active radiation (PAR) is an important factor determining the growth and productivity of plants, and the accurate information of PAR is indispensable for simulating the growth and productivity of plants.

Chapter 5 compared three extrapolation and interpolation methods for predicting daily PAR reaching the earth surface over the Poyang Lake national nature reserve, China. The result revealed that: (1) the triangulated irregular network (TIN) and inverse distance weighted (IDW)-based interpolation method achieved the best prediction of PAR ($R^2 = 0.89, s.e. = 1.02, F = 830.02, P < 0.001$) in all tested methods; (2) the extrapolation method from Nanchang station got moderate result ($R^2 = 0.88, s.e. = 1.07, F = 745.29, P < 0.001$); (3) the extrapolation method from Yongxiu station also produced acceptable prediction ($R^2 = 0.87, s.e. = 1.14, F = 669.76, P < 0.001$); however, (4) the extrapolation methods from Xingzi and Duchang station were not suitable for this specific site for their biased predictions.

Considering the assumptions and principles supporting the extrapolation and interpolation methods, it is concluded that the interpolation method produce more reliable result than the extrapolation methods and hold the greatest potential in all tested methods to be applied over the whole nature reserve.

(5) Water level induced by the Three Gorges Dam affects the radiation regime of *V. spiralis* and may affect the food habitat of Siberian crane

The growth and production of submerged vegetation are controlled primarily by light intensity reaching its canopy, water temperature, CO2 and nutrient concentration. Light intensity likely controls the growth and production of *V. spiralis* as it is highly variable in waters with fluctuating water depth and clarity such as Poyang Lake.

Chapter 6 modelled the photosynthetically active radiation reaching the top of *V. spiralis* (PAR_{tc}) in Lake Dahuchi from 1998 to 2006. PAR_{tc} was calculated from incident radiation while considering losses due to surface reflectance, absorption and scatter within the water column. The results revealed significant between year differences in PAR_{tc}, which was determined primarily by fluctuation in water level. Six years of Secchi disk depth records revealed seasonal switching of the lake from turbid at low water level in autumn, winter and spring to clear at high water level in summer. The highest PAR_{tc} occurred at intermediate water levels, which were reached when the Yangtze River forces Lake Dahuchi out of its turbid state in spring.

The operation of the Three Gorges Dam, which will increass water level of Yangtze River from May to June may force Lake Dahuchi out of its turbid state earlier and increase the Light intensity reaching the canopy and the production of *V. spiralis.* The impact on light regime would become negative when forcing Lake Dahuchi to water levels above 14.5 m. However, it is anticipated that the first would be more frequent than the second. It is concluded that the operation of the Three Gorges Dam will at the short term increase the light regime and productivity of *V. spiralis* and possibly affect the food habitat of Siberian crane in Poyang Lake.

The solar radiation on the top of canopy of *V. spiralis* is determined by that reaching the earth surface, water level, light attenuation and vegetation length (Chapter 6). Chapter 5 compared the extrapolation and interpolation methods for predicting the solar radiation reaching the earth surface within the Poyang Lake national nature

reserve, and established the foundation for estimating the radiation reaching the top of canopy of *V. spiralis*.

Light attenuation in the water column affects the solar radiation reaching the top of canopy of *V. spiralis*. This study revealed that the light (photosynthetically active radiation) attenuation coefficient (Chapter 6) was significantly related to water clarity recorded in the field and derived from MODIS images (Chapter 2).

In addition, the Secchi disk depth demonstrated a remarkable seasonal pattern of water clarity (Chapter 6) in Lake Dahuchi, namely, water clarity was low in winter and spring, increased in April or May to reach the highest values in summer, upon which it gradually declined from September onward. The similar seasonal pattern was observed in other lakes with the nature reserve, even in Poyang Lake from remote sensing image analysis. The dredging activities not only change the seasonal pattern of water clarity in the northern Poyang Lake (Chapter 4), but could decline the water clarity in central and southern Poyang Lake, even within the nature reserve when the backflow from Yangtze River to Poyang Lake happened from July to September (unpublished result). Therefore, we suggested that the dredging activities could decrease the light regime and productivity of *V. spiralis* and negatively affect the food habitat of Siberian crane in Poyang Lake.

(6) Integration of a simulation model of plant biomass with remote sensing and a geographical information system could contribute to evaluate the impact of possible hydrological changes on *V. spiralis.*

A conceptual framework to integrate a simulation model of plant biomass for *V. spiralis* with remote sensing and a geographical information system was introduced in Chapter 7. It is expected that the system, once implemented, could contribute to (i) evaluate the impact of possible hydrological changes in the future on submerged aquatic vegetation which attracts Siberian cranes (ii) enhance the ability to assess the impact of ongoing engineering projects and (iii) assess whether tuber feeding bird populations are constrained by the regional availability of food resources in Lake Poyang.

The model needs several important inputs such as light intensity reaching its canopy, water temperature, CO_2 and nutrient concentration. Chapter 6 estimated the light intensity reaching the top of canopy of vegetation, and made necessary preparation for implementing the model.

8.3 Future works

For assessing the food habitat of Siberian crane, several interrelated issues were addressed in this study. However, this study did not cover all aspects related to the food habitat of Siberian crane. There are some important issues that need to be investigated, and some of the aspects dealt with in this study need further exploration for achieving this objective. The future works relevant to this study are as follow:

(1) Assessing dredging impact

Dredging is an economic activity with pronounced environmental impacts. The dredging activities in northern Poyang Lake increased the water turbidity, and may negatively affect this ecosystem. There is reason for concern about the possible environmental impacts on the ecology of Poyang Lake. So far, the nature and magnitude of these ecological impacts remain unknown. It would be worthwhile to

explore these possible impacts in order to develop scientific knowledge to support the decisions that need to be made by the responsible authorities

(2) Simulating the growth of *V. spiralis*

Plant growth models have been applied in many cases for predicting or understanding the growth of submerged aquatic vegetation. However, such model has not been tested in Poyang Lake. The implementation of simulation model of *V. spiralis* in Poyang Lake will contribute to understand how the environmental factor changes affect the growth and biomass of *V. spiralis*.

(3) Integrating growth simulation of *V. spiralis* with remote sensing and geographical information system

So far, no growth simulation model of submerged aquatic vegetation was found to successfully integrate with remote sensing and a geographical information system, which could be important techniques to derive variables required by the simulation model. The integrated system, once implemented, could predict the spatial distribution, and contribute to evaluate the impact of possible hydrological changes on *V. spiralis.*

(4) Predicting the food habitat of Siberian crane

It is also possible to integrate the food habitat model of Siberian crane with the simulation model of *V. spiralis.* Such integrated system could be used to predict the habitat of Siberian crane, considering the food availability, water level and human disturbance. The system could also be employed to analyze the impact of dredging, Three Gorges Dam or other ongoing engineering projects on the habitat of Siberian crane.

8.4 Conclusion

In this chapter, various investigations undertaken in this study were summarized, relations among these investigations were analyzed, and the several future works relevant to this study were highlighted. It is anticipant that these results would provide the basis for the future works, and the implementation of future works would support the decisions that need to be made by the responsible authorities, as they need to balance the pros and cons of dredging when deciding how to rationally manage this unique lake ecosystem.

BIBLIOGRAPHY

Allee, R. J., and J. E. Johnson. 1999. Use of satellite imagery to estimate surface chlorophyll a and Secchi disc depth of Bull Shoals Reservoir, Arkansas, USA. International Journal of Remote Sensing, 20(6): 1057-1072.

Almorox, J., and C. Hontoria. 2004. Global solar radiation estimation using sunshine duration in Spain. Energy Conversion and Management, 45(9-10): 1529-1535.

Barr, A. G., S. M. McGinn, and S. B. Cheng. 1996. A comparison of methods to estimate daily global solar irradiation from other climatic variables on the Canadian prairies. Solar Energy, 56(3): 213-224.

Bartell, S. M., K. R. Campbell, E. P. H. Best, and W. A. Boyd. 2000. Interim Report for the Upper Mississippi River System - Illinois Waterway System Navigation Study. ENV Report 17. U. S. Army Corps of Engineers, Rock Island District, St. Louis District, St. Paul District.

Best, E. P. H., and W. A. Boyd. 2001a. A simulation model for growth of the submersed aquatic macrophyte American wildcelery (*Vallisneria americana Michx.*). ERDC/EL TR-01-5, U.S. Army Engineer Research and Development Center, Vicksburg, MS.

Best, E. P. H., and W. A. Boyd. 2001b. VALLA (Version 1.0): A simulation model for growth of American wildcelery. ERDC/EL SR-01-1, U.S. Army Engineer Research and Development Center, Vicksburg, MS.

Best, E. P. H., C. P. Buzzelli, S. M. Bartell, R. L. Wetzel, W. A. Boyd, R. D. Doyle, and K. R. Campbell. 2001. Modeling submersed macrophyte growth in relation to underwater light climate: Modeling approaches and application potential. Hydrobiologia, 444: 43-70.

Best, E. P. H., G. A. Kiker, B. A. Rycyzyn, K. P. Kenow, J. Fischer, S. K. Nair, and D. B. Wilcox. 2005. Aquatic plant growth model refinement for the Upper Mississippi River-Illinois Waterway System Navigation Study. ENV Report 51, U. S. Army Corps of Engineers, Rock Island District, St. Louis District, St. Paul District.

Best, E. P. H., A. H. Teeter, and S. K. Nair. 2004. Modeling the impacts of suspended sediment concentration and current velocity on submersed vegetation in an Illinois River Pool, USA. APCRP Technical Notes Collection (ERDC TN-APCRP-EA-07), U.S. Army Engineer Research and Development Center, Vicksburg, MS.

Blanch, S. J., G. G. Ganf, and K. F. Walker. 1998. Growth and recruitment in *Vallisneria americana* as related to average irradiance in the water column. Aquatic Botany, 61(3): 181-205.

Bonvicini Pagliai, A. M., A. M. Cognetti Varriale, R. Crema, M. Curini Galletti, and R. Vandini Zunarelli. 1985. Environmental impact of extensive dredging in a coastal marine area. Marine Pollution Bulletin, 16(12): 483-488.

Bowes, G., T. K. Van, L. A. Garrard, and W. T. Haller. 1977. Adaptation to low light levels by Hydrilla. Journal of Aquatic Plant Management, 15: 32-35.

Brezonik, P. L., S. M. Kloiber, L. G. Olmanson, and M. E. Bauer. 2002. Satellite and GIS tools to assess lake quality. Water Resources Center, University of Minnesota.

Burgess, D. W. 1993. Automatic ship detection in satellite multispectral imagery. Photogrammetric Engineering and Remote Sensing, 59(2): 229-237.

Cai, S., Y. Du, and Y. Zeng. 2002. Main problems of the water and soil environment in the middle and lower reaches of Yangtze River and possible countermeasures. Resources and Environment in the Yangtze Basin, 11(6): 564-568.

Calado, G., and P. Duarte. 2000. Modelling growth of *Ruppia cirrhosa*. Aquatic Botany, 68(1): 29-44.

Campbell, J. W., and T. Aarup. 1989. Photosynthetically available radiation at high latitudes. Limnology and Oceanography, 34(8): 1490-1499.

Carr, G. M., H. C. Duthie, and W. D. Taylor. 1997. Models of aquatic plant productivity: a review of the factors that influence growth. Aquatic Botany, 59: 195-215.

Chambers, P. A., and J. Kalff. 1987. Light and nutrients in the control of aquatic plant community structure. Journal of Ecology, 75: 611-619.

Chander, G., D. L. Helder, B. L. Markham, J. D. Dewald, E. Kaita, K. J. Thome, E. Micijevic, and T. A. Ruggles. 2004. Landsat-5 TM reflective-band absolute radiometric calibration. IEEE Transections on Geoscience and Remote Sensing, 42(12): 2747-2760.

Chander, G., and B. Markham. 2003. Revised Landsat-5 TM radiometric calibration procedures and postcalibration dynamic ranges. IEEE Transections on Geoscience and Remote Sensing, 41(11): 2674-2677.

Chavez, P. S. J. 1988. An improved dark-object subtraction technique for atmospheric scattering correction of multispectral data. Remote Sensing of Environment, 24(3): 459-479.

Chavez, P. S. J. 1996. Image-based atmospheric corrections - revisited and improved. Photogrammetric Engineering and Remote Sensing, 62(9): 1025-1036.

Chen, R., S. Lu, E. Kang, J. Yang, and X. Ji. 2006a. Estimating daily global radiation using two types of revised models in China. Energy Conversion and Management, 47(7-8): 865-878.

Chen, X., S. Bao, H. Li, Z. Wu, W. Fu, X. Cai, H. Zhao, Y. Liu, and G. Peng. 2006b. Modeling the impacts of land use/cover change on sediment load in wetlands of the Poyang Lake basin. Pages 560-570 *in* Proceedings of Hydrology and Management of Forested Wetlands Proceedings of the International Conference. American Society of Agricultural and Biological Engineers, New Bern, North Carolina.

Chen, X., Y. S. Li, Z. Liu, K. Yin, Z. Li, O. W. Wai, and B. King. 2004. Integration of multi-source data for water quality classification in the Pearl River estuary and its adjacent coastal waters of Hong Kong. Continental Shelf Research, 24(16): 1827-1843.

Collins, C. D., and J. H. Wlosinski. 1989. A macrophyte submodel for aquatic ecosystems. Aquatic Botany, 33(3-4): 191-206.

Cooling, M. P., G. G. Ganf, and K. F. Walker. 2001. Leaf recruitment and elongation: an adaptive response to flooding in *Villarsia reniformis*. Aquatic Botany, 70(4): 281-294.

Cooter, E. J., and G. B. Dhakhwa. 1996. A solar radiation model for use in biological applications in the South and Southeastern USA. Agricultural and Forest Meteorology, 78(1-2): 31-51.

Craggs, C., E. Conway, and N. M. Pearsall. 1999. Stochastic modelling of solar irradiance on horizontal and vertical planes at a northerly location. Renewable Energy, 18(4): 445-463.

Crisp, D. J. 2004. The state-of-the-art in ship detection in Synthetic Aperture Radar imagery. DSTO Information Sciences Laboratory, Edinburgh, South Australia.

Dewidar, K., and A. Khedr. 2001. Water quality assessment with simultaneous Landsat-5 TM at Manzala Lagoon, Egypt. Hydrobiologia, 457(1-3): 49 - 58.

Dobberfuhl, D. R. 2007. Light limiting thresholds for submerged aquatic vegetation in a blackwater river. Aquatic Botany, 86(4): 346-352.

Dobesch, H., P. Dumolard, and I. Dyras, editors. 2007. Spatial Interpolation for Climate Data: the Use of GIS in Climatology and Meterology. ISTE Publishing Company.

Doorenbos, J., and W. O. Pruitt. 1984. Guidelines for Predicting Crop Water Requirements. FAO, Rome.

Duane Nellis, M., J. Harrington, A. John, and J. Wu. 1998. Remote sensing of temporal and spatial variations in pool size, suspended sediment, turbidity, and Secchi depth in Tuttle Creek Reservoir, Kansas: 1993. Geomorphology, 21(3-4): 281-293.

El-Metwally, M. 2004. Simple new methods to estimate global solar radiation based on meteorological data in Egypt. Atmospheric Research, 69(3-4): 217-239.

Fok, M., and T. Pang. 2006. Finless porpoises in Wuhan, China. Newsletter of the Department of Ecology & Biodiversity, the University of Hong Kong, 34: 18-20.

Fox, M. F., D. R. Kester, and J. A. Yoder. 2005. Spatial and temporal distributions of surface temperature and chlorophyll in the Gulf of Maine during 1998 using SeaWiFS and AVHRR imagery. Marine Chemistry, 97(1-2): 104-123.

Fraser, R. N. 1998a. Hyperspectral remote sensing of turbidity and chlorophyll a among Nebraska Sand Hills lakes. International Journal of Remote Sensing, 19(8): 1579-1589.

Fraser, R. N. 1998b. Multispectral remote sensing of turbidity among Nebraska Sand Hills lakes. International Journal of Remote Sensing, 19(15): 3011-3016.

Gallegos, H. G., and R. Lopardo. 1988. Spatial variability of the global solar radiation obtained by the solarimetric network in the Argentine Pampa Humeda. Solar Energy, 40(5): 397-404.

Gan, T. Y., O. A. Kalinga, K. Ohgushi, and H. Araki. 2004. Retrieving seawater turbidity from Landsat TM data by regressions and an artificial neural network. International Journal of Remote Sensing, 25(21): 4593-4615.

Giardino, C., M. Pepe, P. A. Brivio, P. Ghezzi, and E. Zilioli. 2001. Detecting chlorophyll, Secchi disk depth and surface temperature in a sub-alpine lake using Landsat imagery. The Science of The Total Environment, 268(1-3): 19-29.

Giusti, E., and S. Marsili-Libelli. 2005. Modelling the interactions between nutrients and the submersed vegetation in the Orbetello Lagoon. Ecological Modelling, 184(1): 141-161.

Greidanus, H. 2006. Findings of the DECLIMS project - Detection and classification of marine traffic from space. *http://earth.esa.int/workshops/seasar2006/participants/87/paper_SeasarDECLIMS12p3.pdf (last accessed 10 December 2006)*.

Greidanus, H., P. Clayton, M. Indregard, G. Staples, N. Suzuki, P. Vachoir, C. Wackerman, T. Tennvassas, J. Mallorqui, N. Kourti, R. Ringrose, and H. Melief. 2004. Benchmarking operational SAR ship detection. Pages 4215-4218 *in* Proceedings of International Geoscience and Remote Sensing Symposium (IGARSS)'04, Anchorage, Alaska.

Gupta, R. P. 2003. Remote Sensing Geology (second edition). Springer-Verlag Berlin Heidelberg, New York.

Hakanson, L., and V. V. Boulion. 2003. A model to predict how individual factors influence Secchi depth variations among and within lakes. International Review of Hydrobiology, 88(2): 212-232.

Handcock, R. N., A. R. Gillespie, K. A. Cherkauer, J. E. Kay, S. J. Burges, and S. K. Kampf. 2006. Accuracy and uncertainty of thermal-infrared remote sensing

of stream temperatures at multiple spatial scales. Remote Sensing of Environment, 100(4): 427-440.
Hansen, J. W. 1999. Stochastic daily solar irradiance for biological modeling applications. Agricultural and Forest Meteorology, 94(1): 53-63.
Harma, P., J. Vepsalainen, T. Hannonen, T. Pyhalahti, J. Kamari, K. Kallio, K. Eloheimo, and S. Koponen. 2001. Detection of water quality using simulated satellite data and semi-empirical algorithms in Finland. The Science of The Total Environment, 268(1-3): 107-121.
Harwell, M. C., and K. E. Havens. 2003. Experimental studies on the recovery potential of submerged aquatic vegetation after flooding and desiccation in a large subtropical lake. Aquatic Botany, 77(2): 135-151.
Hellweger, F. L., P. Schlosser, U. Lall, and J. K. Weissel. 2004. Use of satellite imagery for water quality studies in New York Harbor. Estuarine, Coastal and Shelf Science, 61(3): 437-448.
Herb, W. R., and H. G. Stefan. 2003. Integral growth of submersed macrophytes in varying light regimes. Ecological Modelling, 168(1-2): 77-100.
Hootsmans, M. J. M. 1994. A growth analysis model for *Potamogeton pectinatus L.* Pages 250-286 *in* W. Van Vierssen, M. Hootsmans, and J. Vermaat, editors. Lake veluwe, a macrophyte-dominated system under eutrophication stress. Kluwer Academic Publishers, Dordrecht.
Hossain, S., B. D. Eyre, and L. J. McKee. 2004. Impacts of dredging on dry season suspended sediment concentration in the Brisbane River estuary, Queensland, Australia. Estuarine, Coastal and Shelf Science, 61(3): 539-545.
Huang, B., and B. Jiang. 2002. AVTOP: a full integration of TOPMODEL into GIS. Environmental Modelling & Software, 17(3): 261-268.
Huang, G. 2006. On ecological security and ecological construction of Poyang Lake district (in Chinese). Science & Technology Review, 24: 73-78.
Huisman, J., H. Olff, and L. F. M. Fresco. 1993. A hierarchical set of models for species response analysis. Journal of Vegetation Science, 4(1): 37-46.
Hunt, L. A., L. Kuchar, and C. J. Swanton. 1998. Estimation of solar radiation for use in crop modelling. Agricultural and Forest Meteorology, 91(3-4): 293-300.
ILEC. 2005. Managing lakes and their basins for sustainable use: a report for lake managers and stakeholders. International Lake Environment Committee Foundation, Kusatsu, Japan.
ILEC&UNEP. 2003. World lake vision: a call to action. International Lake Environment Committee Foundation and United Nations Environment Programme, Kusatsu, Japan.
Iziomon, M. G., and H. Mayer. 2002. Assessment of some global solar radiation parameterizations. Journal of Atmospheric and Solar-Terrestrial Physics, 64(15): 1631-1643.
Jahn, L. A., and R. V. Anderson. 1986. The Ecology of Pools 19 and 20, of the Upper Mississippi River: A community Profile. US Fish and Wildlife Service, Biological Report 85(7.6).
Jiang, J., and Q. Huang. 1997. A study of the impact of the three gorges project on the water level of Poyang Lake (in Chinese). Journal of Nature Resources, 12(3): 219-224.
Jonzen, N., B. A. Nolet, L. Santamaria, and M. G. E. Svensson. 2002. Seasonal herbivory and mortality compensation in a swan-pondweed system. Ecological Modelling, 147: 209-219.
Jorgensen, P. V., and K. Edelvang. 2000. CASI data utilized for mapping suspended matter concentrations in sediment plumes and verification of 2-D

hydrodynamic modelling. International Journal of Remote Sensing, 21(11): 2247-2258.

Jorgensen, S. E., H. Loffler, W. Rast, and M. Straskraba. 2005. Lake and reservoir management, Volume 54 (Developments in Water Science). Elsevier Publishers, Amsterdam.

Joshi, S. 2005. Feature article: underwater light field and its comparison to metal halide lighting. Advanced Aquarist's Online Magazine, 8.

Kanai, Y., M. Ueta, N. Germogenov, M. Nagendran, N. Mita, and H. Higuchi. 2002. Migration routes and important resting areas of Siberian cranes (*Grus Leucogeanus*) between northeastern Siberia and China as revealed by satellite tracking. Biological Conservation, 106: 339-346.

Kandirmaz, H. M., L. Yegi Ngil, V. Pestemalci, and N. Emrahoglu. 2004. Daily global solar radiation mapping of Turkey using metepsat satellite data. International Journal of Remote Sensing, 25(11): 2159-2168.

Kimber, A., J. L. Owens, and W. G. Crumpton. 1995. Light availability and growth of wildcelery (*Vallisneria americana*) in upper Mississippi River backwaters. Regulated Rivers: Research & Management, 11(2): 167-174.

Kirk, J. T. O. 1994. Light and Photosynthesis in Aquatic Ecosystems. Cambridge University Press, New York, NY, USA.

Kloiber, S. M., P. L. Brezonik, and M. E. Bauer. 2002a. Application of Landsat imagery to regional-scale assessments of lake clarity. Water Research, 36(17): 4330-4340.

Kloiber, S. M., P. L. Brezonik, L. G. Olmanson, and M. E. Bauer. 2002b. A procedure for regional lake water clarity assessment using Landsat multispectral data. Remote Sensing of Environment, 82(1): 38-47.

Kobayashi, H., and H. Iwabuchi. 2008. A coupled 1-D atmosphere and 3-D canopy radiative transfer model for canopy reflectance, light environment, and photosynthesis simulation in a heterogeneous landscape. Remote Sensing of Environment, 112(1): 173-185.

Korschgen, C. E. 1989. Riverine and deepwater habitats for diving ducks. Pages 157-180 *in* L. M. Smith, R. L. Pederson, and R. M. Kaminski, editors. Habitat management for migrating and wintering waterfowl in North America. Texas Tech University Press, Lubbock.

Korschgen, C. E., and W. L. Green. 1988. American wildcelery (*Vallisneria americana*): ecological considerations for restoration. U.S. Fish and Wildlife Service, Fish and Wildlife Technical Report.

LaMontagne, J. M., L. J. Jackson, and R. M. R. Barclay. 2003. Compensatory growth responses of *Potamogeton pectinatus* to foraging by migrating trumpeter swans in spring stop over areas. Aquatic Botany, 76: 235-244.

Lancaster, P., and K. Salkauskas. 1986. Curve and surface fitting: an introduction. Academic Press, London-Orlando.

Lathrop, R. G. 1992. Landsat thematic mapper monitoring of turbid inland water quality. Photogrammetric Engineering and Remote Sensing, 58(4): 465-470.

Lathrop, R. G., and T. M. Lillesand. 1986. Use of Thematic Mapper data to assess water quality in Green Bay and central Lake Michigan. Photogrammetric Engineering and Remote Sensing, 52(5): 671-680.

Lavery, P., C. Pattiaratchi, A. Wyllie, and P. Hick. 1993. Water quality monitoring in estuarine waters using the Landsat thematic mapper. Remote Sensing of Environment, 46(3): 268-280.

Lewis, M. A., D. E. Weber, R. S. Stanley, and J. C. Moore. 2001. Dredging impact on an urbanized Florida bayou: effects on benthos and algal-periphyton. Environmental Pollution, 115(2): 161-171.

Li, F., W. Ji, N. Zeng, J. Wu, X. Wu, W. Yi, Z. Huang, F. Zhou, J. Barzen, and J. Harris. 2005. Aerial survey of Siberian cranes in the Poyang Lake Basin (in Chinese). Pages 58-65 *in* Q. Wang and F. Li, editors. Crane Research in China. Crane and Waterbird Specialists Group of Chinese Ornithological Society, International Crane Foundation, Yunnan Educational Publishing House.

Li, R., and J. Li. 2004. Satellite remote sensing technology for lake water clarity monitoring: an overview. Environmental Informatics Archives, 2: 893-901.

Lillesand, T. M. 2004. Combining satellite remote sensing and volunteer Secchi disk measurement for lake transparency monitoring. *Available online at: http://www.nwqmc.org/NWQMC-Proceedings/Papers-Alphabetical%20by%20First%20Name/Thomas%20Lillesand-Satellite.pdf (accessed June 8 2006)*.

Lillesand, T. M., and J. W. Chipman. 2001. Satellite-assisted lake water quality: using satellite data to observe regional trends in lake transparency. GIM International, 15(11): 26-29.

Liu, D. L., and B. J. Scott. 2001. Estimation of solar radiation in Australia from rainfall and temperature observations. Agricultural and Forest Meteorology, 106(1): 41-59.

Liu, Y., M. Fang, Q. Feng, and L. Wang. 2003a. An automatic ship detection system using ERS SAR images. Pages 2656-2658 *in* Proceedings of International Geoscience and Remote Sensing Symposium (IGARSS)'03, Toulouse, France.

Liu, Y., A. Islam, and J. Gao. 2003b. Quantification of shallow water quality parameters by means of remote sensing. Progress in Physical Geography, 27(1): 24-43.

Liu, Y., and Y. Xu. 1994. The study of influence and countermeasure of Sanxia Project to Poyang's migratory birds reserve (in Chinese). Journal of Jiangxi Normal University, 18(4): 375-380.

Longley, P. A., M. F. Goodchild, D. J. Maguire, and D. W. Rhind. 2001. Geographic Information Systems and Science John Wiley & Sons.

Lubke, R. A., P. E. Reavell, and P. J. Dye. 1984. The effects of dredging on the macrophytic vegetation of the Boro river, Okavango delta, Botswana. Biological Conservation, 30(3): 211-236.

Ma, R., and J. Dai. 2005. Investigation of chlorophyll-a and total suspended matter concentrations using landsat ETM and field spectral measurement in Taihu Lake, China. International Journal of Remote Sensing, 26(13): 2779-2795.

Madsen, J. D., C. F. Hartleb, and C. W. Boylen. 1991. Photosynthetic characteristics of *Myriophyllum spicatum* and six submersed aquatic macrophyte species native to Lake George, New York. Freshwater Biology, 26(2): 233-240.

McDonnel, M. J., and A. J. Lewis. 1978. Ship detection from Landsat imagery. Photogrammetric Engineering and Remote Sensing, 44(3): 297-301.

McFeeters, S. K. 1996. The use of the Normalized Difference Water Index (NDWI) in the delineation of open water features. International Journal of Remote Sensing, 17(7): 1425-1432.

Meine, C. D., and G. W. Archibald, editors. 1996. The Cranes - Status Survey and Conservation Action Plan. IUCN, Gland, Switzerland and Cambridge, U.K.

Merry, C. J., H. L. McKim, N. Lapotin, and J. R. Adams. 1988. Use of SPOT HRV data in the Corps of Engineers dredging program. Photogrammetric Engineering and Remote Sensing, 54(9): 1295-1299.

Miller, R. L., and B. A. McKee. 2004. Using MODIS Terra 250 m imagery to map concentrations of total suspended matter in coastal waters. Remote Sensing of Environment, 93(1-2): 259-266.

Min, Q. 1995. On the regularities of water level fluctuations in Poyang Lake (in Chinese). Journal of Lake Sciences, 7(3): 281-288.

Mottus, M., J. Ross, and M. Sulev. 2001. Experimental study of ratio of PAR to direct integral solar radiation under cloudless conditions. Agricultural and Forest Meteorology, 109(3): 161-170.

Munawar, M., W. P. Norwood, L. H. McCarthy, and C. I. Mayfield. 1989. *In situ* bioassessment of dredging and disposal activities in a contaminated ecosystem: Toronto Harbour. Hydrobiologia, 188-189(1): 601-618.

Muneer, T., and M. S. Gul. 2000. Evaluation of sunshine and cloud cover based models for generating solar radiation data. Energy Conversion and Management, 41(5): 461-482.

Muneer, T., S. Younes, and S. Munawwar. 2007. Discourses on solar radiation modeling. Renewable and Sustainable Energy Reviews, 11(4): 551-602.

Nayar, S., B. P. L. Goh, L. M. Chou, and S. Reddy. 2003. *In situ* microcosms to study the impact of heavy metals resuspended by dredging on periphyton in a tropical estuary. Aquatic Toxicology, 64(3): 293-306.

Nelson, S. A. C., P. A. Soranno, K. S. Cheruvelil, S. A. Batzli, and D. L. Skole. 2003. Regional assessment of lake water clarity using satellite remote sensing. Journal of Limnology, 62(Suppl. 1): 27-32.

Nolet, B. A., V. N. Fuld, V. Rijswijk, and M. E. C. 2006. Foraging costs and accessibility as determinants of giving-up densities in a swan-pondweed system. Oikos, 112(2): 353-362.

O'Sullivan, P. E., and C. S. Reynolds, editors. 2005. The lakes handbook (volume II): lake restoration and rehabilitation. Blackwell Publishing, Oxford, UK.

Osenberg, C. W., R. J. Schmitt, S. J. Holbrook, K. E. Abu-Saba, and A. R. Flegal. 1994. Detection of environmental impacts: natural variability, effect size, and power analysis. Ecological Applications, 4(1): 16-30.

Paulescu, M., L. Fara, and E. Tulcan-Paulescu. 2006. Models for obtaining daily global solar irradiation from air temperature data. Atmospheric Research, 79(3-4): 227-240.

Pennekamp, J. G. S., R. J. C. Epskamp, W. F. Rosenbrand, A. Mullie, G. L. Wessel, T. Arts, and I. K. Deibel. 1996. Turbidity caused by dredging: viewed in perspective. Terra et Aqua, 64: 10-17.

Poole, H. H., and W. R. G. Atkins. 1929. Photo-electric measurements of submarine illumination throughout the year. Journal of the Marine Biological Association of the United Kingdom, 16(1): 297-324.

Pozdnyakov, D., A. Korosov, H. Grassl, and L. Pettersson. 2005. An advanced algorithm for operational retrieval of water quality from satellite data in the visible. International Journal of Remote Sensing, 26(12): 2669-2687.

Raymond, H. G. K., B. A. Nolet, and D. Bankert. 2006. Movement of foraging tundra swans explained by spatial pattern in cryptic food densities. Ecology, 87(9): 2244-2254.

Rehman, S., and S. G. Ghori. 2000. Spatial estimation of global solar radiation using geostatistics. Renewable Energy, 21(3-4): 583-605.

Richards, J. A., and X. Jia. 2006. Remote Sensing Digital Image Analysis. Springer Berlin Heidelberg.

Rivington, M., G. Bellocchi, K. B. Matthews, and K. Buchan. 2005. Evaluation of three model estimations of solar radiation at 24 UK stations. Agricultural and Forest Meteorology, 132(3-4): 228-243.

Sabins, F. F. 1997. Remote Sensing: Principles and Interpretation, Third edition. W. H. Freeman and Company, New York.

Scheffer, M. 1998. Ecology of Shallow Lakes. Chapman & Hall, London.

Scheffer, M., A. H. Bakema, and F. G. Worteboer. 1993. MEGAPLANT: a simulation model of the dynamics of submerged plants. Aquatic Botany, 45: 341-356.

Schmitt, R. J., C. W. Osenberg, W. J. Douros, and J. Chesson. 1996. The art and science of administrative environmental impact assessment. Pages 281-293 *in* R. J. Schmitt and C. W. Osenberg, editors. Detecting Ecological Impacts: Concepts and Applications in Coastal Habitats. Academic Press, San Diego, CA.

Shankman, D., B. D. Keim, and J. Song. 2006. Flood frequency in China's Poyang lake region: trends and teleconnections. International Journal of Climatology, 26(9): 1255-1266.

Shaw, B., C. Mechenich, and L. Klessig. 2004. Understanding Lake Data (G3582). University of Wisconsin-Stevens Point.

Sipelgas, L., U. Raudsepp, and T. Kouts. 2006. Operational monitoring of suspended matter distribution using MODIS images and numerical modelling. Advances in Space Research, 38(10): 2182-2188.

Song, L., and L. Jin. 2001. Advances of the study on flood control and disaster reduction Poyang Lake (in Chinese). Environment and Exploitation, 16(3): 4-6.

Spencer, K. L., R. E. Dewhurst, and P. Penna. 2006. Potential impacts of water injection dredging on water quality and ecotoxicity in Limehouse Basin, River Thames, SE England, UK. Chemosphere, 63(3): 509-521.

Sponberg, A. F., and D. M. Lodge. 2005. Seasonal belowground herbivory and a density refuge from waterfowl herbivory for *Vallisneria americana*. Ecology, 86(8): 2127-2134.

Suckling, P. W. 1985. Estimating daily solar radiation values in selected mid-latitude regions by extrapolating measurements from nearby stations. Solar Energy, 35(6): 491-495.

Swift, T. J., J. Perez-Losada, S. G. Schladow, J. E. Reuter, A. D. Jassby, and C. R. Goldman. 2006. Water clarity modeling in Lake Tahoe: linking suspended matter characteristics to Secchi depth. Aquatic Sciences, 68(1): 1-15.

Tello, M., C. Lopez-Martinez, and J. J. Mallorqui. 2006. Automatic vessel monitoring with single and multidimensional SAR images in the wavelet domain. ISPRS Journal of Photogrammetry and Remote Sensing, 61(3-4): 260-278.

Tiba, C. 2001. Solar radiation in the Brazilian Northeast. Renewable Energy, 22(4): 565-578.

Trnka, M., Z. Zalud, J. Eitzinger, and M. Dubrovsky. 2005. Global solar radiation in Central European lowlands estimated by various empirical formulae. Agricultural and Forest Meteorology, 131(1-2): 54-76.

Tunaley, J. K. E. 2004. Algorithms for ship detection and tracking using satellite imagery. Pages 1804-1807 *in* Proceedings of International Geoscience and Remote Sensing Symposium (IGARSS)'04, Anchorage, Alaska, USA.

Tymvios, F. S., C. P. Jacovides, S. C. Michaelides, and C. Scouteli. 2005. Comparative study of Angstrom's and artificial neural networks' methodologies in estimating global solar radiation. Solar Energy, 78(6): 752-762.

Van Genderen, J. L., R. Gens, Z. Vekerdy, A. Prakash, J. Cornelis, and P. Boekarts. 1998. Tutorial on remote sensing image and data fusion - version 2 (Multimedia CD-ROM). ITC, Enschede, the Netherlands.

Van Nes, E. H. 2002. Controlling complexity in individual-based models of aquatic vegetation and fish communities. Wageningen University.

Van Nes, E. H., M. Scheffer, M. S. v. d. Berg, and H. Coops. 2003. Charisma: a spatial explicit simulation model of submerged macrophytes. Ecological Modelling, 159: 103-116.

Van Vierssen, W., M. Hootsmans, and J. Vermaat. 1994. Lake veluwe, a macrophyte-dominated system under eutrophication stress. Kluwer Academic Publishers, Dordrecht.

Vignolo, A., A. Pochettino, and D. Cicerone. 2006. Water quality assessment using remote sensing techniques: Medrano Creek, Argentina. Journal of Environmental Management, 81(4): 429-433.

Wang, B. 1999. Calculation of solar radiation: (3) Calculation of extraatmosphere solar radiation on horizontal surface (in Chinese). Solar Energy, 4: 11-12.

Wang, J. 2002. Three Borges Project: the largest water conservancy project in the world. Public Administration and Development, 22: 369-375.

Wang, X. J., and T. Ma. 2001. Application of remote sensing techniques in monitoring and assessing the water quality of Taihu Lake. Bulletin of Environmental Contamination and Toxicology, 67(6): 863-870.

Wang, Z., J. H. W. Lee, and D. Cheng. 2005. Impacts of the TGP project on the Yangtze River ecology and management strategies. International Journal of River Basin Management, 3(4): 237-246.

Wildish, D. J., and M. L. H. Thomas. 1985. Effects of dredging and dumping on benthos of Saint John Harbour, Canada. Marine Environmental Research, 15(1): 45-57.

Wilson, T. B., and T. P. Meyers. 2007. Determining vegetation indices from solar and photosynthetically active radiation fluxes. Agricultural and Forest Meteorology, 144(3-4): 160-179.

Winokur, R. S. 2000. SAR symposium keynote address. Johns Hopkins APL Technical Digest, 21(1): 5-11.

Wong, L. T., and W. K. Chow. 2001. Solar radiation model. Applied Energy, 69(3): 191-224.

Wu, G., J. De Leeuw, A. K. Skidmore, H. H. T. Prins, and Y. Liu. 2007a. Comparison of MODIS and Landsat TM5 images for mapping tempo-spatial dynamics of Secchi disk depths in Poyang Lake national nature reserve, China. International Journal of Remote Sensing, In Press, Accepted Manuscript.

Wu, G., J. De Leeuw, A. K. Skidmore, H. H. T. Prins, and Y. Liu. 2007b. Concurrent monitoring of vessels and water turbidity enhances the strength of evidence in remotely sensed dredging impact assessment. Water Research, 41(15): 3271-3280.

Wu, Y., and W. Ji. 2002. Study on Jiangxi Poyang Lake national nature reserve. Forest Publishing House, Beijing.

Xiong, X., and X. Hu. 2003. Effects of Poyang Lake Control Project on the wetland ecosystem in Poyang Lake region. Journal of Jiangxi Normal University, 27(1): 89-93.

Xu, D., M. Xiong, and J. Zhang. 2001. Analysis on hydrologic characteristics of Poyang Lake. Yangtze River, 32(2): 21-27.

Yang, H. S., A. Dobermann, J. L. Lindquist, D. T. Walters, T. J. Arkebauer, and K. G. Cassman. 2004. Hybrid-maize--a maize simulation model that combines two crop modeling approaches. Field Crops Research, 87(2-3): 131-154.

Yang, K., and T. Koike. 2002. Estimating surface solar radiation from upper-air humidity. Solar Energy, 72(2): 177-186.

Zhang, F., B. Wu, L. Zhang, H. Huang, and Y. Tian. 2006a. Illicit vessel identification in inland waters using SAR image. Page 64190S *in* Proceedings of SPIE, Volume 6419-Geoinformatics 2006: Remotely Sensed Data and Information. SPIE, Wuhan, China.

Zhang, Y. 2005. Surface water quality estimation using remote sensing in the gulf Dinland and the finnish archipelago sea. Helsinki University of Technology Laboratory of Space Technology, Espoo.

Zhang, Y., and B. Qin. 2002. The basic characteristic and climatological calculation of the photosynthetically available radiation in Taihu region (in Chinese). Acta Energiae Solaris Sinica, 23(1): 1-6.

Zhang, Y., B. Qin, G. Zhu, G. Gao, L. Luo, and W. Chen. 2006b. Effect of sediment resuspension on underwater light field in shallow lakes in the middle and lower reaches of the Yangtze River: A case study in Longgan Lake and Taihu Lake. Science in China Series D: Earth Sciences, 49(Supplement 1): 114-125.

Zhao, B., B. He, Y. Zhu, and G. Yuan. 2003. Modelling for dynamic monitoring transparency of Lake Dianchi water-body (in Chinese). Environment Science and Technology, 26(2): 16-17.

Zhong, Y., and S. Chen. 2005. Impact of dredging on fish in Poyang Lake. Jiangxi Fishery Sciences and Technology, 1: 15-18.

AUTHOR'S BIOGRAPHY

Wu, Guofeng was born on the 21st of December 1969 in Heilongjiang, China.

In 1994 he obtained Bachelor Degree on Cartography from the former Wuhan Technical University of Surveying and Mapping, China. He acquired Professional Master Degree on Geographical Information System (GIS) for Cadastral Applications from the International Institute for Geo-Information Science and Earth Observation (ITC), the Netherlands in 1999, and Master of Science Degree on Cartography and GIS from the Wuhan University (the former Wuhan Technical University of Surveying and Mapping), China in 2001. In November 2003, he was awarded a scholarship by the Netherlands Foundation for the Advancement of Tropical Research (WOTRO) and ITC to pursue a PhD Degree at ITC and Wageningen University in the Netherlands.

He works at the School of Resource and Environmental Sciences of Wuhan University, China since 1994. He teaches several GIS-related courses including computer program, data structure, GIS and spatial database. His major research interests cover multimedia electronic map, GIS, remote sensing and their applications in lake ecosystems.

ITC DISSERTATION LIST

1. **Akinyede** (1990), Highway cost modelling and route selection using a geotechnical information system
2. **Pan, Heping** (1990), 90-9003-757-8, Spatial structure theory in machine vision and applications to structural and textural analysis of remotely sensed images
3. **Bocco Verdinelli, G.** (1990), Gully erosion analysis using remote sensing and geographic information systems: a case study in Central Mexico
4. **Sharif, M**. (1991), Composite sampling optimization for DTM in the context of GIS
5. **Drummond, J.** (1991), Determining and processing quality parameters in geographic information systems
6. **Groten, S.** (1991), Satellite monitoring of agro-ecosystems in the Sahel
7. **Sharifi, A.** (1991), 90-6164-074-1, Development of an appropriate resource information system to support agricultural management at farm enterprise level
8. **Zee, D. van der** (1991), 90-6164-075-X, Recreation studied from above: Air photo interpretation as input into land evaluation for recreation
9. **Mannaerts, C.** (1991), 90-6164-085-7, Assessment of the transferability of laboratory rainfall-runoff and rainfall - soil loss relationships to field and catchment scales: a study in the Cape Verde Islands
10. **Wang, Zeshen** (1991), 90-393-0333-9, An expert system for cartographic symbol design
11. **Zhou, Yunxian** (1991), 90-6164-081-4, Application of Radon transforms to the processing of airborne geophysical data
12. **Zuviria, M. de** (1992), 90-6164-077-6, Mapping agro-topoclimates by integrating topographic, meteorological and land ecological data in a geographic information system: a case study of the Lom Sak area, North Central Thailand
13. **Westen, C. van** (1993), 90-6164-078-4, Application of Geographic Information Systems to landslide hazard zonation
14. **Shi, Wenzhong** (1994), 90-6164-099-7, Modelling positional and thematic uncertainties in integration of remote sensing and geographic information systems
15. **Javelosa, R.** (1994), 90-6164-086-5, Active Quaternary environments in the Philippine mobile belt
16. **Lo King-Chang** (1994), 90-9006526-1, High quality automatic DEM, digital elevation model generation from multiple imagery
17. **Wokabi, S.** (1994), 90-6164-102-0, Quantified land evaluation for maize yield gap analysis at three sites on the eastern slope of Mt. Kenya
18. **Rodriguez, O.** (1995), Land Use conflicts and planning strategies in urban fringes: a case study of Western Caracas, Venezuela
19. **Meer, F. van der** (1995), 90-5485-385-9, Imaging spectrometry & the Ronda peridotites
20. **Kufoniyi, O.** (1995), 90-6164-105-5, Spatial coincidence: automated database updating and data consistency in vector GIS
21. **Zambezi, P.** (1995), Geochemistry of the Nkombwa Hill carbonatite complex of Isoka District, north-east Zambia, with special emphasis on economic minerals
22. **Woldai, T.** (1995), The application of remote sensing to the study of the geology and structure of the Carboniferous in the Calañas area, pyrite belt, SW Spain
23. **Verweij, P.** (1995), 90-6164-109-8, Spatial and temporal modelling of vegetation patterns: burning and grazing in the Paramo of Los Nevados National Park,

Colombia

24. **Pohl, C.** (1996), 90-6164-121-7, Geometric aspects of multisensor image fusion for topographic map updating in the humid tropics
25. **Jiang, Bin** (1996), 90-6266-128-9, Fuzzy overlay analysis and visualization in GIS
26. **Metternicht, G.** (1996), 90-6164-118-7, Detecting and monitoring land degradation features and processes in the Cochabamba Valleys, Bolivia. A synergistic approach
27. **Hoanh Chu Thai** (1996), 90-6164-120-9, Development of a Computerized Aid to Integrated Land Use Planning (CAILUP) at regional level in irrigated areas: a case study for the Quan Lo Phung Hiep region in the Mekong Delta, Vietnam
28. **Roshannejad, A.** (1996), 90-9009-284-6, The management of spatiotemporal data in a national geographic information system
29. **Terlien, M.** (1996), 90-6164-115-2, Modelling spatial and temporal variations in rainfall-triggered landslides: the integration of hydrologic models, slope stability models and GIS for the hazard zonation of rainfall-triggered landslides with examples from Manizales, Colombia
30. **Mahavir, J.** (1996), 90-6164-117-9, Modelling settlement patterns for metropolitan regions: inputs from remote sensing
31. **Al-Amir, S.** (1996), 90-6164-116-0, Modern spatial planning practice as supported by the multi-applicable tools of remote sensing and GIS: the Syrian case
32. **Pilouk, M.** (1996), 90-6164-122-5, Integrated modelling for 3D GIS
33. **Duan Zengshan** (1996), 90-6164-123-3, Optimization modelling of a river-aquifer system with technical interventions: a case study for the Huangshui river and the coastal aquifer, Shandong, China
34. **Man, W.H. de** (1996), 90-9009-775-9, Surveys: informatie als norm: een verkenning van de institutionalisering van dorp - surveys in Thailand en op de Filippijnen
35. **Vekerdy, Z.** (1996), 90-6164-119-5, GIS-based hydrological modelling of alluvial regions: using the example of the Kisaföld, Hungary
36. **Pereira, Luisa** (1996), 90-407-1385-5, A robust and adaptive matching procedure for automatic modelling of terrain relief
37. **Fandino Lozano, M.** (1996), 90-6164-129-2, A framework of ecological evaluation oriented at the establishment and management of protected areas: a case study of the Santuario de Iguaque, Colombia
38. **Toxopeus, B.** (1996), 90-6164-126-8, ISM: an interactive spatial and temporal modelling system as a tool in ecosystem management: with two case studies: Cibodas biosphere reserve, West Java Indonesia: Amboseli biosphere reserve, Kajiado district, Central Southern Kenya
39. **Wang, Yiman** (1997), 90-6164-131-4, Satellite SAR imagery for topographic mapping of tidal flat areas in the Dutch Wadden Sea
40. **Saldana-Lopez, Asunción** (1997), 90-6164-133-0, Complexity of soils and Soilscape patterns on the southern slopes of the Ayllon Range, central Spain: a GIS assisted modelling approach
41. **Ceccarelli, T.** (1997), 90-6164-135-7, Towards a planning support system for communal areas in the Zambezi valley, Zimbabwe; a multicriteria evaluation linking farm household analysis, land evaluation and geographic information systems
42. **Peng, Wanning** (1997), 90-6164-134-9, Automated generalization in GIS
43. **Lawas, C.** (1997), 90-6164-137-3, The resource users' knowledge, the neglected input in Land resource management: the case of the Kankanaey farmers in Benguet, Philippines

44. **Bijker, W.** (1997), 90-6164-139-X, Radar for rain forest: A monitoring system for land cover Change in the Colombian Amazon
45. **Farshad, A.** (1997), 90-6164-142-X, Analysis of integrated land and water management practices within different agricultural systems under semi-arid conditions of Iran and evaluation of their sustainability
46. **Orlic, B.** (1997), 90-6164-140-3, Predicting subsurface conditions for geotechnical modelling
47. **Bishr, Y.** (1997), 90-6164-141-1, Semantic aspects of interoperable GIS
48. **Zhang, Xiangmin** (1998), 90-6164-144-6, Coal fires in Northwest China: detection, monitoring and prediction using remote sensing data
49. **Gens, R.** (1998), 90-6164-155-1, Quality assessment of SAR interferometric data
50. **Turkstra, J.** (1998), 90-6164-147-0, Urban development and geographical information: spatial and temporal patterns of urban development and land values using integrated geo-data, Villaviciencia, Colombia
51. **Cassells, C.** (1998), 90-6164-234-5, Thermal modelling of underground coal fires in northern China
52. **Naseri, M.** (1998), 90-6164-195-0, Characterization of salt-affected soils for modelling sustainable land management in semi-arid environment: a case study in the Gorgan Region, Northeast, Iran
53. **Gorte B.G.H.** (1998), 90-6164-157-8, Probabilistic segmentation of remotely sensed images
54. **Tegaye, Tenalem Ayenew** (1998), 90-6164-158-6, The hydrological system of the lake district basin, central main Ethiopian rift
55. **Wang, Donggen** (1998), 90-6864-551-7, Conjoint approaches to developing activity-based models
56. **Bastidas de Calderon, M.** (1998), 90-6164-193-4, Environmental fragility and vulnerability of Amazonian landscapes and ecosystems in the middle Orinoco river basin, Venezuela
57. **Moameni, A.** (1999), Soil quality changes under long-term wheat cultivation in the Marvdasht plain, South-Central Iran
58. **Groenigen, J.W. van** (1999), 90-6164-156-X, Constrained optimisation of spatial sampling: a geostatistical approach
59. **Cheng, Tao** (1999), 90-6164-164-0, A process-oriented data model for fuzzy spatial objects
60. **Wolski, Piotr** (1999), 90-6164-165-9, Application of reservoir modelling to hydrotopes identified by remote sensing
61. **Acharya, B.** (1999), 90-6164-168-3, Forest biodiversity assessment: A spatial analysis of tree species diversity in Nepal
62. **Akbar Abkar, Ali** (1999), 90-6164-169-1, Likelihood-based segmentation and classification of remotely sensed images
63. **Yanuariadi, T.** (1999), 90-5808-082-X, Sustainable land allocation: GIS-based decision support for industrial forest plantation development in Indonesia
64. **Abu Bakr**, **Mohamed** (1999), 90-6164-170-5, An integrated agro-economic and agro-ecological framework for land use planning and policy analysis
65. **Eleveld, M.** (1999), 90-6461-166-7, Exploring coastal morphodynamics of Ameland (the Netherlands) with remote sensing monitoring techniques and dynamic modelling in GIS
66. **Yang, Hong** (1999), 90-6164-172-1, Imaging spectrometry for hydrocarbon microseepage
67. **Mainam, Félix** (1999), 90-6164-179-9, Modelling soil erodibility in the semiarid zone of Cameroon
68. **Bakr, Mahmoud** (2000), 90-6164-176-4, A stochastic inverse-management

approach to groundwater quality

69. **Zlatanova, Z.** (2000), 90-6164-178-0, 3D GIS for urban development
70. **Ottichilo, Wilber K.** (2000), 90-5808-197-4, Wildlife dynamics: An analysis of change in the Masai Mara ecosystem
71. **Kaymakci, Nuri** (2000), 90-6164-181-0, Tectono-stratigraphical evolution of the Cankori Basin (Central Anatolia, Turkey)
72. **Gonzalez, Rhodora** (2000), 90-5808-246-6, Platforms and Terraces: Bridging participation and GIS in joint-learning for watershed management with the Ifugaos of the Philippines
73. **Schetselaar, Ernst** (2000), 90-6164-180-2, Integrated analyses of granite-gneiss terrain from field and multisource remotely sensed data. A case study from the Canadian Shield
74. **Mesgari, Saadi** (2000), 90-3651-511-4, Topological Cell-Tuple structure for three-dimensional spatial data
75. **Bie, Cees A.J.M. de** (2000), 90-5808-253-9, Comparative performance analysis of agro-ecosystems
76. **Khaemba, Wilson M**. (2000), 90-5808-280-6, Spatial statistics for natural resource management
77. **Shrestha, Dhruba** (2000), 90-6164-189-6, Aspects of erosion and sedimentation in the Nepalese Himalaya: highland-lowland relations
78. **Asadi Haroni, Hooshang** (2000), 90-6164-185-3, The Zarshuran Gold Deposit Model applied in a mineral exploration GIS in Iran
79. **Raza, Ale** (2001), 90-3651-540-8, Object-oriented temporal GIS for urban applications
80. **Farah, Hussein** (2001), 90-5808-331-4, Estimation of regional evaporation under different weather conditions from satellite and meteorological data. A case study in the Naivasha Basin, Kenya
81. **Zheng**, **Ding** (2001), 90-6164-190-X, A neural-fuzzy approach to linguistic knowledge acquisition and assessment in spatial decision making
82. **Sahu, B.K.** (2001), Aeromagnetics of continental areas flanking the Indian Ocean; with implications for geological correlation and reassembly of Central Gondwana
83. **Alfestawi, Y.** (2001), 90-6164-198-5, The structural, paleogeographical and hydrocarbon systems analysis of the Ghadamis and Murzuq Basins, West Libya, with emphasis on their relation to the intervening Al Qarqaf Arch
84. **Liu, Xuehua** (2001), 90-5808-496-5, Mapping and modelling the habitat of Giant Pandas in Foping Nature Reserve, China
85. **Oindo, Boniface Oluoch** (2001), 90-5808-495-7, Spatial patterns of species diversity in Kenya
86. **Carranza, Emmanuel John** (2002), 90-6164-203-5, Geologically constrained mineral potential mapping
87. **Rugege, Denis** (2002), 90-5808-584-8, Regional analysis of maize-based land use systems for early warning applications
88. **Liu, Yaolin** (2002), 90-5808-648-8, Categorical database generalization in GIS
89. **Ogao, Patrick** (2002), 90-6164-206-X, Exploratory visualization of temporal geospatial data using animation
90. **Abadi, Abdulbaset M.** (2002), 90-6164-205-1, Tectonics of the Sirt Basin – Inferences from tectonic subsidence analysis, stress inversion and gravity modelling
91. **Geneletti, Davide** (2002), 90-5383-831-7, Ecological evaluation for environmental impact assessment
92. **Sedogo, Laurent G.** (2002), 90-5808-751-4, Integration of participatory local and

regional planning for resources management using remote sensing and GIS

93. **Montoya, Lorena** (2002), 90-6164-208-6, Urban disaster management: a case study of earthquake risk assessment in Carthago, Costa Rica
94. **Ahmad, Mobin-ud-Din** (2002), 90-5808-761-1, Estimation of net groundwater use in irrigated river basins using Geo-information techniques: A case study in Rechna Doab, Pakistan
95. **Said, Mohammed Yahya** (2003), 90-5808-794-8, Multiscale perspectives of species richness in East Africa
96. **Schmidt, Karin** (2003), 90-5808-830-8, Hyperspectral remote sensing of vegetation species distribution in a Saltmarsh
97. **Lopez Binnquist, Citlalli** (2003), 90-3651-900-4, The endurance of Mexican Amate Paper: Exploring additional dimensions to the sustainable development concept
98. **Huang, Zhengdong** (2003), 90-6164-211-6, Data integration for urban transport planning
99. **Cheng, Jianquan** (2003), 90-6164-212-4, Modelling spatial and temporal urban growth
100. **Campos dos Santos, Jose Laurindo** (2003), 90-6164-214-0, A biodiversity information system in an Open Data/Metadatabase Architecture
101. **Hengl, Tomislav** (2003), 90-5808-896-0, PEDOMETRIC MAPPING, Bridging the gaps between conventional and pedometric approaches
102. **Barrera Bassols, Narciso (**2003), 90-6164-217-5, Symbolism, knowledge and management of soil and land resources in indigenous communities: Ethnopedology at global, regional and local scales
103. **Zhan, Qingming** (2003), 90-5808-917-7, A hierarchical object-based approach for urban land-use classification from remote sensing data
104. **Daag, Arturo S.** (2003), 90-6164-218-3, Modelling the erosion of Pyroclastic Flow Deposits and the Occurrences of Lahars at Mt. inatubo, Philippines
105. **Bacic, Ivan** (2003), 90-5808-902-9, Demand-driven land evaluation with case studies in Santa Catarina, Brazil
106. **Murwira, Amon** (2003), 90-5808-951-7, Scale matters! A new approach to quantify spatial heterogeneity for predicting the distribution of wildlife
107. **Mazvimavi, Dominic** (2003), 90-5808-950-9, Estimation of flow characteristics of ungauged catchments. A case study in Zimbabwe
108. **Tang, Xinming** (2004), 90-6164-220-5, Spatial object modelling in fuzzy topological spaces with applications to land cover change
109. **Kariuki, Patrick** (2004), 90-6164-221-3, Spectroscopy and swelling soils; an integrated approach
110. **Morales, Javier** (2004), 90-6164-222-1, Model driven methodology for the design of geo-information services
111. **Mutanga, Onisimo** (2004), 90-5808-981-9, Hyperspectral remote sensing of tropical grass quality and quantity
112. **Sliuzas, Ricardas V.** (2004), 90-6164-223-X, Managing informal settlements: a study using geo-information in Dar es Salaam, Tanzania
113. **Lucieer, Arko** (2004), 90-6164-225-6, Uncertainties in segmentation and their visualisation
114. **Corsi, Fabio** (2004), 90-8504-090-6, Applications of existing biodiversity information: Capacity to support decision-making
115. **Tuladhar, Arbind** (2004), 90-6164-224-8, Parcel-based geoinformation system: Concepts and guidelines
116. **Elzakker, Corné van** (2004), 90-6809-365-7, The use of maps in the exploration of geographic data

117. **Nidumolu, Uday Bhaskar** (2004), 90-8504-138-4, Integrating Geoinformation models with participatory approaches: applications in land use analysis
118. **Koua, Etien L.** (2005), 90-6164-229-9, Computational and visual support for exploratory Geovisualization and Knowledge Construction
119. **Blok, Connie A.** (2005), Dynamic visualization variables in animation to support monitoring of spatial phenomena
120. **Meratnia, Nirvana** (2005), 90-365-2152-1, Towards database support for moving object data
121. **Yemefack, Martin** (2005), 90-6164-233-7, Modelling and monitoring Soil and Land Use Dynamics within Shifting Agricultural Landscape Mosaic Systems
122. **Kheirkhah, Masoud** (2005), 90-8504-256-9, Decision support system for floodwater spreading site selection in Iran
123. **Nangendo, Grace** (2005), 90-8504-200-3, Changing forest-woodlandsavanna mosaics in Uganda: with implications for conservation
124. **Mohamed, Yasir Abbas** (2005), 04-15-38483-4, The Nile Hydroclimatology: impact of the Sudd wetland (Distinction)
125. **Duker, Alfred, A.** (2005), 90-8504-243-7, Spatial analysis of factors implicated in *mycobacterium ulcerans* infection in Ghana
126. **Ferwerda, Jelle, G.,** (2005), 90-8504-209-7, Charting the quality of forage: Measuring and mapping the variation of chemical components in foliage with hyperspectral remote sensing
127. **Martinez, Javier** (2005), 90-6164-235-3, Monitoring intra-urban inequalities with GIS-based indicators. With a case study in Rosario, Argentina
128. **Saavedra, Carlos** (2005), 90-8504-289-5, Estimating spatial patterns of soil erosion and deposition in the Andean region using Geoinformation techniques. A case study in Cochabamba, Bolivia
129. **Vaiphasa, Chaichoke** (2006), 90-8504-353-0, Remote sensing techniques for mangrove mapping
130. **Porwal, Alok** (2006), 90-6164-240-X, Mineral potential mapping with mathematical geological models
131. **Werff, Harald van der** (2006), 90-6164-238-8, Knowledge-based remote sensing of complex objects: recognition of spectral and spatial patterns resulting from natural hydrocarbon seepages
132. **Vlag, Daniël van de** (2006), 90-8504-384-0, Modeling and visualizing dynamic landscape objects and their qualities
133. **Joshi, Chudamani** (2006), 90-8504-470-7, Mapping cryptic invaders and invisibility of tropical forest ecosystems: *Chromolaena odorata* in Nepal
134. **Bandara, K.M.P.S.** (2006), 90-8504-406-5, Assessing irrigation performance by using remote sensing
135. **Dilo, Areti** (2006), 90-8504-461-8, Representation of and Reasoning with Vagueness in Spatial Information. A system for handling vague objects
136. **Debba, Pravesh** (2006), 90-8504-462-6, Sampling scheme optimization from hyperspectral data
137. **Huisman, Marco** (2006), 90-6164-246-9, Assessment of rock mass decay in artificial slopes
138. **Lemmens, Rob** (2006), 90-6164-250-7, Semantic interoperability of distributed geo-services
139. **Chacón Moreno, Eulogio** (2007), 90-8504-559-2, Ecological and spatial modeling: Mapping ecosystems, landscape changes, and plant species distribution in Llanos del Orinoco, Venezuela
140. **Amer, Sherif** (2007), 90-6164-253-1, Towards spatial justice in urban health services planning

141. **Obakeng, Obolokile Thothi** (2007), 90-6164-254-X, Soil moisture dynamics and evapotranspiration at the fringe of the Botswana Kalahari, with emphasis on deep rooting vegetation
142. **Cho, Moses Azong** (2007), 978-90-8504-622-6, Hyperspectral remote sensing of biochemical and biophysical parameters
143. **Farifteh, Jamshid** (2007), 978-90-6164-259-6, Imaging Spectroscopy of salt-affected soils: Model-based integrated method
144. **Minang, Peter Akong**, (2007), 978-90-6164-260-2, Implementing global environmental policy at local level: community carbon forestry perspectives in Cameroon
145. **Noomen, Marleen F.** (2007), 978-90-8504-671-4, Hyperspectral reflectance of vegetation affected by underground hydrocarbon gas seepage
146. **Trias Aditya Kurniawan Muhammad**, (2007), 978-90-6164-261-9, The National Atlas as a Metaphor for Improved Use of a Geospatial Data Infrastructure
147. **Alkema, Dinand** (2007), 978-90-6164-239, Simulating floods. On the application of 2D-hydraulic models for flood hazard and risk assessment
148. **Ruitenbeek, Frank van** (2007), 978-90-6164-262-6, Hydrothermal processes in the Archean – New insights from imaging spectroscopy
149. **Turdukulov, Ulanbek D.** (2007), 978-90-6164-264-0, Visualizing the evolution of image features in time-series: supporting the exploration of sensor data
150. **Sobhan, Md. Istiak** (2007), 978-90-8504-809-1, Species discrimination from a hyperspectral perspective

PE&RC PHD EDUCATION CERTIFICATE

With the educational activities listed below the PhD candidate has complied with the educational requirements set by the C.T. de Wit Graduate School for Production Ecology and Resource Conservation (PE&RC) which comprises of a minimum total of 32 ECTS (= 22 weeks of activities)

Review of Literature (5.6 ECTS)

- Impact of the Three Gorges Dam on the distribution of Siberian crane food habitat in Poyang Lake, China (2003-2004)

Writing of Project Proposal (7 ECTS)

- Impact of the Three Gorges Dam on the distribution of the Siberian crane food habitat in Poyang Lake, China (2003-2004)

Post-Graduate Courses (4.2 ECTS)

- Advanced geostatistical methods; ITC (2005)
- IDL basic programming; ITC (2006)
- Advanced remote sensing; ITC (2006)

Competence Strengthening / Skills Courses (1.4 ECTS)

- Scientific writing course; ITC (2005)

Discussion Groups / Local Seminars and Other Meetings (5 ECTS)

- PhD tutorial of NRM; ITC (2004-2007)
- PhD and research seminars; ITC (2004-2007)

PE&RC Annual Meetings, Seminars and the PE&RC Weekend (1.8 ECTS)

- PhD weekend (2004)
- Research day of NRM; ITC (2005-2007)

International Symposia, Workshops and Conferences (7 ECTS)

- The international conference on Poyang Lake ecological system (2005)
- The fourth international symposium on multispectral image processing and pattern recognition (2005)
- The international workshop on Poyang Lake Ecosystem (2007)